CDF/DOC/BOTTOM/CDFR/7815
July 25, 2006- Version 5.0

$Br(B_s \to D_s\pi\pi\pi)/Br(B^0 \to D^+\pi\pi\pi)$ $D_s \to \phi\pi(3\pi, K^*K)$, $D^+ \to K\pi\pi$ with $355pb^{-1}$ in Run II

G. Bauer, A. Belloni, A. Bolshov, B. Iyutin, Ch. Paus

Massachusetts Institute of Technology

Abstract

We conducted a study of the ratio of the branching fractions $\frac{Br(B_s^0 \to D_s^+ 3\pi)}{Br(B^0 \to D^- 3\pi)}$ where $D_s \to \phi\pi(K^*K, 3\pi)$, $D^+ \to K\pi\pi$. This study is an update to the first observation and branching fraction measurement of $B_s^0 \to D_s^+ 3\pi$ covered by CDF note 7504. Major changes compare to the previous analysis:

- Added $110pb^{-1}$ more luminosity
- Added `LOWPT` trigger data
- Used PDG 2006 numbers
- Added two new D_s modes:
  - $D_s \to K^*K$
  - $D_s \to \pi\pi\pi$

After correcting for the relative trigger and reconstruction efficiencies we measure

$$\frac{f_s}{f_d}\frac{Br(B_s^0 \to D_s^+ 3\pi)}{Br(B^0 \to D^- 3\pi)} = 0.271 \pm 0.025(Stat) \pm 0.021(Syst) \pm 0.037(BR)$$

Using the PDG 2006 value for $f_s/f_d = 0.259 \pm 0.038$ we obtain

$$\frac{Br(B_s^0 \to D_s^+ 3\pi)}{Br(B^0 \to D^- 3\pi)} = 1.05 \pm 0.10(Stat) \pm 0.08(Syst) \pm 0.15(f_s/f_d) \pm 0.14(BR)$$

This analysis is a technical prerequisite to a more challenging measurement of $\frac{Br(B_s \to D_s^+ D_s^-)}{Br(B^0 \to D_s^+ D^-)}$ with the same decay channels for charm mesons.

1 Introduction

The measurement of B_s mixing, one of the flagship CDF B physics analysis in Run II, is statistically limited at the moment. Fully reconstructed $B_s \to D_s 3\pi$ provide a good addition to the B_s sample reconstructed with the other hadronic modes [17] and capable to improve the sencitivity of B_s mixing measurement.

The $B_s^0 \to \ D_s^+ 3\pi$ measurement is also a technical prerequisite to a more challenging observation and measurement of $B_s \to D_s^+ D_s^-$. $B_s \to D_s^+ D_s^-$ has a pure CP even final state and $B_s \to D_s^{(*)+} D_s^{(*)-}$ has a predominantly CP even final state. These modes are the major contributors to the phase-space difference between the even and the odd B_s decay channels. Measuring the total branching fraction of double charm B_s decays should give a handle to estimate $\frac{\Delta\Gamma}{\Gamma}$.

$B_s \to D_s^+ D_s^-$ measurement is difficult due to the small branching fractions of charm meson decays available for full hadronic reconstruction. Our estimate is that with the current data sample of $355 pb^{-1}$ we will be able to see significant $B_s \to D_s^+ D_s^-$ signal only combining two hadronic trigger paths and several D_s decay modes.

To test our tools we use similar but more populated modes. To suppress systematics we study ratios of branching fractions. Several of them will give us a good case to test and tune our techniques.

$$\frac{Br(B_s^0 \to \ D_s^+ 3\pi)}{Br(B^0 \to \ D^- 3\pi)}, \quad (D_s^+ \to \phi\pi(3\pi, K^* K), D^+ \to K\pi\pi) \tag{1}$$

$$\frac{Br(B^0 \to \ D_s^+ D^-)}{Br(B^0 \to \ D^- 3\pi)}, \quad (D_s^+ \to \phi\pi(3\pi, K^* K), D^+ \to K\pi\pi) \tag{2}$$

$$\frac{Br(B_s \to D_s^+ D_s^-)}{Br(B^0 \to \ D_s^+ D^-)}, \quad (D_s^+ \to \phi\pi(3\pi, K^* K), D^+ \to K\pi\pi) \tag{3}$$

All the listed decay modes have six tracks in the final state and share similar topology with two secondary resonances decaying into three tracks each. In $B_s^0 \to \ D_s^+ 3\pi$ and $B^0 \to \ D^- 3\pi$ stand-alone pions are predominantly coming from a_1 decay treated in reconstruction as a resonance with no lifetime. Using the same D_s and D^+ decay modes for all B decays allows to optimize reconstruction and reduce systematics.

This setup provides a lot of possibilities for crosschecks and additional studies. The analysis described in this note measures the first ratio. Second ratio is measured in [3]. The study of the third ratio will finish the sequence.

This note is an update of the measurement done with $243 pb^{-1}$ [1]. Below is the elaborate list of changes with respect to the previous analysis:

- $355 pb^{-1}$ luminosity compared to $243 pb^{-1}$ used before increase statistics by $\approx 50\%$.

- LOWPT triggers add $\approx 40\%$ statistics.
- $D_s \to K^*K$ and $D_s \to \pi\pi\pi$ modes add $\approx 80\%$ signal statistics. The addition of the two modes does not dramatically reduce the error of the measurement because of the high combinatorial and physics background for these modes. Nevertheless studying those modes adds an indepedent crosscheck and makes the analysis more complete.
- L00 hits are kept improving signal reconstruction.
- Monte Carlo version 5.3.4 is replacing version 5.3.3 providing better agreement with data with lower systematics.
- Several physics background were revealed since last winter and added to the analysis.
- New 2005 PDG values were used for calculations.

2 Data Samples and NTuple Production

2.1 Datasets and Run Ranges

We used `xbhd0d` hadronic dataset produced from data collected with Two Track Triggers. Hadronic modes were reconstructed using data passed `B_CHARM` and `LOWPT` trigger paths. We used a standard most up to date good run list recommended by BPAK group. It contains 1348 runs with the last run number 186598 and total luminosity of $355pb^{-1}$. The runlist was enforced on data and was used to generate realistic Monte Carlo.

2.2 Preparing Tracks for the Analysis.

We use the standard analysis recommendations from the B Group [4] for a non-lifetime analysis. Tracks were refit with the addition of L00 hits. This feature was not implemented in Monte Carlo and required additional tuning. The most up-to-date energy loss corrections, magnetic field scaling and COT covariance matrix scaling are applied. We use alignment "pass 17" to properly position silicon hits. Several track quality cuts were applied.

- At least 3 SVX r-ϕ hits.
- COT parent with 10 axial and 10 stereo hits.
- Track transfer momentum greater than 350 MeV.

This analysis does not reconstruct the Primary Vertex (PV) on an event-by-event basis. For all modes, the beamline coordinates at the z position of each candidate vertex are taken as the PV.

2.3 Vertex Fits and General Pre-Selection Cuts

Candidates for each decay are reconstructed from the bottom up in the Ntuple-Maker. For $B_s^+ \to D_s^+ 3\pi, D_s \to \phi\pi$ we start with a $\phi \to KK$. We combine two tracks and apply loose cuts followed by a vertex fit. We use ϕ candidate to make D_s^+ candidates by adding another track.

Triple pion combinations are formed from all eligible tracks and fitted to have a common origin using the standard vertex fit. Vertex quality requirements are applied on these vertices. In addition, a loose invariant mass cut allows for significant reduction of otherwise overwhelming combinatorics from random tracks in the event. For a triple pion combination to come from a B meson in $B \to D3\pi$ decay, it has to have an invariant mass no larger than $m_B - m_D$.

This procedure is done for each event and all reconstructed intermediate particles are stored in the separate collections. To reconstruct $B^0 \to D^+ 3\pi$ we run over D_s and 3π collections, and apply 6-track vertex fit on all eligible combinations.

There are cuts which applied at intermediate stages of the reconstruction. The sequence of cuts is optimized to reduce the computation time and disk usage. The typical order of cuts is

- Candidates with the same track content and assignment are removed.
- Candidates with wrong charge are removed. I some cases we store the "*Wrong Charge*" events for background studies.
- Two on-line trigger tracks are required for B candidates. No trigger track requirements for D candidates.
- The raw mass is calculated based on the track momenta (fully prepared track) and candidates are only accepted within a loose mass window.
- In some cases with particularly bad combinatorics fast linearized fit is performed. Loose cut on χ^2 of a linearized fit is applied.
- A loose mass window (± 100 MeV) is applied to D-meson candidates. After that D-meson masses are constrained to their PDG values while fitting the parent B candidate.
- A full vertex fit is performed and the resulting $\chi^2_{R\phi}$, the fitted mass and the L_{xy} are used to reject candidates. Cuts are only applied at this stage if tighter cuts are applied later in the analysis.

Here we have to mention the existence of self-reflections produced by swapping candidate tracks. Swaps which do not change particle assignment are dropped during the STNTuple production. Swaps which do change particle hypothesis (kaon to pion or vice versa) are left in the sample and may contribute to the signal. The systematics due to this effect is discussed in section 8.6.

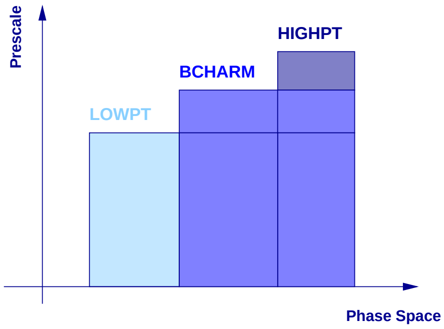

Figure 1: Picture representation of hadronic trigger paths. Visualization of the generalized triggers selection requirements (phase space) versus the effective trigger prescale.

2.4 Trigger Confirmation

In this analysis `B_CHARM` and `LOWPT` trigger paths are used.

Each B candidate is required to have a trigger pair. Trigger is confirmed for every event and for each candidate in the event. For event we check trigger bit information. For `B_CHARM` sample we take events with one of the following trigger bits set.

- `L3_B_CHARM`
- `L3_B_CHARM_L1_SEVEN_TRK2`
- `L3_B_CHARM_L1_DPS`
- `L3_B_CHARM_L1_UPS`
- `L3_B_CHARM_L1_FPS`

For `LOWPT` sample we take events with one of the following trigger bits

- `L3_B_CHARM_LOWPT`
- `L3_B_CHARM_LOWPT_L1_SEVEN_TRK2`
- `L3_B_CHARM_LOWPT_L1_DPS`
- `L3_B_CHARM_LOWPT_L1_UPS`
- `L3_B_CHARM_LOWPT_L1_FPS`

In addition to the trigger bit confirmation for event we do SVT matching for each candidate. We follow the procedure described in [5]. The SVT matching algorithm is based on the svtsim [6] package.

To promote a track to being an *on-line trigger track* we require the p_T and d_0 as stored in the SVTD bank to comply with: $p_T > 2$ GeV and 0.0120 cm $< |d_0| < 0.1$ cm.

The such determined on-line trigger tracks are confirmed and stored to make various pair trigger decisions. Later in the analysis we require candidates from `B_CHARM` sample to pass `B_CHARM` trigger confirmation and candidate from `LOWPT` sample to pass `LOWPT` trigger confirmation.

3 Monte Carlo Simulation

We have several applications for Monte Carlo in this analysis.

- cut optimization
- templates for signal and reflections
- efficiency study

There are several components in the simulation.

- quark production mechanism
- fragmentation
- b hadron decay
- decay branching fractions
- good run list selection
- description of the trigger
- description of the reconstructed quantities

The first four issues require input from theory and other experiments. The last three are related to CDF experiment.

3.1 B Hadron Generation and Decay

This analysis deals with an exclusive reconstruction and a clean signal. No cuts were applied which would require knowledge of the underlying event structure and no systematics from the background tracks is expected. Therefore we simplify our task by simulating B mesons only.

We use BGenerator [7] to create B mesons. It is based on NLO calculations [8] and the fragmentation is implemented using the Peterson fragmentation function [9]. BGenerator only produces B mesons, no fragmentation products are present. For the B meson decays we use EvtGen package [10].

There is a descrepancy between the Monte Carlo generated transverse momentum spectrum of the B mesons and the spectrum seen in data. In this analysis we used the default spectrum which produces better agreement between data and Monte Carlo for our modes. The systematic due to the difference is described in section 8.3.

The decay tables used to generate Monte Carlo are quoted (table 3 and 5). We found out that Monte Carlo description of the subresonance structure of the three-pion in $B^0 \rightarrow D^- 3\pi$ does not agree with data. We had to use the most recent knowledge from BaBar [11] along with our own studies to update our decay table 21. A possible systematics due to the decay table is discussed in section 8.5

3.2 Realistic Simulation

To reflect time dependent changes in the detector condition and trigger tables we developed a realistic Monte Carlo [12]. Run to run changes include the parameters of the triggers at `Level1` and `Level2`, the position of the beam line, the silicon detector conditions and the alignment. We generate Monte Carlo for each run from a good run list recommended by BPAK group. The number of generated events is proportional to run luminosity.

Monte Carlo misses a few runs with a total luminosity of about $30pb^{-1}$. A short summary of the missed runs is given in the table 2 We use these runs for our analysis assuming that reconstruction efficiency for candidates behaves similarly. The study of this effect for more populated modes $B_s \rightarrow D_s\pi$ and $B^0 \rightarrow D^+\pi$ is described in the systematic chapter in [18]. It was found that the ratio of reconstruction efficiencies for B^0 and B_s does not depend on run number.

The generation of the events is done with `BGenerator` [7]. The generation, decay and `GEANT` simulation of the detector response are done using the 5.3.4 version of `cdfSim`. The response of the trigger simulation is done using the `TRGSim++` executable as available with the 5.3.4 release of CDF software. The production executable used is the `ProductionExe` as available from the 5.3.4 release. The trigger decision is simulated using the `TRGSim++` executable of the realistic trigger simulation package. This executable confirms cuts equivalent to those for the trigger paths at L2 on the `SVTD_StorableBank` information available in the event record.

To confirm trigger in Monte Carlo we use exactly the same procedure we apply to data (section 2.4). The only difference is that we have to use `Level2` trigger bits instead of `Level3` bits to confirm trigger for the event (for example `L2_B_CHARM` instead of `L3_B_CHARM`). SVT matching procedure used to confirm trigger for candidate is the same.

`B_CHARM` and `LOWPT` triggers are prescaled. The prescale factor is run dependent and have to be accounted for. We read the number of events before and after prescale from the database and find an average prescale value for each trigger path for each run. If there are several triggers of the same type in the run (for example `L3_B_CHARM` and `L3_B_CHARM_L1_SEVEN_TRK2`) we combine the number of events to calculate `B_CHARM` "effective prescale". Effective prescale is always equal or less than one.

In our realistic Monte Carlo number of generated events is proportional to run luminosity. To add prescale to the simulation a rundom number between 0 and 1 is generated. The event is passed if random number is smaller than the effective prescale for the generated run. The run dependent prescale profiles are shown on figure 4. Our experience with data shows that treating prescale run by run is enough to achive good agreement for the relative `B_CHARM` and

LOWPT yields. Treating luminosity on a section level is not nesessary for our statistics.

3.3 Comparing Data and Monte Carlo

We performed a detailed comparison of the Monte Carlo simulation with data. For this purpose we used our most populated channel $B^0 \to D^- 3\pi$. For sideband subtractions we used area equivalent to 2 normal deviations under the signal and only right sideband with clean combinatorial background as shown on figure 6.

Before making comparison we run Monte Carlo and data through several preparation steps.

- Monte Carlo and data samples are divided into B_CHARM and LOWPT subsamples confirming trigger for event and for candidate.
- Run by run prescale is aplied to Monte Carlo.
- B_CHARM and LOWPT combined together for data and Monte Carlo. If there are duplicate events than B_CHARM event is taken.

We made a dedicated comparison for single track values: transverse momentum, radial angle, impact parameter, rapidity and number of silicon hits. Data for all 6 candidate tracks was combined into one histogram to improve statistics.

To check the validity of the underlying theory, production and fragmentation it is sufficient to study track p_T and η distributions (figure 7 and figure 8 on the left). Zoom-in into the low momentum region (figure 7 on the right) shows good agreement as well. Comparing impact parameter of the track (figure 9 on the left), radial angle (figure 8 on the right) and number of silicon hits (figure 9 on the right) we validated the performance of the trigger and tracking algorythms.

While comparing distributions of cut variables we set the relevant cuts to looser values (figures 10, 11 and 13). The default cut value is marked with vertical gray line.

One of the difficulties we faced with $B^0 \to D^- 3\pi$ Monte Carlo is to reproduce 3-pion mass spectrum. Even with tuned decay table (table 21) based on recent BaBar paper [11] combined with our own study discussed in section 8.5 Monte Carlo 3π invariant mass distribution does not reproduce low energy turn-on in data.

Figure 14 on the left shows the comparison for the 3-pion invariant mass. The wide resonance of a_1 is shifted toward the higher mass values. It could be due to the incomplete knowledge of a_1 decay structure or poor description of a_1 Breit-Wigner shape in Monte Carlo. The shape of the contribution from non-resonant component agrees better. The spike of $D_s \to \pi\pi\pi$ is clearly visible in data. The size of the feature agrees with the expected amount of $B^0 \to D_s^+ D^-, D_s^+ \to \pi\pi\pi$ contribution estimated from double charm reconstruction [3] (figure 61 on the right).

The right part of figure 14 shows the invariant mass of 2 pions (out of 3). To make this plot from two possible combinations of 2 pions with total charge zero we take the one which is heavier. As expected the distribution shows a good ρ resonance. Small resonance near 1.3GeV in data may probably be $f_2(1270)$.

Figure 18 shows the transverse momentum of the 3π treated as a resonance on the left. The opening angle of such a resonance with respect to B is shown on the right. A good agreement of these kinematic variables for 3π gives an extra footing to our tuned decay file (section 8.5).

Complicated 3-pion subresonance structure could be a topic for a separate study. In this note we only estimate the systematic related to this issue (section 8.5).

3.4 L00 hits.

For this analysis we used `STNtuple` produced using `L00` silicon hits. We used hit smearing module [13] to correct `L00` hits efficiency and resolution. The module does the following.

- Loops over the hit list in the beginning of the event.
- Smears `L0` and `L00` MC hits to achieve a resolution measured on data
- Randomly drops a proportion of `L00` hits to correct for Monte Carlo overefficiency
- Proceed with track refitting

Monte Carlo distributions of affected values agree with data. Number of silicon hits per track is shown on figure 9 on the left. 2-dimensional χ^2 of the B-meson is shown on figure 11 on the left. L_{xy} error of the B-meson is shown on figure 19.

3.5 Efficiencies extracted from the Monte Carlo

For $B^0 \rightarrow D^- 3\pi$ we generated 60×10^6 signal events with decay file quoted in table 3. We apply detector simulation, trigger, reconstruction, run by run prescale the way it is described in the previous sections.

For $B_s^0 \rightarrow D_s^+ 3\pi$ we generated 60×10^6 events of combined sample with 3 different D_s^+ decay modes table (5). We scaled their relative ratios with the best knowledge of branching fractions from PDG to ease the study of cross talks between the modes. This Monte Carlo is used for $B_s^0 \rightarrow D_s^+ 3\pi, D_s \rightarrow K^* K$ and $B_s^0 \rightarrow D_s^+ 3\pi, D_s \rightarrow \pi\pi\pi$. For $B_s^0 \rightarrow D_s^+ 3\pi, D_s \rightarrow \phi\pi$ we use a dedicated signal Monte Carlo with 60×10^6 events.

To get a number of events we fit signal Monte Carlo with double Gaussian and integrate the region containing 95.45% of the signal. Fit parameters are saved to use for signal template. All the fits are shown on figures 30, 31, 32, 33. The final yield numbers used to calculate efficiencies are summarized in table 15.

4 Cut Optimization

We used several guidelines to choose our analysis cuts.

- Cut should have non trivial separation power between signal and background. The top plots on figures 10, 11 and 13 compares data sideband and signal Monte Carlo. It gives intuition about the separation power of the cuts we use.

- Cut should be unique (uncorrelated). It should reduce background unreachable by other cuts.

- We constrained ourselves by using signal Monte Carlo only therefore we can not use cuts which rely on the structure of underlying event i.e. any kind of isolation cuts.

The final values are chosen with a help of optimization procedure. It requires a lot of repetitive runs over data. To reduce the size of the input file and speed up the process we apply a set of loose cuts before the optimization (table 7). For optimization we only use sideband on the right from the signal (figure 6) to avoid bias from misreconstructed decays present in the left sideband.

For B^0 we use [5.2 to 6.0] GeV mass window, for B_s we use [5.3 to 6.5] GeVmass window. We deliberately decided to optimize only with respect to combinatorial background to avoid bias with unknown systematics. We fit mass distribution with a sum of flat and exponent omitting the signal region. Monte Carlo effective signal width is used to estimate the extent of the blind region and the width of the signal used for significance calculations. The mass of the signal is shifted by -4.85MeV inline with the estimated difference between data and Monte Carlo.

The process is iterative. It was started with values taken from the similar analysis [5]. Each cut was varied in reasonable limits. While one cut was varied the others were fixed to default values. In the beginning, procedure applies default cuts to Monte Carlo and scales Monte Carlo yield to the provided expected number of signal candidates. The step by step algorithm is described below.

1. Get default cut values and variation windows

2. Get the expected signal yield with default cuts

3. Fit MC signal with default cuts

4. Scale MC to the provided signal yield

    (a) Change one cut while fixing the others at default values
    (b) Fit scaled MC signal, get the effective width
    (c) Chose blind region as $\pm 3\sigma$ of MC signal effective width
    (d) Fit data with background function omitting the blind region
    (e) Integrate data background within $\pm 2.0\sigma$ signal region (the effective width is taken from MC and corrected by $2.0MeV$, mean value is shifted by -4.85MeV)
    (f) Integrate scaled MC signal in $\pm 2.0\sigma$ region

(g) Save $\frac{SignalMC}{\sqrt{SignalMC+BGData}}$

(h) Go to next cut value

(i) If done with the cut go to next cut

(j) If done with all the cuts, - print results

5. The default cuts and variation windows are changed according to results

6. The procedure is started from the beginning

While running procedure shows a dynamic fit for visual quality check (figure 20). As an output it gives the efficiency and significance curves as functions of cut value for every optimized cut. Figures 21 and 22 show the significance and efficiency curves for $B^0 \to D^- 3\pi$, figures 23 and 24 show the significance and efficiency curves for $B_s^0 \to D_s^+ 3\pi, D_s \to \phi\pi$, figures 25 and 26 show the significance and efficiency curves for $B_s^0 \to D_s^+ 3\pi, D_s \to K^* K$, figures 27 and 28 show the significance and efficiency curves for $B_s^0 \to D_s^+ 3\pi, D_s \to \pi\pi\pi$.

Procedure usually takes several iterations to converge. The final values for cuts were guidelined by efficiency and significance curves. We usually chose to cut at the maximum of the significance. If the significance distribution had a plato the cut was set to the value at the beginning of the plato. The final results are summarized in tables 8 and 9.

The optimization was done on `B_CHARM` and `LOWPT` samples prescaled and combined the way it is described in section 3. Despite the fact that the same analysis cuts were applied to `B_CHARM` and `LOWPT` samples the implicit online trigger cuts and offline trigger confirmation cuts were different.

5 Templates for Signal and Background.

The background fitting model affects the quality of the total fit and may significantly change the estimated signal. Earlier analysis [5] shows that fitting model gives one of the largest inputs into systematics. The fit finction for every mode consist of three major parts.

- **Signal** - sharp resonant peak at B^0 or B_s mass with width defined by detector and reconstruction resolution.
- **Combinatorial background** - a smooth featureless background due to the accidental combinations of the tracks from underlying event happened to pass the analysis cuts.
- **Physics background** - a spiky background with a lot of features due to the incomplete or incorrect reconstruction of the decays similar to signal in mass, decay content and topology.

In this analysis a good part of the effort was spent to identify and estimate physics backgrounds. We were able to single out several decay modes providing a significant contribution to the background within the fit window. For these modes a dedicated Monte Carlo samples were generated to create fitting templates. The rest of the physics backgrounds were studied with the help of *"semi-generic"* Monte Carlo. For example to study physics backgrounds for $B^0 \to D^-3\pi$, $D^- \to K^+\pi^-\pi^-$ a semi-generic Monte Carlo $B \to D^-X$ was generated. Here B stands for the combination of B_d, B_u and B_s mesons, X - stands for "anything" and D^--meson is forced to decay to $K^+\pi^-\pi^-$.

5.1 Signal Templates.

B^0 signal Monte Carlo predominantly consist of $B^0 \to D^+a_1, D^+ \to K\pi\pi, a_1 \to \pi\pi\pi$ (table 3). The estimate of the systematic error due to the sample composition is done in section 8.5.

In B_s signal Monte Carlo 3π subresonance structure was defined to be the same (table 5). Different D_s modes were scaled with respect to each other by using the best PDG knowledge. This was done to simplify the estimate of the cross talk between the modes. $D_s \to \pi\pi\pi$ subresonance breakdown is also not well established. The estimate of the systematic error due to the sample composition is described in section 8.5.

We use multiple Gaussians to fit our signals. $B^0 \to D^-3\pi$ signal is fitted with triple Gaussian and $B_s^0 \to D_s^+3\pi$ is fitted with double Gaussian.

$$f_{Sig} = f_1\mathcal{G}(m|\mu_1\sigma_1) + (1-f_1)\mathcal{G}(m|\mu_2\sigma_2) \tag{4}$$

The Gaussians within one template were constrained to have a common mean value. The ratios of their norms and widths were fixed from Monte Carlo. The yield was integrated using the *effective width* - the window containing 95.45% of the signal.

The width and mass of the signal is not well described by Monte Carlo. By using the high statistics $B^0 \to D^-3\pi$ mode we measured the difference of the signal shape in data and Monte Carlo. The signal fit parameters are summarized in table 12. Followig this table the widths of the signal Gaussians for all the modes were corected by $17 \pm 3\%$. The mass templates for $B^0 \to D^-3\pi$ fit were shifted by $-4.8MeV$.

$B_s^0 \to D_s^+3\pi$ modes have about a hundred events each and fit values, if left free, fluctuate significantly due to the low statistics. To avoid it only norm and mass of the signal were left floating while fitting B_s modes. Fit systematics is estimated in section 8.7.

5.2 Background Templates $B^0 \to D^+\pi\pi\pi$.

$B^0 \to D^-3\pi$ background fitting function consist of combinatorial background and physics background. For the combinatorial background we use the sum of a flat shape and an exponent.

$$f_{Comb} = f_1 exp(m|\mu\tau) + f_2 \tag{5}$$

To derive the shape we used a reconstruction of $B^0 \to D^-3\pi$ with wrong charge correlation between D^+-meson and kaon in $D^- \to K^+\pi^-\pi^+$ decay. Wrong charge data sample still has a small reflection of B^0 mass peak. We used a linear combination of right charge and wrong charge plots to eliminate the presence of signal. Fitted in wider interval from 4.5 to 6.5GeV fitting hypothesis shows a good agreement with data (figure 29).

Physics background includes modes similar to signal with misreconstructed decay products. Lost neutrals or extra tracks and wrong mass assignments represent a majority of the physics background sometimes called reflections. We were able to single out several modes with a significant contribution to the fitted region:

- Cabibo suppressed modes with kaon reconstructed as pion
- $B^0 \to D^{*-}3\pi$ modes with lost π_0 from $D^* \to D^+\pi^0$
- $\Lambda_b \to \Lambda_c 3\pi, \Lambda_c \to pK\pi$ with proton reconstructed as pion
- $B_s^0 \to D_s^+ 3\pi, D_s \to K^* K$ with kaon reconstructed as pion

The task of generating a truly generic Monte Carlo is very resource consuming. For some of the most significant reflections a dedicated Monte Carlo samples were generated. The rest of the backgrounds were generated as a part of *"semi-generic"* Monte Carlo. For $B^0 \to D^- 3\pi$ mode we generated a semi-generic Monte Carlo $B^0 \to D^- X$, where the D^- was forced to decay to $K^+\pi^-\pi^-$. Figure 34 shows decomposition of the semi-generic Monte Carlo into several statistically significant parts. Below all the mentioned reflections and templates for them are reviewed in details.

- The double horn structure near 5.1GeV is due to $D^{*-}3\pi$ decays where π^0 or γ from $D^{*-} \to D^-\gamma(\pi^0)$ is lost. We generated dedicated Monte Carlo with 10 times more statistics compare to our data sample. Table 4 shows the decay file. For 3π composition we only consider a_1 and $\rho\pi$ hypothesis. The reflections of these two modes are different in shape and current data sample is big enough to distinguish them. The shape of each mode is well described with a sum of 4 Gaussians (figure36).

  In this analysis we are not very concerned about particular shape and origin of physics background as long as it is well reproduced by Monte Carlo. As a side note we may speculate that double-horn structure is the result of $B \to D^* 3\pi$ decay followed by $D^{*+} \to D^+\pi^0$ where D^* is partially polarized. As a result, the angle between the π^0 and the D^* momentum follows $cos^2(\theta)$ law. Most of the time, pion will be released either in the direction of D^* momentum, or in the opposite direction. At the same time D^+ tends to continue collinear to D^*. Depending on whether the pion was released forward or backward with respect to the D^* momentum, the reconstructed B mass ends up in one of the two horns.

- Analysis [5] confirmed a 5% presence of Cabibo supressed $B \to D^+K$ in $B \to D^+\pi$. We also expect to see Cabibo suppressed modes for $B^0 \to D^- 3\pi$. Since none of them are properly studied yet we use our best guess to estimate their input. We built our Cabibo decay table using analogy with the signal modes substituting one d quark with s quark. It gives us $K\pi\pi$ for $\pi\pi\pi$, ρK for $\rho\pi$ and K_1 for a_1 (Table 4). We found out that the shape of the reconstructed mass distribution does not significantly depend on the composition of the sample. In section 8.7 we did additional studies for systematics due to poorly known Cabibo branching and composition. Cabibo shapes are shown on figure 38. They are fitted with Breit-Wigner distribution smeared with Gaussian and multiplied by a plateau formed by two Error functions.

$$f_{Cab} = (\mathcal{G}(m|\mu_1\sigma_1) \otimes \mathcal{B}(m|\mu_1\Gamma)) \cdot erf(m|\mu_2\sigma_2) \cdot erf(m|\mu_3\sigma_3) \tag{6}$$

- $\Lambda_b \to \Lambda_c 3\pi, \Lambda_c \to pK\pi$ with proton misreconstructed as pion ends up partially under the signal. It is fitted with function 6.
- From the semi-generic $D^+ \to K\pi\pi$ background we remove Cabibo suppressed modes and $B^0 \to D^{*-}3\pi$ modes since we create a separate templates for them. The rest is fitted with sum of the linear and a reverse exponent (figure 35 on the left).

$$f_{SG} = N_{SG}((\mu_{01} - f_{01}m) + (\mu_{02} - f_{02}m)(1 - exp(m|\mu_1\tau_1)) + (\mu_{03} - f_{03}m)(1 - exp(m|\mu_2\tau_2))) \tag{7}$$

  Linear turn-on corresponds to decays with the same stable content but lost γ. Exponential turn-ons at around 5.14 GeV correspond to misreconstructed modes with one lost pion.
- $B_s^0 \to D_s^+ 3\pi$ with kaon from $D_s \to KK\pi$ misreconstructed as pion forms a narrow peak under the signal. To model this reflection we used semi-generic $D_s X$ Monte Carlo where $D_s \to \phi\pi(K^*K, 3\pi)$ (figure 35 on the right). 80% of the contribution to this reflection structure is coming from $D_s \to K^*K$ subresonance. It is fitted with a sum of the linear and two reverse exponents. Several gaussians are thrown in to account for spikes. The contribution of this template is much smaller compared to the contribution of the semi-generic $D^+ \to K\pi\pi$. It does not change the signal yield significantly and only added for completeness.
- $B^0 \to D_s^+ D^-$ with $D_s \to 3\pi$ has the same final state as our signal. This decay goes through $b \to ccs$ transition and should be separated from bulk of the decaus which go through $b \to cud$. Template for this mode is fitted with one Gaussian. (figure 35

When full data fit is performed most of the parameters are fixed and only norms of some of the reflections are left floating. The detailed description of the fitting process is given in section 6

5.3 Background templates $B_s^0 \to D_s^+ 3\pi$.

We use the same approach for $B_s^0 \to D_s^+ 3\pi$. Background fitting function is divided into combinatorial background and physics background. 3 different sets of templates are created for 3 modes. We use the sum of the flat and exponent (function 5) for the combinatorial background. Among physics background several modes required a dedicated study.

- Cabibo suppressed modes with kaon reconstructed as pion
- $B_s \to D_s^{*-}3\pi$ modes with lost π_0 from $D^* \to D^+\pi^0$
- $\Lambda_b \to \Lambda_c 3\pi, \Lambda_c \to pK\pi$ with proton reconstructed as pion ($D_s \to K^*K$ only)
- $B^0 \to D^- 3\pi$ with pion reconstructed as kaon ($D_s \to K^*K$ only)
- Reflection from semi-generic $D^+ \to K\pi\pi$ ($D_s \to K^*K$ only)
- Reflection from semi-generic $D^0 \to K\pi$ ($D_s \to K^*K$ only)

We generate three *"semi-generic"* Monte Carlos for $B_s^0 \to D_s^- X$ for three D_s decays: $D_s \to \phi\pi$, $D_s^- \to K^*K$ and $D_s^- \to \pi\pi\pi$. Figures 39 40 and 41 show decomposition of the semi-generic Monte Carlos into several statistically significant parts. Below all the mentioned reflections and templates for them are reviewed in details.

- For each D_s mode we generated a separate Monte Carlo to study $B_s \to D_s^* 3\pi$ where $D_s^* \to D_s\pi^0(\gamma)$. Table 6 shows the decay file. From all the 3π sub-resonances we only use a_1 for the template assuming that it dominates 3π by analogy with $B^0 \to D^{*+}3\pi$. The dedicated systematic study of this assumption is described in section 8.5. Figures 42, 43 and 44 show the templates for tree D_s modes. They are fitted with function 6.

- To generate Cabibo suppressed modes for $B_s^0 \to D_s^+ 3\pi$ we used the approach similar to $B^0 \to D^- 3\pi$ substituting particles with s quark instead of particles with d quark in the decay table. The substitute gives $K\pi\pi$ for $\pi\pi\pi$, ρK for $\rho\pi$ and K_1 for a_1. $B^0 \to D_s^+ D^-$ mode is added as a known contributor (table 6). The shape of the template does not significantly depend on the sample composition. The distributions are fitted with function 6. Fit is shown on figures 42, 43 and 44.

- $B_s^0 \to D_s^+ 3\pi, D_s \to \phi\pi$ has a noticable contribution from $D_s \to f_0\pi, f_0 \to KK$ (table 19) founded by [15] based on Dialitz analysis of 701 D_s decays. We fit it with the simple Gaussian and correct the width by $2.0 MeV$.

- $B_s^0 \to D_s^+ 3\pi, D_s \to K^*K$ has a big contribution from $B^0 \to D^- 3\pi$ with one pion reconstructed as a kaon. In $B_s^0 \to D_s^+ 3\pi, D_s \to \phi\pi$ this contribution is negligible due to the narrow ϕ mass window. The reflection is fitted with four Gaussians (figure 46).

- $B_s^0 \to D_s^+ 3\pi, D_s \to K^*K$ has a contribution from non resonant $D_s^+ \to KK\pi$. $B_s^0 \to D_s^+ 3\pi, D_s \to \phi\pi$ is much less affected by this reflection because of the narrow ϕ mass window. The contribution from this mode goes under the signal since its particle content is identical to K^*K. We have to remove it to use $D_s \to K^*K$ branching fraction in our calculations. We fit it with a Gaussian and correct its width by $2.0 MeV$.

- $B_s^0 \to D_s^+ 3\pi, D_s \to K^*K$ also has a big contribution from $\Lambda_b \to \Lambda_c 3\pi, \Lambda_c \to pK\pi$. It is fitted with function 6 (figure 46).

- $B_s^0 \to D_s^+ 3\pi, D_s \to K^* K$ reconstruction contains reflections from the B modes decaying by $D^+ \to K\pi\pi$ and $D^0 \to K\pi$. When pion is reconstructed as kaon the mass of the candidate moves to the right. It makes a noticeable contribution under the signal (figure 45). The reflection is fitted with function 7.

- From the semi-generic $D_s \to \phi\pi(K^* K, 3\pi)$ background we remove Cabibo suppressed modes and $B_s \to D_s^* 3\pi$ modes. The rest is fitted with sum of the linear and two reverse exponents (figures 39, 39 and 39). Linear turn-on corresponds to similar decays with lost γ. Two exponential turn-ons correspond to misreconstructed modes with one or two lost pions.

When fit is performed most of the template parameters are fixed. Some normalizations are left floating, some are fixed to values estimated from our best knowledge. The detailed description of the fitting process is given in section 6

6 General Fit Model

Every fit consist of several templates. The shapes of the templates are fixed and only normalization is left floating. Normalizations of low-statistics templates are fixed to the estimated values. Table 13) shows the summary of the normalization parameters. Entry *"free"* in this table means that the normalization parameter for the template is floating (the rest of the template parameters are still fixed). For some of the fixed templates table shows the ratio of the template to the signal in percents. For those cases when data was used to scale Monte Carlo table shows the expected count of the events in plain numbers. Mass parameters of all the templates are corrected by -4.8MeV - the mass difference between data and Monte Carlo measured from $B^0 \to D^- 3\pi$ signal.

All fits have several common backgrounds which are treated identically.

- **Combinatorial background** is fitted with a linear combination of flat and exponent (function 5). All 3 parameters are left floating: normalization and slope for exponent and normalization for flat.

- **Semi-Generic Background** has different source but similar shape in all the modes. It is fitted with function 7 for every mode. Only normalization is left floating in data fit. All the mass parameters are corrected by -4.8MeV.

- **Cabibo** contribution has similar shape and functional representation for all four modes. It is fitted with function 6. All mass parameters are corrected by -4.8MeV. To calculate the relative norm of the Cabibo suppressed mode we used current measurement for $B^0 \to D^+\pi$ and $B^0 \to D^+ K$ branchings quoted in table 18. The reconstruction efficiency for Cabibo mode is summarized in table 16. We found that Cabibo contribution should be $6.9\% \pm 2\%$ of the signal and used this number for all three-pion modes in this analysis.

The rest of the tempaltes differ from mode to mode. Most of the parameters of the templates were fixed. Overall normalizations of the templates were treated depending on the statistics of the reflectiong mode and our knowledge about it.

- Normalization was left free for the high statistics reflections like $B^0 \to D^{*+}3\pi$
- Normalization was fixed with respect to the signal yield for low statistics reflections with known branching fraction ($\Lambda_b \to \Lambda_c 3\pi$)
- Normalization was fixed to absolute number for low statistics reflection with a yield of reflecting mode measured in one of our analysis on the same dataset ($B^0 \to D_s^+ D^-$)

I several subsections below the choice of the normalization strategy is described in details for every template.

6.1 Features of $B^0 \to D^- 3\pi$ Fit Model.

To fit our $B^0 \to D^- 3\pi$ signal we used templates described in section 5.

- **Signal** is fitted with triple Gaussian with common mass. The ratios for the norms and widths are fixed from Monte Carlo. 3 parameters are left floating: width and norm of the narrowest Gaussian and common mass.
- $D^{*+}a_1$ template has 4 Gaussians. Only overall norm is set free in the final fit.
- $D^{*+}\rho\pi$ template has 4 Gaussians. Only overall norm is set free in the final fit.
- $\Lambda_b \to \Lambda_c 3\pi, \Lambda_c \to pK\pi$ contribution is fitted with Breit-Wigner (function 6). All the mass parameters are corrected by -4.8MeV. The norm is fixed to $3\% \pm 1\%$ with respect to B^0 signal. To calculate norm we used measurement of $f_\Lambda/f_d \times \Lambda_b \to \Lambda_c\pi/B^0 \to D\pi$ by CDF [14]. We assumed the same ratio for the modes with tree pions in the final state. Efficiency of reconstruction is measured from Monte Carlo and listed in table 16. We also used known branching fractions quoted in table 18.
- $B_s^0 \to D_s^+ 3\pi$ reflection where $D_s \to KK\pi$ is fitted together with the rest of semi-generic $D_s \to \phi\pi(K^*K, 3\pi)$. We were able to scale Monte Carlo yield with respect to data by using fully reconstructed signal modes $B_s \to D_s 3\pi, D_s \to \phi\pi(K^*K, 3\pi)$. The reconstructed reflections of three modes were scaled down, summed up and fitted together (figure 35). About 2/3 of the reflection is coming from $D_s \to K^*K$. The template changes signal yield by $< 1\%$. The norm of the temlate is fixed in agreement with our data yields for reflecting modes.
- $B^0 \to D_s^+ D^-$ reflection where $D_s \to \pi\pi\pi$ goes under the signal peak. We were able to scale Monte Carlo yield with respect to data by using fully reconstructed signal modes $B^0 \to D_s D^+, D_s \to 3\pi$ [3]. The template changes signal yield by $< 1\%$. The norm of the temlate is fixed in agreement with our data yields for reflecting modes.

6.2 Features of $B_s^0 \rightarrow\ D_s^+ 3\pi$ Fit Models (All D_s Channels).

- **Signal** was fitted with doule Gaussian with common mass. The ratios for the norms and widths were fixed from Monte Carlo. Only three parameters were left floating: width and norm of the narrowest Gaussian and common mass.

- $D^{*+}a_1$ template was fitted with Breit-Wigner (function 6) with different parameters for each mode. Only overall norm of this template was set free in the final fits. The fit for $B_s^0 \rightarrow\ D_s^+ 3\pi, D_s \rightarrow \pi\pi\pi$ reduced the contribution of $D^{*+}a_1$ template to zero. There is not enough statistics to make any significant statement about it.

6.3 Features of $B_s^0 \rightarrow\ D_s^+ 3\pi, D_s \rightarrow \phi\pi$ Fit Model.

- $B^0 \rightarrow\ D_s^+ D^-, D_s^+ \rightarrow \phi\pi$ reconstructed mass distributions has contribution from $D_s \rightarrow f_0\pi$. We generated a realistic Monte Carlo with the correct ratio between $D_s \rightarrow \phi\pi, \phi \rightarrow KK$ and $D_s \rightarrow f_0\pi, f_0 \rightarrow KK$ (table 19). We used $B_s^0 \rightarrow\ D_s^+ 3\pi, D_s \rightarrow \phi\pi$ signal from data to calculate the scaling factor for our Monte Carlo. This factor was used to scale norm of $D_s \rightarrow f_0\pi$ template to data yield for current luminocity. The norm of the template was fixed to $(3.5 \pm 2)\%$ of the signal in the final fit. The large error is due to the uncertainty on the branching fraction of $D_s \rightarrow f_0\pi, f_0 \rightarrow KK$ measured by [15].

6.4 Features of $B_s^0 \rightarrow\ D_s^+ 3\pi, D_s \rightarrow K^*K$ Fit Model.

- $B^0 \rightarrow\ D^- 3\pi$ reflection is fitted with four Gaussians. To calculate the norm of the reflection we used our $B^0 \rightarrow\ D^- 3\pi$ signal Monte Carlo. We calculated $B^0 \rightarrow\ D^- 3\pi$ Monte Carlo scale factor (4.513) by dividing signal Monte Carlo yield 14839 ± 122 from table 16 to the observed signal yield 3288 ± 76 from table 17). We integrated the yield of the $B^0 \rightarrow\ D^- 3\pi$ Monte Carlo reflection neglecting very small ($< 1\%$) feed from $B_s^0 \rightarrow\ D_s^+ 3\pi, D_s \rightarrow K^*K$ back to $B^0 \rightarrow\ D^- 3\pi$. The template and the integrated nomber are shown on figure 46 on the left. It has 639 events which we scaled the reflection template down to 141.5 *events*. Technically it was done by multiplying the overall norm of the template by 1/4.513. The norm of this template was fixed during the data fit. All the mass parameters of the template were corrected by -4.8MeV. All the width parameters were corrected by 17%.

- $\Lambda_b \rightarrow \Lambda_c 3\pi, \Lambda_c \rightarrow pK\pi$ contribution for this mode was calculated to be consistent with similar estimate for $B^0 \rightarrow\ D^- 3\pi$ based on resent CDF measurement [14]. It was fitted with Breit-Wigner function 6. All the mass parameters were corrected by -4.8MeV. The norm was fixed to absolute number of 20 ± 9 *events*.

- $B_s^0 \rightarrow\ D_s^+ 3\pi, D_s \rightarrow K^*K$ reconstructed mass distributions has contribution from non-resonant $D_s \rightarrow KK\pi$. We generated a realistic Monte Carlo with the known ratio between $D_s \rightarrow \phi\pi, \phi \rightarrow KK$ and non-resonant $D_s \rightarrow KK\pi$ (table 19). We used $B_s^0 \rightarrow\ D_s^+ 3\pi, D_s \rightarrow \phi\pi$ mode to calculate the scaling factor for our Monte Carlo with respect to data. This factor was used to scale norm of non-resonant $D_s \rightarrow KK\pi$

template to current data luminocity. The norm of the template was fixed to $(9 \pm 4)\%$ of the signal in the final fit. The large error is due to the uncertainty on the branching fraction of $D_s \to KK\pi$ measured by [15].

- $D^+ \to K\pi\pi$ semi-generic backgrounds was fitted with function 7. We used $B^0 \to D^- 3\pi$ mode to calculate the scaling factor for our Monte Carlo with respect to actual yield from data. Very large error on the norm covers for the limited knowledge of the content of the semi-generic Monte-Carlo. All the mass parameters were corrected by -4.8MeV. The norm was fixed.

- $D^0 \to K\pi$ semi-generic backgrounds was fitted with function 7. To calculate the norm of the template we scaled $B^+ \to D^0\pi, D^0 \to K\pi$ contributions to the actual yiled from the same luminocity data [16]. Very large error on the norm covers for the limited knowledge of the content of the semi-generic Monte-Carlo. All the mass parameters were corrected by -4.8MeV. The norm was fixed.

The final fits for all the modes for `B_CHARM` and `LOWPT` combined are shown on figures 47, 48 and 49. Magnified plots for $B^0 \to D^- 3\pi$ and $B_s^0 \to D_s^+ 3\pi, D_s \to K^*K$ show the fine structure of the background under the signal.

7 Extraction of Branching Fractions

The result of the data fit for $B^0 \to D^- 3\pi$ is shown on figure 47. The results of the data fits for three $B_s^0 \to D_s^+ 3\pi$ modes are shown on figures 48 and 49. The fit and the calculation of the binned χ^2 are done in $[4.6, 6.5]$GeV interval. To calculate binned χ^2 probability of the fit we combined adjacent low statistics bins to count at least 20 events per each binned entry. Signal yields for $B_s^0 \to D_s^+ 3\pi$ with uncertainties is summarized in table 17. Signal template is integrated to include 95.45% of the signal.

Branching fractions which were used for calculations are summarized in table 19. The ratios of different D_s branching fractions are known better than their absolute values. We use $Br(D_s \to \phi\pi, \phi \to K^+K^-)$ as a common denominator. This D_s branching is traditionally best measured and also enters directly into the formula for $\mathrm{Br}(B^0 \to D_s^+ D^-, D_s^+ \to \phi\pi)/\mathrm{Br}(B^0 \to D^- 3\pi)$. Below we listed the formulas we used to calculate ratios of branching fractions.

$$\frac{f_s}{f_d} \frac{Br(B_s^0 \to D_s^+ 3\pi(\phi\pi))}{Br(B^0 \to D^- 3\pi)} = \frac{N(D_s 3\pi)}{N(D3\pi)} \cdot \frac{\epsilon(D3\pi)}{\epsilon(D_s 3\pi)} \cdot \frac{Br(D^+ \to K\pi\pi)}{Br(D_s^+ \to \phi\pi^+, (KK))} \tag{8}$$

$$\frac{f_s}{f_d} \frac{Br(B_s^0 \to D_s^+ 3\pi(K^*K))}{Br(B^0 \to D^- 3\pi)} = \frac{N(D_s 3\pi)}{N(D3\pi)} \cdot \frac{\epsilon(D3\pi)}{\epsilon(D_s 3\pi)} \cdot \frac{Br(D^+ \to K\pi\pi)}{\frac{Br(D_s^+ \to K^* K^+, (K^-\pi^+))}{Br(D_s^+ \to \phi\pi^+, (KK))} \cdot Br(D_s^+ \to \phi\pi^+, (KK))} \tag{9}$$

$$\frac{f_s}{f_d}\frac{Br(B_s^0 \rightarrow\ D_s^+ 3\pi(3\pi))}{Br(B^0 \rightarrow\ D^- 3\pi)} = \frac{N(D_s 3\pi)}{N(D3\pi)} \cdot \frac{\epsilon(D3\pi)}{\epsilon(D_s 3\pi)} \cdot \frac{Br(D^+ \rightarrow K\pi\pi)}{\frac{Br(D_s \rightarrow \pi\pi\pi)}{Br(D_s^+ \rightarrow \phi\pi^+,(KK))} \cdot Br(D_s^+ \rightarrow \phi\pi^+,(KK))} \tag{10}$$

Using values of efficiencies from table 15, yields from table 17 for three different $B \rightarrow D_s 3\pi$ modes separately we obtain:

$$\frac{f_s}{f_d}\frac{Br(D_s^+ 3\dot{P}i : PhiPi)}{Br(B^0 \rightarrow\ D^- 3\pi)} = 0.263 \pm 0.029(Stat) \pm 0.035(BR) \tag{11}$$

$$\frac{f_s}{f_d}\frac{Br(D_s^+ 3\dot{P}i : KSK)}{Br(B^0 \rightarrow\ D^- 3\pi)} = 0.274 \pm 0.053(Stat) \pm 0.045(BR) \tag{12}$$

$$\frac{f_s}{f_d}\frac{Br(D_s^+ 3\dot{P}i : 3Pi)}{Br(B^0 \rightarrow\ D^- 3\pi)} = 0.293 \pm 0.067(Stat) \pm 0.054(BR) \tag{13}$$

Where $(BR_{\phi\pi})$ is the error due to $Br(D^+ \rightarrow K\pi\pi)/Br(D_s \rightarrow \phi\pi)$ and (BR) is the rest of the branching error. Using the latest PDG value $\frac{f_s}{f_d} = 0.259 \pm 0.038$ we calculate the ratio of branching fractions for three different $B \rightarrow D_s 3\pi$ modes separately. For our dataset, we obtain:

$$\frac{Br(B_s^0 \rightarrow\ D_s^+ 3\pi, D_s \rightarrow \phi\pi)}{Br(B^0 \rightarrow\ D^- 3\pi)} = 1.02 \pm 0.11(Stat) \pm 0.15(f_s/f_d) \pm 0.14(BR) \tag{14}$$

$$\frac{Br(B_s^0 \rightarrow\ D_s^+ 3\pi, D_s \rightarrow K^* K)}{Br(B^0 \rightarrow\ D^- 3\pi)} = 1.06 \pm 0.20(Stat) \pm 0.16(f_s/f_d) \pm 0.17(BR) \tag{15}$$

$$\frac{Br(B_s^0 \rightarrow\ D_s^+ 3\pi, D_s \rightarrow \pi\pi\pi)}{Br(B^0 \rightarrow\ D^- 3\pi)} = 1.13 \pm 0.26(Stat) \pm 0.17(f_s/f_d) \pm 0.21(BR) \tag{16}$$

The error on D_s branching fractions is clearly dominating. The systematic error is not quoted yet. It is discussed in the next section.

8 Systematic Uncertainties

For the moment this analysis is statistically limited. Several sources of systematic uncertainty were studied to make sure that systematic error is significantly smaller than statistical error.

8.1 Luminosity and run ranges

We thoroughly checked that we use the same luminosity for our $B^0 \to D^-3\pi$ and $B_s^0 \to D_s^+3\pi$ signals. Figure 50 on the left shows the run ranges comparison for data for all four modes. Full mass range from 4.5GeV to 6.5GeV is used.

We also checked that we use consistent Monte Carlo. Figure 50 on the right shows the run ranges comparison for all the signal Monte Carlo samples we use in the analysis. On figure 12 mentioned earlier we compare our signal and Monte Carlo for high statistics mode to check the quality of our realistic Monte Carlo.

To get from $20Tb$ of data sample to $10Kb$ final mass distribution it requres an analysis performed in several stages over thousands files. The plots for run ranges provide a simple visual check that all the modes contain the same data and Monte Carlo. No systematics assigned to run dependent efficiency or luminosity handling.

The alternative method of prescaling was tested to assure the correctness of our approach. The data sample was divided into four run ranges with distinct data taking conditions. The prescale values for these distinct run ranges were derived directly from data. The method is described in [18]. No systematic error is assigned.

The `SVT` χ^2 cut was changed during the datataking from $\chi^2 < 25$ to $\chi^2 < 10$. To estimate the systematic due to the efect from the upper bound two different sets of Monte Carlo with two quoted selection cuts were generated. The effect was estimated to be less than 1%. Refer to [18] for the details of this study. 1% systematic error was assigned to this effect.

8.2 B and D lifetimes

Our knowledge of B and D lifetimes comes from the world average measurements. The values of the average lifetimes are given as input to the B meson decay simulation. Incorrect lifetime may change trigger or reconstruction efficiency, as the two-track trigger is based on track displacement.

In order to estimate the size of this effect, we varied the B and D meson lifetimes by their world average measurement errors, as listed in Table 20. We then re-weighted the Monte Carlo with respect to $c\tau$ distribution and calculated the corrected efficiency. The relative changes in efficiencies after rescaling Monte Carlo are listed in the table 27. The errors are propagated into the total systematic uncertainty.

8.3 The B p_T spectrum.

A discrepancy was noticed between B meson p_T spectrum observed in data to that obtained from Monte Carlo simulation, as shown on Figure 51. The data spectrum is the spectrum of B hadrons measured in inclusive J/ψ channel with $|\eta(J/\psi)| < 0.6$ [19]. The Monte Carlo spectrum is obtained from the `BGen` output before the trigger requirements were applied. The discrepancy between data and Monte Carlo can be attributed to the fact that Peterson fragmentation model [9] diverges at very low p_T of the b quark.

To study the difference we recalculated our efficiencies by using Monte Carlo generated for B_s mixing analysis [17]. It has several different features:

- The new B-meson P_T spectrum measured by [19]
- Cut on $\eta < 1.3$ of the generated b-quaks
- Peterson fragmentation is turned off

The differences between the two sets of Monte Carlo cover all the known concerns. From the difference in efficiencies, we assign $\pm 3.0\%$ systematic uncertainty due to B_s meson p_T spectrum effects.

8.4 The ϕ^0 invariant mass window

In $B_s^0 \to D_s^+ 3\pi, D_s \to \phi\pi$ reconstruction $\phi^0 \to K^+K^-$ invariant mass is required to be within $[1.01, 1.029]$ GeV/c^2. The rest of B_s selection cuts are very similar to cuts used for B^0 and their validity is well covered by comparison of data and Monte Carlo (section 3.3).

We fitted $\phi^0 \to K^+K^-$ invariant mass distribution with a Breit-Wigner function convoluted with a Gaussian (figure 53). The background is modeled with a linear function.

The resolution (Gaussian) component of our fit came out cosistent with 1.37 ± 0.26 MeV/c^2 found by independent analysis [20] for low-p_T kaons ($p_T < 1.5$ GeV/c). The width of the Breit-Wigner component agreed with the world average (4.26 MeV/c^2).

Integrating signal in the selection region, we determined that absolute efficiency of the cut is 84.21% for Monte Carlo and 83.77% for data. The variation of the cut efficiency between data and Monte Carlo are well below 1% level. This study was done on $243pb^{-1}$ reconstructed with 5.3.1 version of `CDF` software.

ϕ mass window cut also undergo our routine study of selection related systematics (section8.10). In this study we scaled the ratio of data and Monte Carlo yields to 1.0 at the default cut values. Then we monitored the deviation of this ratio from 1.0 while shifting the sides of ϕ mass window (figure 54). While we were varying one side of the window we fixed the other side at default value. We found no sign of significant trend due to the possible difference of ϕ resonance shape in data and Monte Carlo.

The study was also done using the larger statistics of sample of $\phi \to KK$ from $B_s \to D_s\pi$ mode. The comparison between data and Monte Carlo could be found in [18].

No systematic was assigned to this selection cut.

8.5 Sample composition effect for $B^0 \to D^- 3\pi$.

Due to the limited knowlege of 3π resonant structure default Monte Carlo does not reproduce the data 3π invariant mass distribution (figure 60 on the left). The top part of the plot shows the comparison of data right sideband with signal Monte Carlo and the bottom part shows the comparison of data sideband subtracted signal with the same Monte Carlo. This plot and the rest of the study were done using $241pb^{-1}$ of `B_CHARM` sample. To make the comparison we corrected 3π invariant mass of the sideband candidates using the formula:

$$M(3\pi)_{corr} = M(3\pi)_{raw} \times \frac{\sqrt{M(B^0)^2_{PDG} - M(D^+)^2_{PDG}}}{\sqrt{M(B^0)^2_{reco} - M(D^+)^2_{PDG}}} \tag{17}$$

The distributions of the 3π invariant mass before and after the correction for wider sideband and looser cuts is shown on figure 55. Our B^0 signal consists of several components:

- $B^0 \to D^+ a_1$
- $B^0 \to D^+ \rho\pi$
- $B^0 \to D^+ 3\pi$
- $B^0 \to D^+ D_s (D_s \to 3\pi)$.

Mass distributions of these components have characteristic shapes clearly distinguishable from each other. We created templates for each of the components and estimated their relative contribution by fitting data.

Figure 56 shows the shapes of $B^0 \to D^+ 3\pi$, $B^0 \to D^+ \rho\pi$, and $B^0 \to D^+ a_1$ templates. They were fitted with Breit-Wigner distribution smeared with Gaussian and multiplied by a plateau formed by two Error functions (formula 6). Figure 57 on the left shows the templated fit of default Monte Carlo. It returns the relative contributions of the templated channels compared with *"real"* HEPG information based counts in table 22.

The disagreement of a_1 numbers is well within the statistics of the Monte Carlo sample. The similarity of the $\rho\pi$ and 3π templates made it difficult for the fit to distinguish between them. Fit overestimates $\rho\pi$ contribution by 22% *"borrowing"* events from 3π non-resonant component. This number is used later to estimate the systematic uncertainty of our procedure.

The fit of the similar data distribution (figure 57 on the right) returns much lower contribution for $\rho\pi$ and no contribution from non-resonant 3π. The mass and the width parameters of a_1 were alowed to float. The found relative conributions agreed with the recent update from `BaBar` [11] which describes $B^0 \to D^+ a_1$ mode as "dominant". Based on this knowledge we lowered the contribution of $\rho\pi$ and 3π modes in our signal Monte Carlo from 50% to 10% (table 21). The new Monte Carlo describes data better (figure 60 on the right). The plot was made using $355 pb^{-1}$ of `B_CHARM` sample.

The rest of the disagreement between data snd Monte Carlo was taken into account as a systematic uncertainty. Several effects were considered.

- The position and shape of a_1 mass peak was not reproduced well. To estimate systematics we generated Separate Monte Carlo with a_1 mass shifted by 80 Mev toward better agreement with data (figure 61 red histogram). Efficiency did not change significantly (table 23). We do not assign any systematic to this effect.

- Our fit for the fractions of a_1 3π and $\rho\pi$ has a good power separating a_1 from the other two mides. Its performance is worse separating $\rho\pi$ from 3π (table 22). To estimate systematics we compared the efficiency for pure a_1 mode with efficiency for admixture specified by decay table 21. The analysis efficiencies for all three components are summarized in table 25. This approach assumes 100% error on the fraction of $\rho\pi$ and 3π components compared to 22% found fitting Monte Carlo a page earlier. The ratio of the efficiencies came out as 1.026 ± 0.015. We assign $\pm 2.5\%$ systematic error to this effect.

- We generated $B^0 \rightarrow D^+ a_1$ signal Monte carlo with the simplest *"phase space"* decay model (`PHSP`). We observed no statistically significant change in efficiency.

We assign overall systematic error of $\pm 2.5\%$ due to the uncertainty in sample composition. This study was done using $243 pb^{-1}$ of `B_CHARM` sample. `5.3.1` version of CDF software was used.

As a cross-check we compared the 3π invariant mass distribution in data for $B^0 \rightarrow D^- 3\pi$ and $B_s^0 \rightarrow D_s^+ 3\pi, D_s \rightarrow \phi\pi$ (figure 63). Our statistics for B_s mode is very low. The error bars on the mass plots are larger than pure statistical error due to the sideband subtraction. With the statistics we have we may safely state that two distributions agree.

8.6 Duplicates and Self Reflections.

After applying all the analysis cuts, many events contain more than one candidate. This is especially true for 6-track modes where combinatorics is high. There are two major sources of multiple candidates. We call them *duplicates* and *self-reflections*.

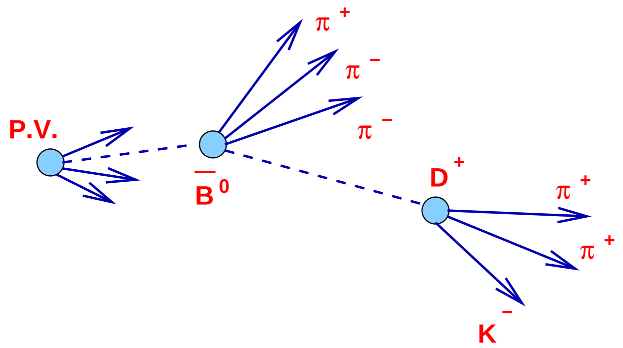

Figure 2: Picture representation of $B^0 \rightarrow D^- 3\pi$ decay. Reflections are coming from swapping the tracks inside candidate and with underlying event.

- We call *duplicate* the event when one or several tracks from the primary vertex or from other decays could be used for the candidate reconstruction. 6-tracks decays are particularly vulnerable for this drawback due to the lower momentum of the tracks. Since the momentum of the mistreated track is mostly combinatorial the distribution of duplicates is very similar to combinatorial background. The effect deteriorates overall significance of the signal but does not affect the efficiency.

- *Self-reflections* arise when reconstruction swaps tracks inside the candidate. For example it may swap direct pion from B and one of the products of D^+ decay (figure 2). self-reflections have very similar characteristics and effectively amplify the signal. The effect does not cancel in ratio since different decay modes have different susceptibility to self-reflections. The correction to the efficiency should be made.

In this analysis we only correct for self-reflections and leave all the duplicates in our sample mostly because we use signal Monte Carlo only and can not study any of the effects related to underlying event. Duplicates do not affect efficiency and only add combinatorial background.

The study shows that data and Monte Carlo contain the same amount of self-reflections. The results are summarized in table 11. We only compare data and Monte Carlo for statistically significant mode $B^0 \to D^- 3\pi$. For B_s modew we only checked that the input due to the self reflections is well below the resolution of our statistics. If we find two candidates with the same track content we leave the first which is usually the candidate with higher transverse momentum. No systematics is assigned to this effect.

8.7 Fit Systematics.

There are several parameters in the fit which could affect the yield and are not defined very well. In this study we address all the known concerns.

- Due to the small signal yields for $B_s^0 \to D_s^+ 3\pi$ modes we have to fix width of the signal template to the value obtained from Monte Carlo. The width correction procedure is described in section 5.1. The correction came out with the error. We use the error to estimate our fit systematics varying signal width by one standard deviation.

- We have a contribution of non-combinatorial background in the signal region for $B^0 \to D^- 3\pi$. For semi-generic background shape we change the norm within one standard deviation. For small contributions with fixed norm: Cabibo, Λ_b and B_s we change norm by $\pm 50\%$.

- $B^0 \to D^- 3\pi$ signal has longer tails compare to $B_s^0 \to D_s^+ 3\pi$ modes. We take this effect into account by integrating every signal in 95.45% window. No systematics is assigned.

The results for fit systematics are summarized in table 26. Several sensitive fit parameters were also varied by $\pm 2\sigma$ to make sure that the uncertainty does not diverge uncontrollably. In the final number for fit uncertainty (table 29) we only use results from $\pm 1\sigma$ and $\pm 50\%$ variations.

8.8 Semi-generic template systematics.

Although the continuum physics background does not fall directly under the signal its shape used for templated fit can indirectly affect the signal yields. The shape of this background depends on the many branching fractions of various B decays that contribute to it. The branching fractions in B^0 have been measured relatively well. The branching fractions for most of the B_s decays have not been measured but assumed from the similar B^0 branching fractions. To estimate the systematic error which could arise we tried to vary the shape and population of the physics backgrounds used in B_s fits and see the effect of such variations on the signal yield. For this we divide the events of semi-generic template into three categories:

- B_s decays to D_s^+ with extra products (signal modes being subtracted)
- B_s decays to D_s^* (main reflection modes and $D_s^+ D_s^*$ mode being subtracted)
- The rest of the B_s, B^0 and B^+ decays.

The resulting breakdown is shown on figure 52 contribution of the decay category is proportional to the area of the correspondent colored segment.

To estimate the systematics due to the shape of semi-generic background we performed three templated fits for $B_s^0 \to D_s^+ 3\pi, D_s \to \phi\pi$. Each of the fits had one of the three categories dropped. We used formula 7 to parametrize the fit. The variation of the yield goes into the estimate of our systematic uncertainty due to the shapes of semi-generic Monte Carlo. We assigne the same $\pm 3\%$ systematics for all three $B_s^0 \to D_s^+ 3\pi$ modes (table 26) since K^*K and 3π statistics is too limited to make similar study significant.

8.9 XFT efficiency for kaons relative to pions

It has been shown [21], that the `XFT` system has different efficiency for tracks generated by kaons and pions. For the study of direct CP assymetry in $D \to hh$ decays this difference was one of the dominant sources for systematic uncertainty. A detailed study of the `XFT` efficiency has been preformed with the following conclusions:

- Pions and kaons may have a different `XFT` efficiency due to the different ionization patterns in the `COT`
- This effect is not reproduced by Monte Carlo.
- A study of this effect was done in data using a sample of $D^+ \to K\pi\pi$ decays. The study showed a 6 % inefficiency of kaons relative to pions in `XFT` *1-miss* configuration.
- No inefficiency was found in *2-miss* configuration of `XFT`.

In order to evaluate the systematic uncertainty associated with the effect, we introduced it a posteriori into the Monte Carlo simulation as a 6% inefficiency for every kaon track to make a trigger track. We compared the relative Monte Carlo efficiencies before and after the effect was introduced as shown in table 28. The ratio of efficiencies has changed by 0.2 %.

The same study was done using the `XFT` efficiency curves provided by [21] (figure 64). In this study `XFT` efficiency was a function of p_T of the track and the actual run number. The ratio of efficiencies obtained using these effieciency curves is 0.1 %. 0.2% systematic uncertainty was assigned to this effect.

8.10 Cut Efficiency Systematics.

The agreement of data and Monte Carlo was tested in section 3.3. The difference is small but has to be taken into account as systematics error. We study the change of the ratio of the yields for data and Monte Carlo with respect to cut value. We scale the ratio to 1.00 at the default cut values and look for deviation while scanning cut one by one within reasonable intervals.

Study for $B^0 \to\ D^- 3\pi$ is shown at figure 65. Impact parameter of B meson and χ^2 of the fit have a significant 1.03 ± 0.02 deviation from 1.00. The minimum transverse momentum of the track has a noticable deviation of 4%. We take 5% for the cut systematics of these three cuts.

Similar study for $B_s^0 \to\ D_s^+ 3\pi, D_s \to \phi\pi$ is shown on figure 66. Statistical error is much bigger and all of the deviations are well within the error. χ^2 dependence shows some noticeable downtrend. We average 9 points of the plot and get 0.94 ± 0.04

$B_s^0 \to\ D_s^+ 3\pi, D_s \to K^* K$ and $B_s^0 \to\ D_s^+ 3\pi, D_s \to \pi\pi\pi$ modes have very low statistic and similar studies are dominated by statistical errors and background fluctuations.

We take 5% as cut systematics for all the modes. This systematic is considered correlated when three modes are combined.

8.11 D^+ Veto Study.

$B_s^0 \to\ D_s^+ 3\pi, D_s \to K^* K$ reconstruction has a large reflection from $B^0 \to\ D^- 3\pi$ under the signal peak when one of the pions from $D^+ \to K\pi\pi$ is reconstructed as a kaon. To be consistent with B-mixing analysis [17] we were considering a possibility of applying D^+ veto to our $B_s^0 \to\ D_s^+ 3\pi, D_s \to K^* K$ reconstruction. For this we substitute the *bachelor kaon* in $D_s \to K^* K$ with pion and calculate the invariant mass. Figures 67 and 68 show mass distributions of reconstructed $B_s \to D_s 3\pi$ and $D_s \to K^* K$ with and without D^+ veto. Figures show that it is possible to eliminate D^+ presence by forbidding ± 24 MeV window around reconstructed D^+ mass with a lost of $\approx 40\%$ of B_s signal for both data and Monte Carlo (table 24). Figure 69 shows data fits with and without D^+ veto. To make data fit with D^+ veto all the templates had to be redone and their scaling parameters recalculated. Comparison shows that veto does not improve the signal and requires additional study of systematics. The latter is especially cumbersome since Monte Carlo does not reproduce widths of the narrow peaks (table 12). Without D^+ veto reconstruction has a big $B^0 \to\ D^- 3\pi$ reflection under the signal. The norm of this reflection could be exactly calculated from data and study of the relevant systematics could be easilly handled (section 8.7).

8.12 Comparison of the Prescale Performance.

Prescale factor for `LOWPT` and `B_CHARM` have been calculated in the past with a different approach. A sample of `B_CHARM` triggers have been selected based on the third level bits. Than the ratio of the number of events $(\texttt{LOWPT} + \texttt{B\_CHARM})/\texttt{B\_CHARM}$ has been performed. This number is less or equal than one by construction and deviate from 1 because of the prescale (in fact all `B_CHARM` events should be also `LOWPT`).

It is possible that prescaling this way one may better consider the variable signal to noice ratio at `Level1` trigger level as a function of instantaneous luminosity. To study the effect we calculated Monte Carlo efficiency for `B_CHARM` and `LOWPT` separately for B_s and B_0 channels in four run ranges:

1. 138809 - 164304 from the beginning of the data set to the beginning of svt 4/5 configuration.
2. 164305 - 168889 from the beginning of svt 4/5 configuration to the 2003 shutdown
3. 168889 - 179056 runs up to bad COT period.
4. 184208 - 186598 post COT recovery up to the end of the dataset.

We measured Monte Carlo efficiencies in $B_d \to D_0\pi$ and $B_s \to D_s\pi$ samples for these 4 run regions separately in `B_CHARM` and `LOWPT` trigger data samples. The ratios of efficiencies versus the run range are shown on figures 58. The point corresponding to the last run range is off by approximately 2σ from the average.

Without studiying the nature of the deviation we estimated systematic error by reweighting the last point on figure 58 to the average value as shown on figure 59. The systematics of $\pm 1.0\%$ was assigned to this effect.

8.13 SVT χ^2 Cut.

In this analysis we used $\chi^2 < 25$ cut as a matching criteria of offline tracks to SVT. This cut has been tightened to $\chi^2 < 15$ for a big fraction of the dataset.

- range 1: run 138809 - 178757 $\chi^2 < 25$. Luminosity 228 pb^{-1}.
- range 2: run 178844 - 186598 $\chi^2 < 15$. Luminosity 127 pb^{-1}.

To estimate to effect of the cut on svt χ^2 two Monte Carlo sets were produced:

- $B_d \to D^+ 3\pi$ with svt $\chi^2 < 25$ and svt $\chi^2 < 15$
- $B_s \to D_s 3\pi$ with svt $\chi^2 < 25$ and svt $\chi^2 < 15$

The ratios of efficiencies produced with two Monte Carlo sets have been compared. The systematic effect of 1.0% has been estimated from the variation of the ratio of efficiencies.

8.14 Summary of Systematic Effects

For now the contributions to our systematics are sample composition and fit systematics as listed in Table 29. The part of the systematic uncertainty related to $B^0 \to D^- 3\pi$ is common for all the modes. It is propagated without change to the combined result. The individual systematic errors for $B_s^0 \to D_s^+ 3\pi$ modes are combined statistically in the final number. For the separate numbers the individual systematics and systematics due to $B^0 \to D^- 3\pi$ are combined in squares.

9 Final Results.

We calculate systematic error separately for each mode and add it to our result.

$$\frac{f_s}{f_d}\frac{Br(D_s^+ 3\dot{P}i : PhiPi)}{Br(B^0 \to\ D^- 3\pi)} = 0.263 \pm 0.029(Stat) \pm 0.021(Syst) \pm 0.035(BR) \tag{18}$$

$$\frac{f_s}{f_d}\frac{Br(D_s^+ 3\dot{P}i : KSK)}{Br(B^0 \to\ D^- 3\pi)} = 0.274 \pm 0.053(Stat) \pm 0.032(Syst) \pm 0.045(BR) \tag{19}$$

$$\frac{f_s}{f_d}\frac{Br(D_s^+ 3\dot{P}i : 3Pi)}{Br(B^0 \to\ D^- 3\pi)} = 0.293 \pm 0.067(Stat) \pm 0.025(Syst) \pm 0.054(BR) \tag{20}$$

Using the latest PDG value $\frac{f_s}{f_d} = 0.259 \pm 0.038$ we have:

$$\frac{Br(B_s^0 \to\ D_s^+ 3\pi, D_s \to \phi\pi)}{Br(B^0 \to\ D^- 3\pi)} = 1.02 \pm 0.11(Stat) \pm 0.08(Syst) \pm 0.15(f_s/f_d) \pm 0.14(BR) \tag{21}$$

$$\frac{Br(B_s^0 \to\ D_s^+ 3\pi, D_s \to K^* K)}{Br(B^0 \to\ D^- 3\pi)} = 1.06 \pm 0.20(Stat) \pm 0.12(Syst) \pm 0.16(f_s/f_d) \pm 0.17(BR) \tag{22}$$

$$\frac{Br(B_s^0 \to\ D_s^+ 3\pi, D_s \to \pi\pi\pi)}{Br(B^0 \to\ D^- 3\pi)} = 1.13 \pm 0.26(Stat) \pm 0.10(Syst) \pm 0.17(f_s/f_d) \pm 0.21(BR) \tag{23}$$

9.1 Combining Results.

$B_s^0 \to\ D_s^+ 3\pi, D_s \to \phi\pi$ dominates the measurement due to the hich statistics and low background. Addition of the other two modes lowers the statistical error by $\approx$ 20%. We found no significant difference in weighting results by measured statistics or by expected yield. In the final version we weight them by Monte Carlo efficiency (expected yield):

$$\frac{Br(B_s^0 \to\ D_s^+ 3\pi)}{Br(B^0 \to\ D^- 3\pi)} = \frac{N_1 + N_2 + N_3}{N_0} \cdot \frac{\epsilon_0}{\epsilon_1 + r_2\epsilon_2 + r_3\epsilon_3} \cdot \frac{Br(D^+ \to K^-\pi^+\pi^+)}{Br(D_s^+ \to \phi\pi^+)} \tag{24}$$

Where

$r_2 = \frac{\Gamma(K^+\bar{K}^*(892)^0, \bar{K}_0^* \to K^-\pi^+)}{\Gamma(\phi\pi^+)}$,

$r_3 = \frac{\Gamma(\pi\pi\pi)}{\Gamma(\phi\pi^+)}$.

N_i - number of observed events (data yield)
ϵ_i - Monte Carlo efficiency

Index $i = 0$ is used for $B^0 \rightarrow D^- 3\pi$ and indeces $i = 1, 2, 3$ are used for decays with $\phi\pi$, K^*K and $\pi\pi\pi$ correspondently.

Total statistical error is provided by the first term of the product with data yields. The second term with Monte Carlo efficiencies provides a combination of non-correlated branching errors. The third term is the source of correlated branching error which is the same for all three channels. Taking all mentioned into accound fo our dataset we found:

$$\frac{f_s}{f_d}\frac{Br(B_s^0 \rightarrow D_s^+ 3\pi)}{Br(B^0 \rightarrow D^- 3\pi)} = 0.271 \pm 0.025(Stat) \pm 0.021(Syst) \pm 0.037(BR) \tag{25}$$

Using the latest PDG value $\frac{f_s}{f_d} = 0.259 \pm 0.038$ we have:

$$\frac{Br(B_s^0 \rightarrow D_s^+ 3\pi)}{Br(B^0 \rightarrow D^- 3\pi)} = 1.05 \pm 0.10(Stat) \pm 0.08(Syst) \pm 0.15(f_s/f_d) \pm 0.14(BR) \tag{26}$$

The part of the systematic error coming from $B^0 \rightarrow D^- 3\pi$ was considered correlated. The systematic uncertainties individual for three channels were combined statistically. We treated fit systematics as “individual”. $D_s \rightarrow \pi\pi\pi$ sample composition was treated as “individual” for $B_s^0 \rightarrow D_s^+ 3\pi, D_s \rightarrow \pi\pi\pi$. The rest of the systematics errors were considered common.

The error on D_s branching fractions dominate the measurement. The error on hadron production as well as good part of the branching and systematic error are correlated. We are eager to see the first results from Cleo-C and plug them into our measurement.

Acknowledgments

We are grateful to many people who helped us with support, advice and constructive criticism. We would like to thank Gerry Bauer, Stefano Giagu, Rob Harr, Matt Herndon, Rolf Oldeman, for answering many questions that came up in the process. We would like to thank Ivan Furic whose analysis was heavily referred during this study. We also would like to note Ricardo Lachman, - our summer student, who helped a lot testing our tools.

References

[1] A. Belloni, A. Bolshov, B. Iyutin, Ch. Paus Measurement of the Ratio of Branching Fractions $Br(B_s^0 \rightarrow D_s^+ 3\pi)/Br(B^0 \rightarrow D^- 3\pi)$. CDF note 7504

[2] Bs Mixing group, (Contact: A. Belloni, I.Furic, G. Gomez-Ceballos, I. Kravchenko, N. Leonardo, S. Menzemer, J. Miles, Ch. Paus, J.Piedra) Updated Study of Bs Oscillations in $B_s \rightarrow D_s(3)\pi$ CDF note 7861

[3] A. Belloni, A. Bolshov, B. Iyutin, Ch. Paus Title: Measuring the Ratio of Branching Fractions, $Br(B^0 \to D_s^+ D^-)/Br(B^0 \to D^- 3\pi)$. Draft. CDF note 7495

[4] J. Kroll, Ch. Paus, G. Punzi, J. Russ, and F. Ukegawa, CDF Note 6012

[5] A. Belloni, I.K. Furić, Ch. Paus, "Study of B_s, B^+ and B^0 Yields in the Hadronic B Samples", CDF Note 6614.

[6] B. Ashmanskas, A. Cerri, see CdfCode browser: http://cdfcodebrowser.fnal.gov/CdfCode/source/svtsim/.

[7] K. Anikeev, P. Murat, Ch. Paus, "Description of Bgenerator II", CDF Note 5092.

[8] P. Nason, S. Dawson and R.K. Ellis, Nucl. Phys. **B303** (1988) 607; Nucl. Phys. **B327** (1989) 49.

[9] C. Peterson *et al.*, Phys. Rev. **D27** (1983) 105.

[10] W. Bell, J.P. Fernandez, L. Flores, F. Wuerthwein, R.J. Tesarek, "User Guide For EvtGen CDF", CDF Note 5618.

[11] H.W.Zhao "Study of B Decays into the Final State $D^{(*)}\pi\pi\pi$ at BaBar" hep-ex/0409055

[12] A. Cerri, M. Rescigno, "The CDFII Realistic Simulation Package" - CDF Note in preparation.

[13] S. Menzemer, talk at BPAK Meeting (July 1 2005) `http://www-cdf.fnal.gov/internal/physics/bottom/bpak/`

[14] (D. Acosta et al., The CDF Collaboration) "Measurement of $Br(\Lambda_b \to \Lambda_c \pi)/Br(B^0 \to D^+\pi) \cdot \sigma(\Lambda_b)/\sigma(B^0)$" CDF Note 7427

[15] (Frabetti et al., FNAL E687 Collab) PL B351 591, Dialitz fit, 701 evts

[16] B^0 Mixing group "Updated Study of B^0 Oscillations ..." CDF Note 7722

[17] B_s Mixing group "Updated Study of B_s Oscillations in $B_s \to D_s(3)\pi$" CDF Note 7861

[18] G Bauer, A Belloni, A Bolshov, B Iyutin, Ch Paus "Measurement of the ratio of Branching fractions $Br(B_s \to D_s\pi)/Br(B_d \to D^+\pi)$ with $355pb^{-1}$" CDF Note 7862

[19] M. Bishai *et. al* "The Measurement of the b-hadron Inclusive Cross-section in CDF Run II using $b \to J/\psi X$". CDF Note 6285,

[20] M. Jones, "Initial Performance Studies of the CDF-II Time-of-Flight Detector", CDF Note 5930.

[21] S. Giagu *et. al*, "Relative branching fractions and CP-violating decay rate asymmetries in Cabibo suppressed decays of the D^0 meson." CDF Note 6391

10 Tables

Set	Run Range	Luminocity (pb^{-1})
xbhd0d dataset. Total	$[138809, 186598]$	355
Missed in MC.		30
MC agrees with data.	$[148152, 186079]$	325

Table 1: The summary of the run numbers and luminocities used in the analysis. .

Run range	luminocity (pb^{-1})	Comment
138809-148152	9.3	Wrong Trigger Tables in DB
155368-155742	3.1	No Beamline
156089, 168820, 185545		Unknown
165465, 165466, 166248		No Beamline
181016-181190, 184290	4.6	No Beamline
186081-186598	11.0	Wrong Trigger Tables in DB

Table 2: The summary of the run numbers and luminocities missed in Monte Carlo.

```
Decay anti-B0
0.0090   a_1- D+                        SVS;
0.0005   D+  rho0    pi-                PHSP;
0.0005   D+  pi- pi+ pi-                PHSP;
Enddecay
#
Decay D+
0.0900   K-  pi+  pi+                    D_DALITZ;
Enddecay
#
Decay a_1-
0.6    rho0 pi-                      VVS_PWAVE 1.0 0.0 0.0 0.0 -0.1 0.0;
Enddecay
#
Decay rho0
1.000    pi+ pi-                         VSS;
Enddecay
```

Table 3: Decay table for signal Monte Carlo $B^0 \rightarrow\ D^{-}3\pi$.

```
#
Decay B0
0.0130   D*-  a_1+                     SVV_HELAMP 0.336 0.0 0.88 0.0 0.336 0.0;
0.0010   D*-  rho0  pi+                 PHSP;
0.0077  D*-  pi-  pi+  pi+             PHSP;
0.0005   D-  rho0  K+                  PHSP;
0.0005 D-        pi-         K+        pi+         PHSP;
0.0090   K_1+  D-                        SVS;
Enddecay
#
Decay D-
0.0900   K+  pi-  pi-                    D_DALITZ;
Enddecay
```

Table 4: Decay tables used for $B^0 \rightarrow D^{*}3\pi$ and Cabibo reflection templates.

```
Decay B_s0
0.0090   a_1+ D_s-                        SVS;
0.0005   D_s-  rho0  pi+                 PHSP;
0.0005   D_s-  pi-   pi+   pi+           PHSP;
Enddecay
#
Decay D_s-
0.0228    K*0    K-                      SVS;
0.0180    phi    pi-                     SVS;
0.0004    rho0   pi-                    SVS;
0.0057    f_0    pi-                    PHSP;
0.0020    f_2    pi-                    PHSP;
0.0033    f'_0   pi-                    PHSP;
Enddecay
#
Decay K*0
0.6657      K+  pi-                       VSS;
Enddecay
#
Decay phi
0.4910      K+   K-                        VSS;
Enddecay
#
Decay f_0
0.5200   pi+  pi-                       PHSP;
Enddecay
#
Decay f_2
0.5650   pi+  pi-                       TSS;
Enddecay
#
Decay f'_0
0.5200   pi+  pi-                       PHSP;
Enddecay
#
Decay a_1+
0.6    rho0 pi+                     VVS_PWAVE 1.0 0.0 0.0 0.0 -0.1 0.0;
Enddecay
#
Decay rho0
1.000    pi+ pi-                        VSS;
Enddecay
```

Table 5: Decay table for mixed signal Monte Carlo $B_s^0 \rightarrow\ D_s^+ 3\pi, D_s \rightarrow \phi\pi$.

```
Decay B_s0
0.0090   a_1+ D_s-                      SVS;
0.0005   D_s-  rho0  pi+               PHSP;
0.0005   D_s-  pi-   pi+   pi+         PHSP;
Enddecay
#
Decay D_s-
0.0228    K*0      K-                 SVS;
0.0180    phi      pi-                SVS;
0.0090    K- K+ pi-                   PHSP;
0.0004    rho0     pi-                SVS;
0.0100    f_0      pi-                PHSP;
0.0020    f_2      pi-                PHSP;
0.0033    f'_0     pi-                PHSP;
Enddecay
#
Decay K*0
0.6657      K+  pi-                     VSS;
Enddecay
Decay phi
0.4910      K+   K-                      VSS;
Enddecay
Decay f_0
0.5200   pi+  pi-                     PHSP;
0.4800   K+   K-                      PHSP;
Enddecay
Decay f_2
0.5650   pi+  pi-                     TSS;
Enddecay
Decay f'_0
0.5200   pi+  pi-                     PHSP;
Enddecay
Decay a_1+
0.6    rho0 pi+                   VVS_PWAVE 1.0 0.0 0.0 0.0 -0.1 0.0;
Enddecay
Decay rho0
1.000    pi+ pi-                      VSS;
Enddecay
```

Table 6: Decay table for backgorund templates for $B_s^0 \to\ D_s^+ 3\pi$.

	Cut	Loose	Final
B	$L_{xy}/\sigma(L_{xy})$	> 7	> 16
B	$d0$	< 0.01 cm	< 0.0065 cm
B	$\chi^2_{r\phi}$	< 20	< 14
D^+	$L_{xy}/\sigma(L_{xy})$	> 8	> 15
D^+	$L_{xy}^{\leftarrow B}$	> -0.05 cm	> 0.015 cm
D^+	$\chi^2_{r\phi}$	< 20	< 10

Table 7: $B^0 \rightarrow\ D^- 3\pi$ the set of loose cuts applied before cut optimization compared to the final set of cuts.

	Value	
B	$L_{xy}/\sigma(L_{xy})$	> 16
B	$d0$	< 0.0065 cm
B	$\chi^2_{r\phi}$	< 14
D^+	$L_{xy}/\sigma(L_{xy})$	> 15
D^+	$L_{xy}^{\leftarrow B}$	> 0.015 cm
D^+	$\chi^2_{r\phi}$	< 10
Track	$MinP_T$	$> 0.35 GeV/c$

Table 8: $B^0 \rightarrow\ D^- 3\pi$ cuts after cut optimization for `B_CHARM` and `LOWPT` combined .

Particle	Cut	$B_s \rightarrow D_s 3\pi(\phi\pi)$	$B_s \rightarrow D_s 3\pi(K^* K)$	$B_s \rightarrow D_s 3\pi(\pi\pi\pi)$
B	$\frac{L_{xy}}{\sigma(L_{xy})}$	> 15	> 18	> 21
B	$d0$	< 0.006 cm	< 0.005 cm	< 0.0055 cm
B	$\chi^2_{r\phi}$	< 10	< 8	< 10
D_s	$\frac{L_{xy}}{\sigma(L_{xy})}$	> 10	> 15	> 20
D_s	$L_{xy}^{\leftarrow B}$	> -0.01 cm	> 0.01 cm	> 0.015 cm
D_s	$\chi^2_{r\phi}$	< 10	< 10	< 10
ϕ	M	$[1.010, 1.029]$		
K^*	M		$[0.84, 0.94]$	
Track	$MinP_T$	$> 0.35 GeV/c$	$> 0.35 GeV/c$	$> 0.48 GeV/c$

Table 9: $B_s^0 \rightarrow\ D_s^+ 3\pi, D_s \rightarrow \phi\pi$, $B_s^0 \rightarrow\ D_s^+ 3\pi, D_s \rightarrow K^* K$ and $B_s^0 \rightarrow\ D_s^+ 3\pi, D_s \rightarrow \pi\pi\pi$ optimized cuts for `B_CHARM` and `LOWPT` combined .

Channel	B_CHARM	B_CHARM and LOWPT	Gain %
$B^0 \to D^- 3\pi$	10517 ± 105	14839 ± 122	$41.1\% \pm 1.5\%$
$B_s \to D_s 3\pi(\phi\pi)$	8625 ± 91	12061 ± 107	$39.8\% \pm 2.0\%$
$B_s \to D_s 3\pi(K^* K)$	1706 ± 41	2281 ± 47	$33.7\% \pm 4.0\%$
$B_s \to D_s 3\pi(\pi\pi\pi)$	956 ± 30	1279 ± 35	$33.8\% \pm 4.0\%$

Table 10: Gain due to the addition of LOWPT triggers. Signal Monte Carlo.

Channel	No Self-Reflections	With Self-Reflections	Change %
$B^0 \to D^- 3\pi$ (Data)	3316 ± 76	3371 ± 78	$1.7\% \pm 3.0\%$
$B^0 \to D^- 3\pi$	14839 ± 122	15028 ± 123	$1.3\% \pm 1.0\%$
$B_s \to D_s 3\pi(\phi\pi)$	12061 ± 107	12222 ± 108	$1.3\% \pm 1.0\%$
$B_s \to D_s 3\pi(K^* K)$	2281 ± 47	2300 ± 47	$0.8\% \pm 2.0\%$
$B_s \to D_s 3\pi(\pi\pi\pi)$	1279 ± 35	1279 ± 35	$0.0\% \pm 3.0\%$

Table 11: The rate of Self-Reflections.

Parameter	Value Data	Error Data	Value MC	Error MC	Diff
Signal	3.44272e+01	7.99331e-01	1.55348e+01	1.36388e-01	NA
Mass0	5.27833e+00	3.85689e-04	5.28313e+00	2.91527e-04	-4.8 ± 0.5
Width0	1.06239e-02	3.81835e-04	9.08360e-03	8.59929e-04	$17\% \pm 3\%$
Frac1	7.16131e-01	fixed	7.18522e-01	8.38964e-02	fixed
Mass1	5.27833e+00	fixed to Mass0	5.28309e+00	fixed to Mass	fixed
Width1	1.63328e-02	fixed wrt Width0	1.48076e-02	6.78722e-04	fixed
Frac2	6.77464e-02	fixed	6.78844e-02	9.77520e-03	fixed
Mass2	5.27833e+00	fixed to Mass0	5.28309e+00	fixed to Mass	fixed
Width2	4.25884e-02	fixed wrt Width0	4.10157e-02	8.73302e-03	fixed

Table 12: The comparison of the signal fitted parameters for data and Monte Carlo. $B^0 \to D^- 3\pi$. The values are used to correct the width of the $B^0 \to D_s^+ D^-$signal template.

	$B \to D3\pi$ $D^+ \to K\pi\pi$	$B \to D_s 3\pi$ $D_s \to \phi\pi$	$B \to D_s 3\pi$ $D_s \to K^* K$	$B \to D_s 3\pi$ $D_s \to \pi\pi\pi$
$D^*_{(s)} a_1$	free	free	free	free
$D^*_{(s)} \rho\pi$	free	-	-	-
Cabibo	$6.9\% \pm 2\%$	$6.9\% \pm 2\%$	$6.9\% \pm 2\%$	$6.9\% \pm 2\%$
$\Lambda_b \to \Lambda_c 3\pi, \Lambda_c \to pK\pi$	$3.0\% \pm 1\%$	-	20 ± 9	-
$B^0_s \to D^+_s 3\pi, D_s \to K^* K$	$2.8\% \pm 0.3\%$	-	-	-
$B^0 \to D^- 3\pi$	-	-	155 ± 6	-
$B \to D^0 X, D^0 \to K\pi$	-	-	80 ± 40	-
$B \to D^+ X, D^+ \to K\pi\pi$	-	-	250 ± 50	-
Semi-Generic	free	free	free	free
Combinatorial	free	free	free	free

Table 13: Templates with fixed normalization.

Channel	$B_s \to D_s 3\pi(\phi\pi)$	$B_s \to D_s 3\pi(K^* K)$	$B_s \to D_s 3\pi(\pi\pi\pi)$
$B_s \to D_s 3\pi(\phi\pi)$	100.0%	$0.5\% \pm 0.2\%$	0.0%
$B_s \to D_s 3\pi(K^* K)$	$0.65\% \pm 0.2\%$	100.0%	0.0%
$B_s \to D_s 3\pi(\pi\pi\pi)$	$0.1\% \pm 0.1\%$	0.0%	100.0%

Table 14: Cross talk between different $B_s \to D_s \pi\pi\pi$ channels.

	$B^0 \to D^+ 3\pi$	$B^0 \to D_s 3\pi(\phi\pi)$	$B \to D_s 3\pi(K^* K)$	$B \to D_s 3\pi(\pi\pi\pi)$
Generated ($\times 10^6$)	60.0	60.0	26.2	13.1
Yield MC Combined	14839 ± 122	12061 ± 107	2281 ± 47	1279 ± 35
Eff Combined ($\times 10^{-3}$)	0.247 ± 0.002	0.201 ± 0.003	0.087 ± 0.002	0.098 ± 0.003

Table 15: Efficiencies extracted from Monte Carlo.

	$B^0 \to D^+ 3\pi$	$\Lambda_b \to \Lambda_c 3\pi$	$B^0 \to D^+ K\pi\pi$
Generated ($\times 10^6$)	60.0	20.0	10.4
Yield MC Combined	15831 ± 132	365 ± 19	2839 ± 53
Efficiency ($\times 10^{-3}$)	0.264 ± 0.002	0.018 ± 0.001	0.273 ± 0.005

Table 16: Efficiencies extracted from Monte Carlo.

	$B^0 \to D^+ 3\pi$	$B_s \to D_s 3\pi(\phi\pi)$	$B \to D_s 3\pi(K^* K)$	$B \to D_s 3\pi(3\pi)$
Yield Data Combined	3288 ± 76	160 ± 17	90 ± 17	49 ± 11

Table 17: Yields extracted from Data.

Mode	branching
$\Lambda_c \to pK\pi$	$(5.0 \pm 1.3) \times 10^{-2}$
$B^0 \to D^- \pi^+$	$(3.0 \pm 0.4) \times 10^{-3}$
$B^0 \to D^- K^+$	$(2.0 \pm 0.6) \times 10^{-4}$

Table 18: Relevant branching fractions with uncertainties used to calculate normalizations for reflection templates.

D^+ Decays	Branching
$\Gamma(K^-\pi^+\pi^+)/\Gamma_{total}$	0.092 ± 0.006
D_s Decays	Branching
$\Gamma(D_s \to K^+K^-\pi^+)/\Gamma_{total}$	0.043 ± 0.012
$\Gamma(\phi\pi^+, \phi \to K^+K^-)/\Gamma_{total}$	0.018 ± 0.004
$\Gamma(K^+\bar{K}^*(892)^0, \bar{K}^*(892)^0 \to K^-\pi^+)/\Gamma_{total}$	0.020 ± 0.006
$\Gamma(\pi^+\pi^+\pi^-)/\Gamma_{total}$	0.0101 ± 0.003
$\Gamma(K^+K^-\pi^+ NR)/\Gamma_{total}$	0.009 ± 0.004
$\Gamma(K^+\bar{K}^*(892)^0, \bar{K}^*(892)^0 \to K^-\pi^+/\Gamma(\phi\pi^+, \phi \to K^+K^-)$	1.25 ± 0.12
$\Gamma(\pi^+\pi^+\pi^-)/\Gamma(\phi\pi^+, \phi \to K^+K^-)$	0.565 ± 0.071

Table 19: Relevant branching fractions and ratios of branching fractions with uncertainties.

Meson	Lifetime
B_s	1.461 ± 0.057 ps
B^0	1.536 ± 0.014 ps
D_s^+	490 ± 9 fs
D^+	1040 ± 7 fs

Table 20: B and D meson lifetimes and errors used to estimate systematic effects by rescaling the Monte Carlo

```
Decay anti-B0
0.0060   a_1- D+          SVS;
0.0011   D+  rho0    pi-  PHSP;
0.0022   D+  pi+ pi- pi-  PHSP;
Enddecay
#
Decay a_1+
0.4920   rho0 pi+        VVS_PWAVE;
0.5080   rho+ pi0        VVS_PWAVE;
Enddecay
```

```
Decay anti-B0
0.0090   a_1- D+          SVS;
0.0005   D+  rho0    pi-  PHSP;
0.0005   D+  pi- pi+ pi-  PHSP;
Enddecay
#
Decay a_1+
0.4920   rho0 pi+        VVS_PWAVE;
Enddecay
```

Table 21: Decay tables used for $B^0 \to D^- 3\pi$ sample composition systematics study. Default decay table on the left. Corrected decay table on the right.

	$A1$	$\rho\pi$	3π
MC (HEPG):	2531	1077	2338
MC Fit:	2453	1317	2176
DATA Fit:	865	99	0
Old .dec	0.006	0.0011	0.0022
New .dec	0.009	0.0005	0.005
Syst:	3.0%	22.0%	6.9%
Stat MC:	2%	3.0%	2.0%
Stat DATA:	3.4%	10%	-

Table 22: The results of the 3π invariant mass templated fit for Monte Carlo and data.

Decay	MC yield.
$B \to D^+ a_1$	2456 ± 35
$B \to D^+ a_1$. Shifted 80 Mev.	2465 ± 36
Efficiency ratio	1.00 ± 0.02

Table 23: Efficiency study for different a_1 mass assignments as a part of a systematic study.

	no D^+ Veto	with D^+ veto	loss
$B_s^0 \to D_s^+ 3\pi, D_s \to K^* K$ data	91 ± 17	50 ± 11	$-44\% \pm 20\%$
$B_s^0 \to D_s^+ 3\pi, D_s \to K^* K$ MC	2708 ± 55	1653 ± 40	$-39\% \pm 3\%$

Table 24: Loss in $B_s^0 \to D_s^+ 3\pi, D_s \to K^* K$ signal yield due to D^+ veto for data and Monte Carlo

Mode	$B^0 \to D^+ a_1$	$B^0 \to D^+ \rho\pi$	$B^0 \to D^+ 3\pi$	Tot
ϵ^{tot} (%)	0.0218 ± 0.0002	0.0206 ± 0.0002	0.0208 ± 0.0002	0.0213 ± 0.0002

Table 25: Monte Carlo Efficiencies for the components of the B^0 signal. `B_CHARM` trigger only.

Varied Parameter	Variation	Min	Max	Diff
$B^0 \to D^+3\pi$		3288 ± 76	3288 ± 76	
Mass Range	[4.6, 6.5]	3288 ± 76	3314 ± 77	1.0%
PhysBG Norm	$\pm 1\sigma$	3322 ± 74	3266 ± 76	0.6%
Cabibo Norm	$\pm 50\%$	3304 ± 75	3270 ± 78	0.5%
Λ_b Norm	$\pm 50\%$	3289 ± 76	3287 ± 76	0.0%
B_s Norm	$\pm 50\%$	3299 ± 77	3278 ± 77	0.3%
$B_s \to D_s 3\pi(\phi\pi)$		160 ± 17	160 ± 17	
Width	$\pm 1\sigma$	159 ± 17	162 ± 17	$\pm 1.3\%$
$D_s \to f_0\pi$	$\pm 50\%$	157 ± 17	163 ± 17	$\pm 1.9\%$
$D_s X$	Sec 8.8	162 ± 16	165 ± 17	$\pm 3.0\%$
$B_s \to D_s K\pi\pi$	$\pm 1\sigma$	160 ± 17	161 ± 17	$\pm 0.6\%$
$B_s \to D_s K\pi\pi$ Mass Shift	± 2.5 MeV/c	160 ± 17	161 ± 17	$\pm 0.6\%$
$B_s \to D_s 3\pi(K^*K)$		90 ± 17	90 ± 17	
Width	$\pm 1\sigma$	88 ± 18	92 ± 18	$\pm 2.2\%$
Λ_b Norm	$\pm 50\%$	90 ± 17	90 ± 17	$\pm 0.0\%$
B^0 Norm	$\pm 1\sigma$	84 ± 18	97 ± 18	$\pm 7.8\%$
$D^+X(K\pi\pi)$ Norm	$\pm 50\%$	88 ± 17	93 ± 17	$\pm 3.3\%$
$D^0X(K\pi)$ Norm	$\pm 50\%$	89 ± 17	91 ± 17	$\pm 1.1\%$
$D_s \to KK\pi$	$\pm 1\sigma$	90 ± 17	90 ± 17	$\pm 0.0\%$
$D_s X$	Sec 8.8			$\pm 3.0\%$
$B_s \to D_s 3\pi(3\pi)$		49 ± 11	49 ± 11	
Width	$\pm 1\sigma$	48 ± 10	49 ± 10	$\pm 2.0\%$
$D_s X$	Sec 8.8			$\pm 3.0\%$

Table 26: Fit systematic errors. Vary the most sensitive parameters. Entry *Sec 8.8* refers to the section where this systematic is described.

Effect	Syst. Uncertainty [%]
B_s lifetime	$\pm 2.1\%$
D_s^+ lifetime	$\pm 0.0\%$
B^0 lifetime	$\pm 0.4\%$
D^+ lifetime	$\pm 0.0\%$

Table 27: Table of systematic uncertainties due to uncertainties on meson lifetimes

—	B^0	B_s
Generated	59999335	59999335
Passed	15733	13330
ϵ^{tot} (%)	0.0262 ± 0.0002	0.0222 ± 0.0002
Ratio(B_s/B^0)	old	new
—	0.8485 ± 0.0010	0.8473 ± 0.0010

Table 28: The Luminosity averaged and prescaled efficiencies for the combined `B_CHARM` and `LOWPT` triggers in 5.3.4 Monte Carlo. As obtained from Monte Carlo that introduced a 6 % inefficiency for a kaon to make a trigger track. From the comparison of the ratios of efficiencies we assign a 0.2 % systematic due to XFT simulation.

Effect	Syst. Uncertainty [%]
BP_T spectrum	±3.0%
B_s lifetime	±2.1%
Trigger	±1.1%
$B^0 \to D^- 3\pi$ composition	±2.5%
$D_s \to \pi\pi\pi$ composition	±3.0%
$B^0 \to D^+ 3\pi$ Fit	±1.3%
$B_s \to D_s 3\pi(\phi\pi)$ Fit	±3.9%
$B_s \to D_s 3\pi(K^* K)$ Fit	±9.3%
$B_s \to D_s 3\pi(\pi\pi\pi)$ Fit	±3.6%
Selection Requirements	±5.0%
Common	±6.9%
$B_s \to D_s 3\pi(\phi\pi)$	±3.9%
$B_s \to D_s 3\pi(K^* K)$	±9.3%
$B_s \to D_s 3\pi(\pi\pi\pi)$	±4.7%

Table 29: Table of systematic errors.

11 Figures

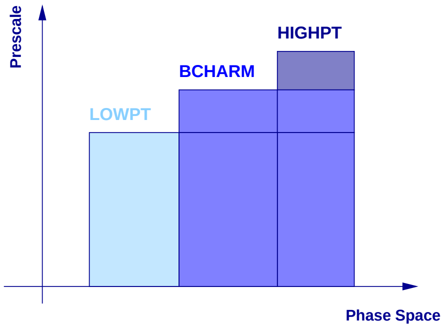

Figure 3: Picture representation of hadronic trigger paths. Visualise the selection requirements of the generalized triggers(phase space) versus the effective trigger prescale.

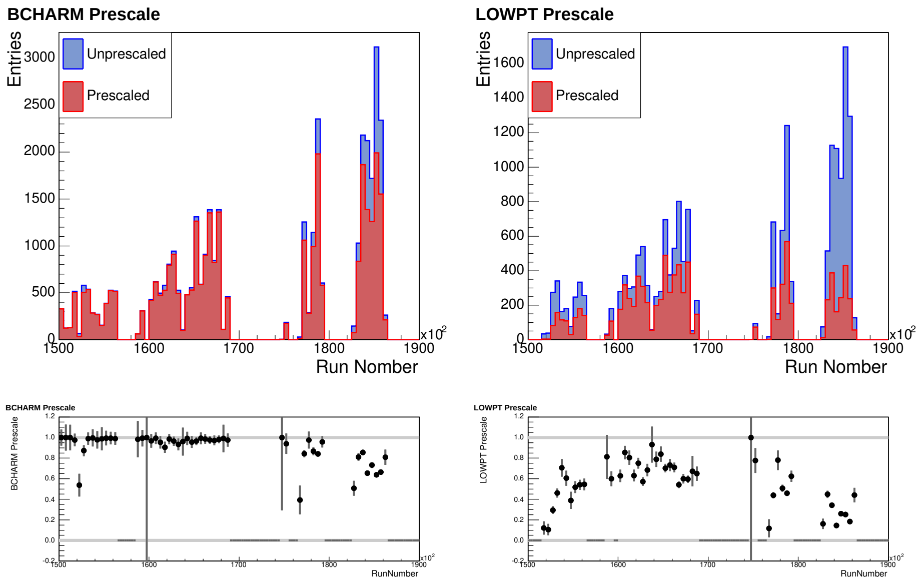

Figure 4: Implementation of effective prescale for every run. `B_CHARM` on the left and `LOWPT` on the right.

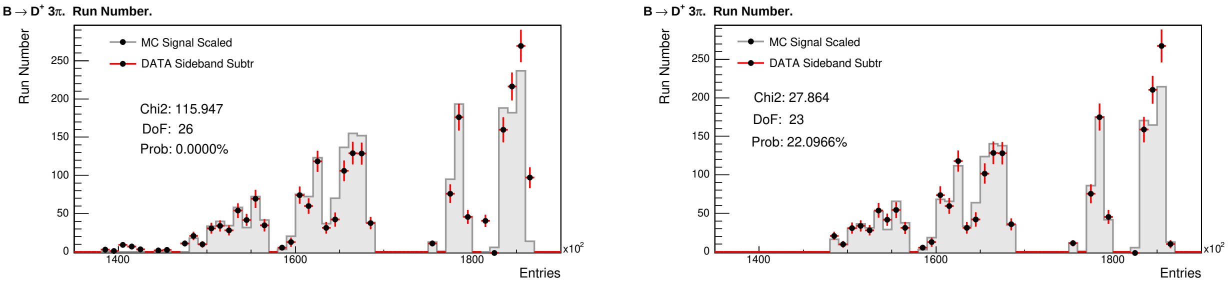

Figure 5: Run range comparison for data and Monte Carlo. Full luminocity on the left. Runs where Monte Carlo is missing removed on the right.

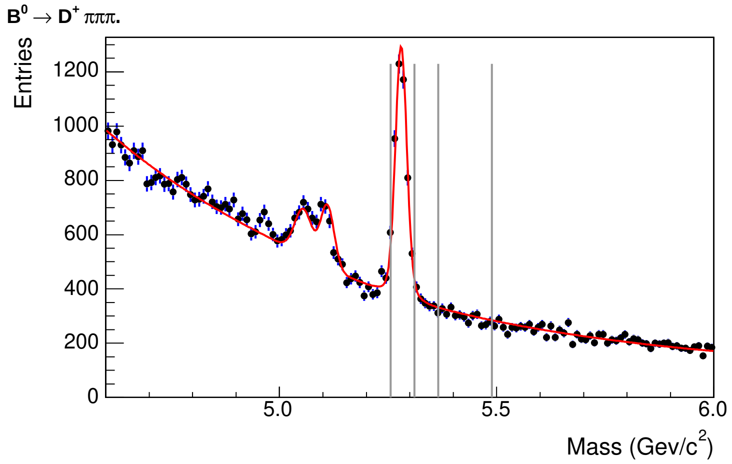

Figure 6: Sidebands used for data and MC compartison. Only right sideband is used due to the presence of physics background on the left.

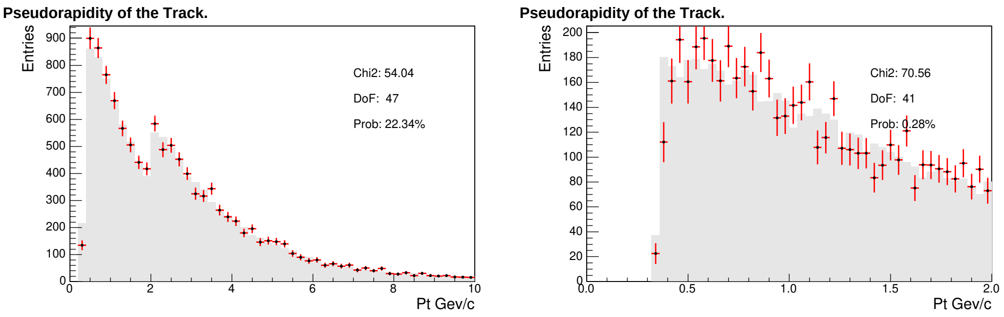

Figure 7: Compare signal $B^0 \to D^+3\pi$ Monte Carlo and sideband subtracted data. Transverse momentum of the track. Wide range on the left, zoom into low momentum on the right. All 6 tracks are used.

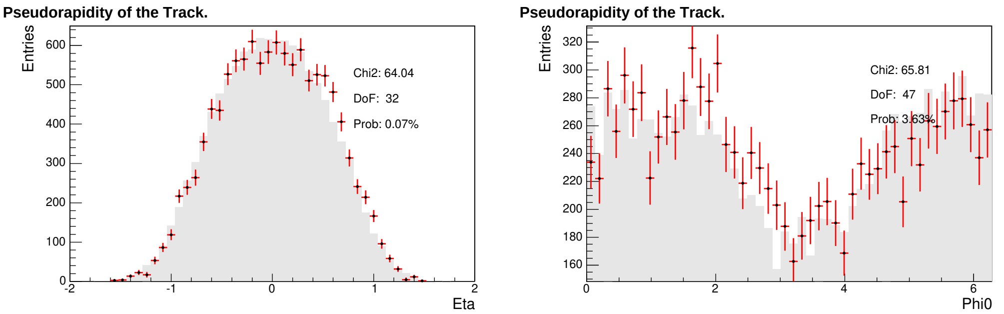

Figure 8: Compare signal $B^0 \to D^+3\pi$ Monte Carlo and sideband subtracted data. Pseudorapidity of the track on the left, ϕ_0 angle of the track on the right. All 6 tracks are used.

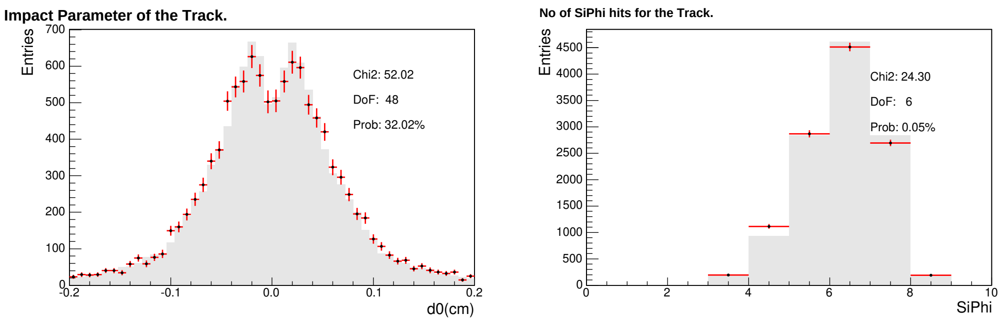

Figure 9: Compare signal $B^0 \to D^+3\pi$ Monte Carlo and sideband subtracted data. Impact parameter of the track on the left, Number of $R\phi$ silicon hits per track on the right. All 6 tracks are used.

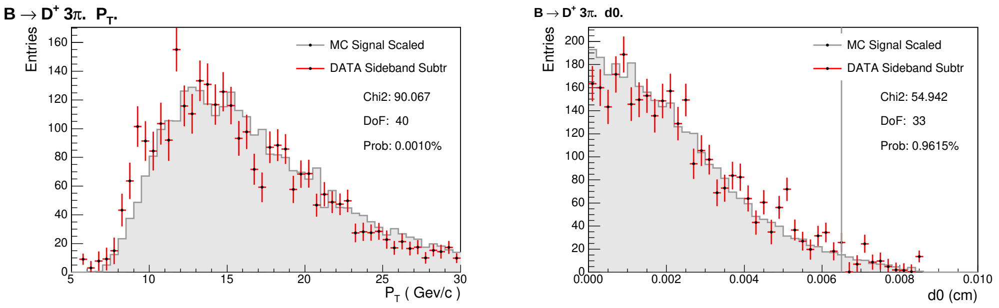

Figure 10: Data and MC comparison. Transverse momentum of the B_0 meson on the left. Impact parameter of the B_0 meson on the right.

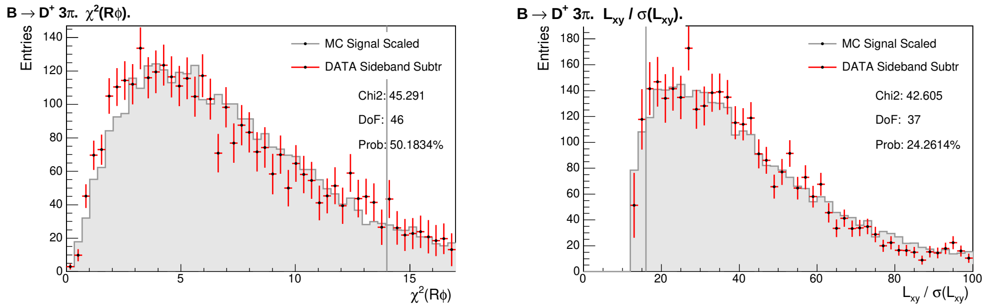

Figure 11: Data and MC comparison. $2D\chi^2$ of the B_0 meson on the left. L_{xy} significance of the B_0 meson on the right.

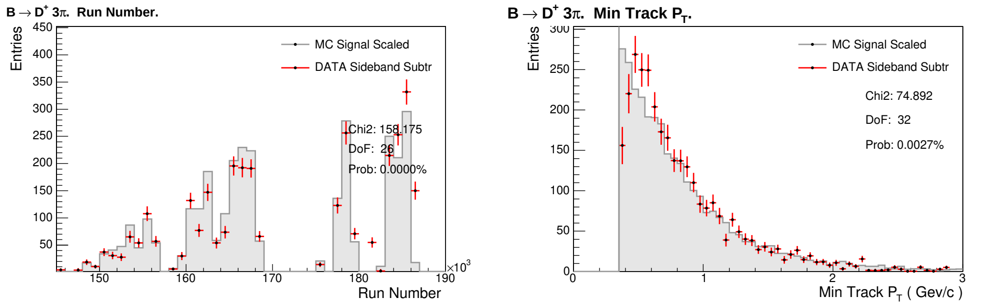

Figure 12: Compare signal $B^0 \to D^+3\pi$ Monte Carlo and sideband subtracted data. Run number of candidate on the left, minimum track p_T on the right.

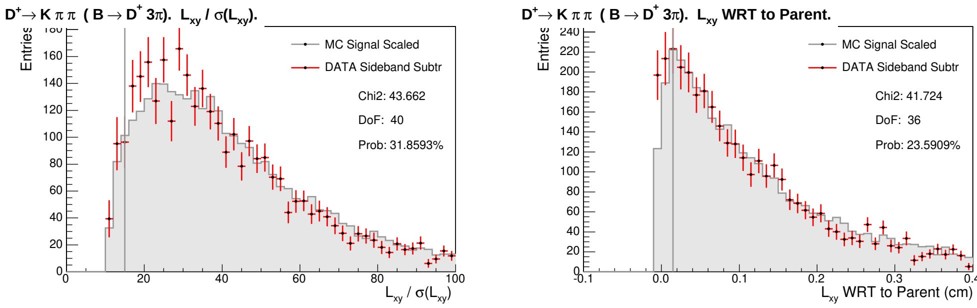

Figure 13: L_{xy} significance of the D^+ meson on the left. L_{xy} of the D^+ meson with respect to B_0 meson on the right..

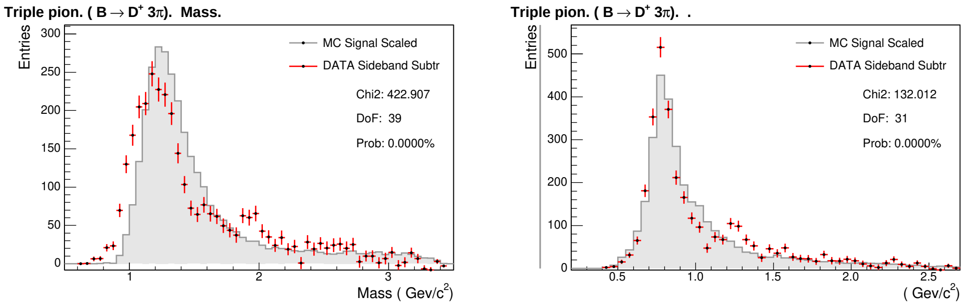

Figure 14: Compare signal $B^0 \to D^+3\pi$ Monte Carlo and sideband subtracted data. Invariant mass of the 3 pions on the left. Invariant mass of 2 pions on the right.

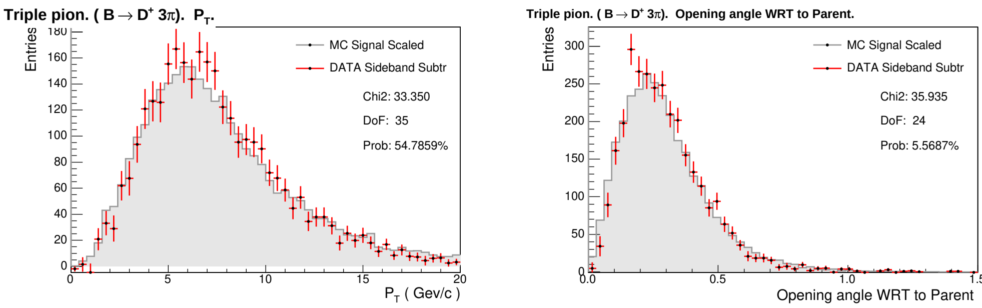

Figure 15: Compare signal $B^0 \to D^+3\pi$ Monte Carlo and sideband subtracted data. Transverse momentum of the 3π treated as a resonance and an opening angle of such a resonance with respect to B.

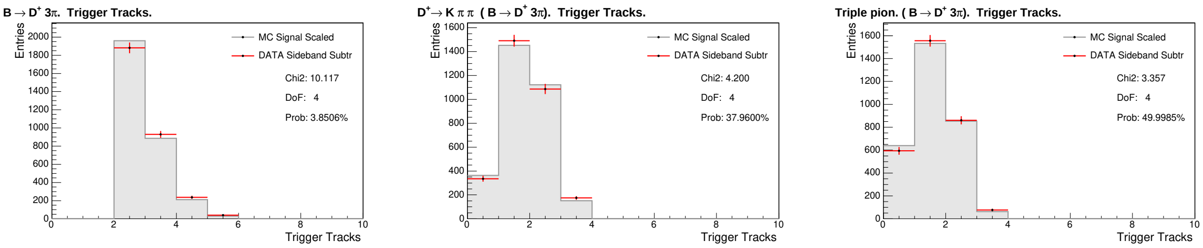

Figure 16: Compare signal $B^0 \to D^+3\pi$ Monte Carlo and sideband subtracted data. Number of trigger tracks among decay products of B-meson, D^+-meson and 3π.

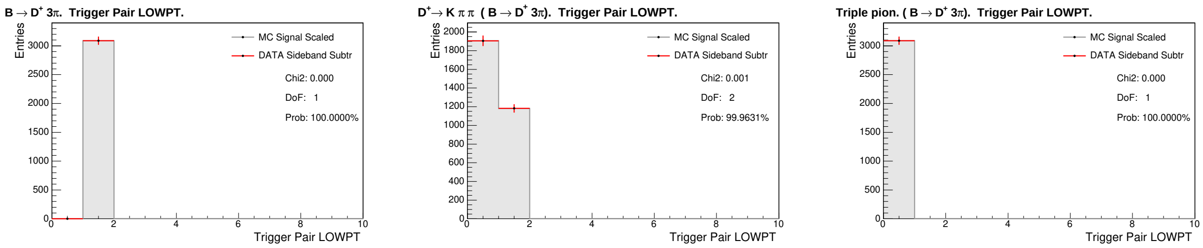

Figure 17: Compare signal $B^0 \to D^+3\pi$ Monte Carlo and sideband subtracted data. Number of `LOWPT` trigger pairs among decay products of B-meson, D^+-meson and 3π.

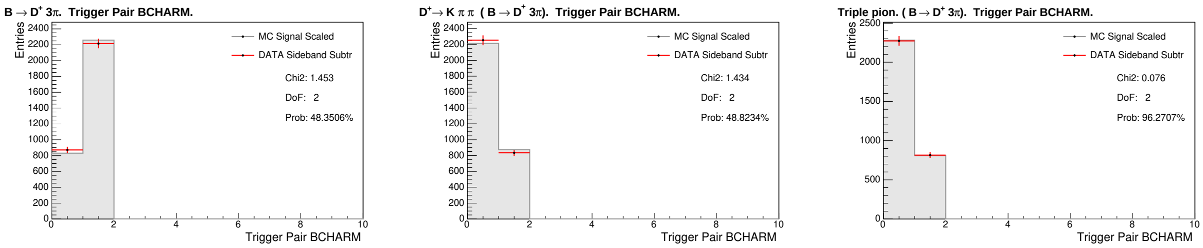

Figure 18: Compare signal $B^0 \to D^+3\pi$ Monte Carlo and sideband subtracted data. Number of `LOWPT` trigger pairs among decay products of B-meson, D^+-meson and 3π.

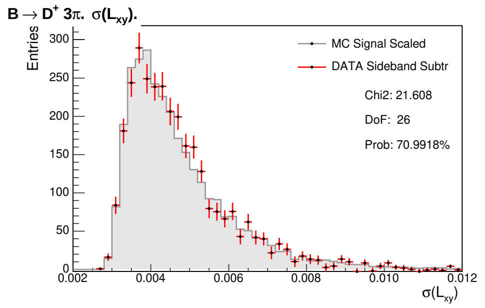

Figure 19: Compare signal $B^0 \to D^+ 3\pi$ Monte Carlo and sideband subtracted data. $\sigma(L_{xy})$ of B.

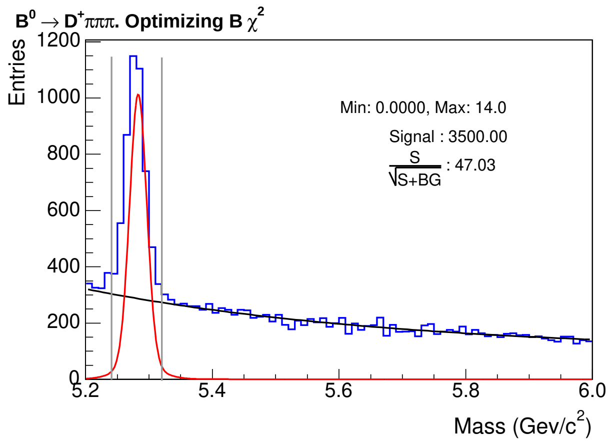

Figure 20: Fitting the signal and background during optimization. Plot shows a snapshot of the optimization process for L_{xy} significance of the B. Grey lines show the region used to calculate signal significance.

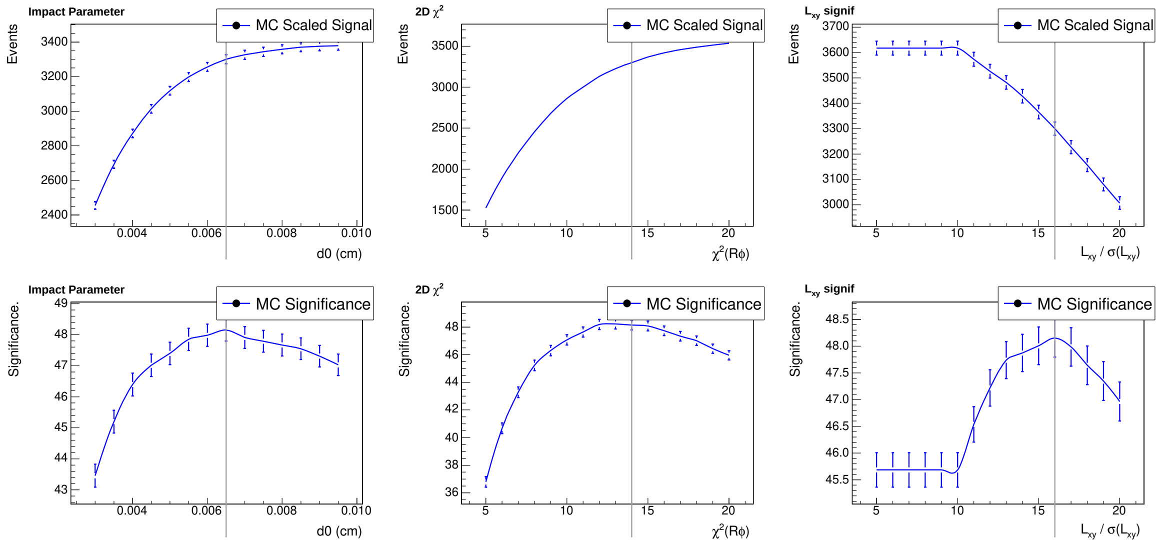

Figure 21: Cut optimization plots for $B^0 \rightarrow \ D^- 3\pi$: L_{xy} significance of the B, impact parameter of the B, and 2D χ^2 of the$B$ for B_CHARM and LOWPT combined Top plots show number of Monte Carlo scaled signal events, bottom plots - significance $\sigma = S/\sqrt{S+B}$ of the scaled Monte Carlo signal.

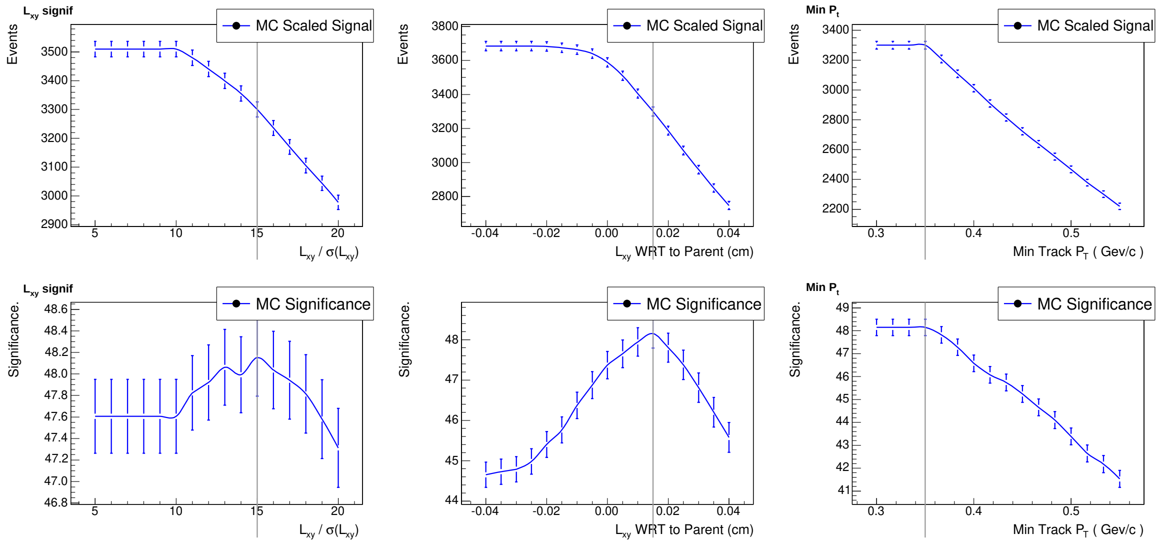

Figure 22: Cut optimization plots for $B^0 \rightarrow \ D^- 3\pi$: L_{xy} significance of the D^+, L_{xy} of the D^+ with respect to B and Minimum P_T of the track for B_CHARM and LOWPT combined Top plots show number of Monte Carlo scaled signal events, bottom plots - significance $\sigma = S/\sqrt{S+B}$ of the scaled Monte Carlo signal.

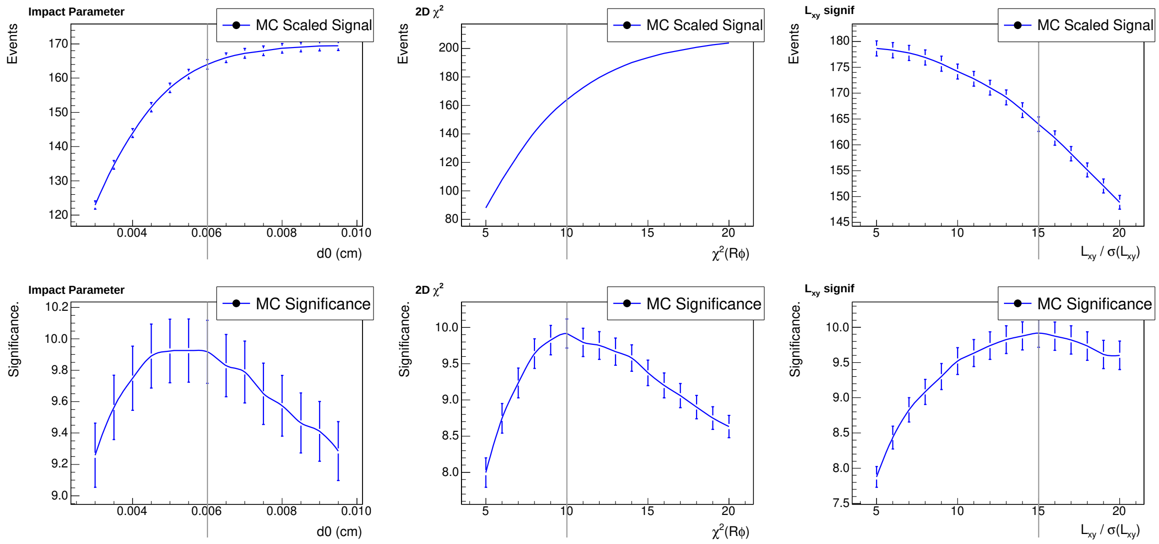

Figure 23: Cut optimization plots for $B_s^0 \rightarrow \ D_s^+ 3\pi, D_s \rightarrow \phi\pi$: L_{xy} significance of the B, impact parameter of the B, and 2D χ^2 of the$B$ for `B_CHARM` and `LOWPT` combined Top plots show number of Monte Carlo scaled signal events, bottom plots - significance $\sigma = S/\sqrt{S+B}$ of the scaled Monte Carlo signal.

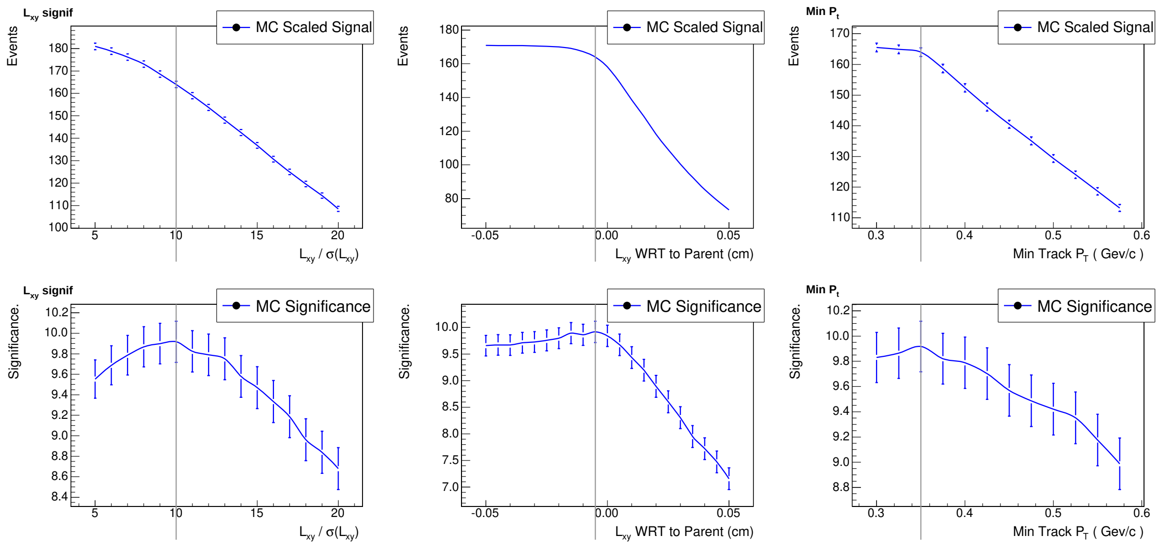

Figure 24: Cut optimization plots for $B_s^0 \rightarrow \ D_s^+ 3\pi, D_s \rightarrow \phi\pi$: L_{xy} significance of the D^+, L_{xy} of the D^+ with respect to B and minimum P_T of the track for `B_CHARM` and `LOWPT` combined Top plots show number of Monte Carlo scaled signal events, bottom plots - significance $\sigma = S/\sqrt{S+B}$ of the scaled Monte Carlo signal.

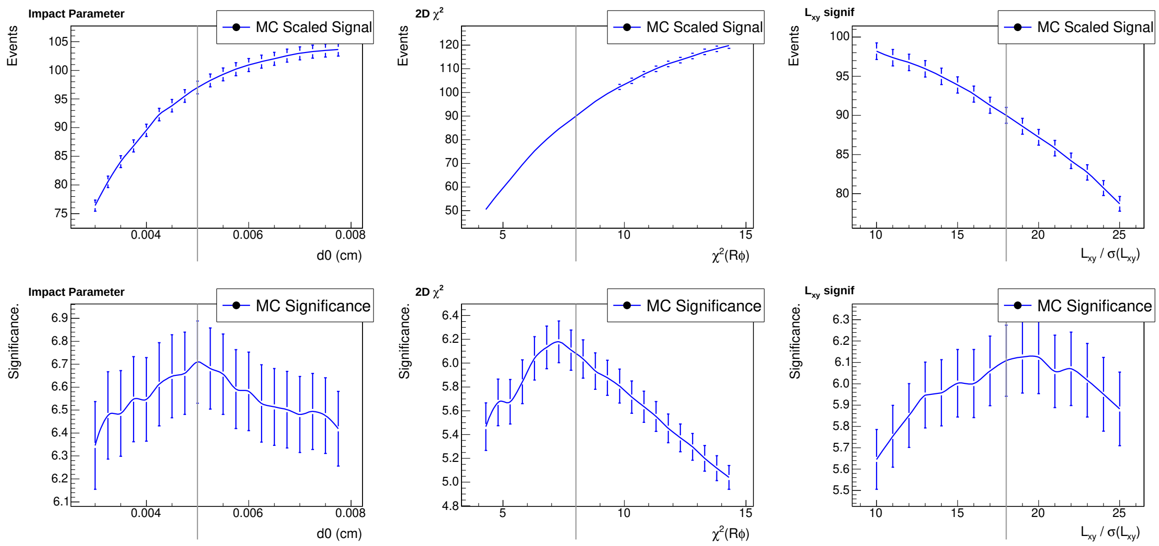

Figure 25: Cut optimization plots for $B_s^0 \to D_s^+ 3\pi, D_s \to K^* K$: L_{xy} significance of the B, impact parameter of the B, and 2D χ^2 of the$B$ for `B_CHARM` and `LOWPT` combined Top plots show number of Monte Carlo scaled signal events, bottom plots - significance $\sigma = S/\sqrt{S+B}$ of the scaled Monte Carlo signal.

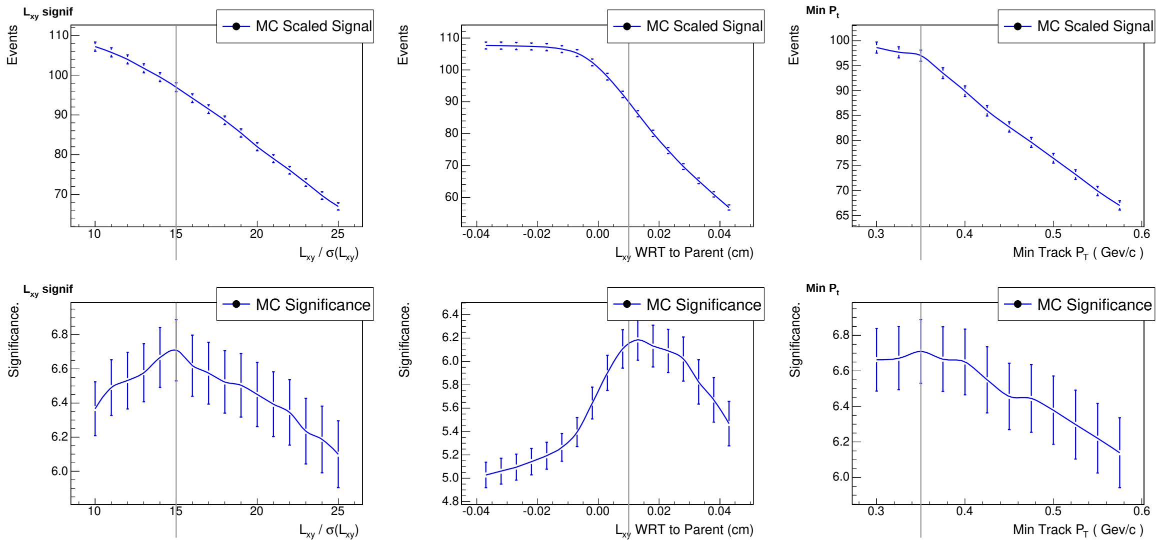

Figure 26: Cut optimization plots for $B_s^0 \to D_s^+ 3\pi, D_s \to K^* K$: L_{xy} significance of the D^+, L_{xy} of the D^+ with respect to B and minimum P_T of the track for `B_CHARM` and `LOWPT` combined Top plots show number of Monte Carlo scaled signal events, bottom plots - significance $\sigma = S/\sqrt{S+B}$ of the scaled Monte Carlo signal.

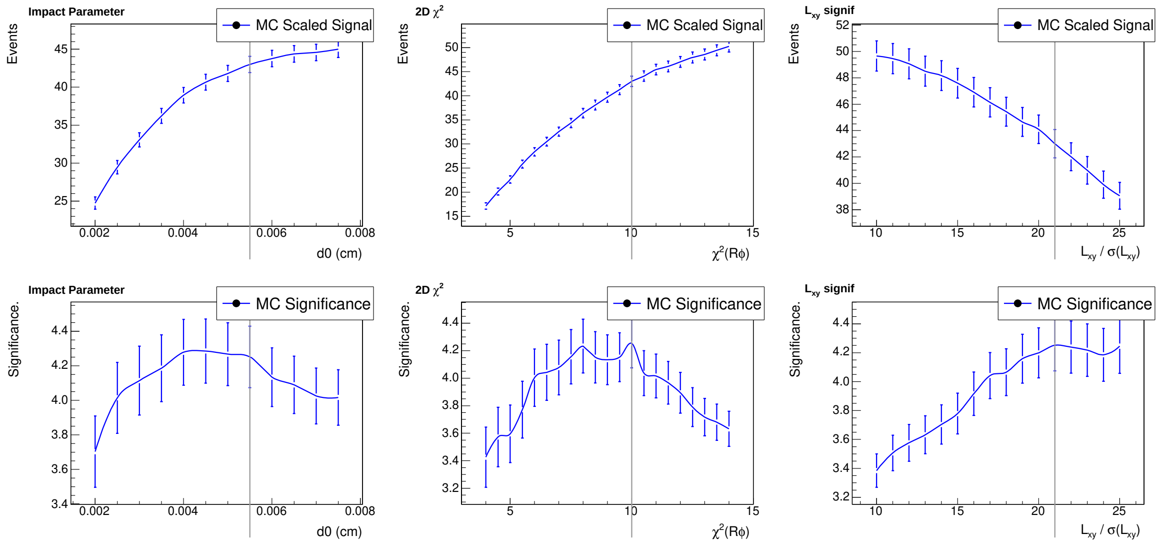

Figure 27: Cut optimization plots for $B_s^0 \rightarrow\ D_s^+ 3\pi, D_s \rightarrow \pi\pi\pi$: L_{xy} significance of the B, impact parameter of the B, and 2D χ^2 of the$B$ for B_CHARM and LOWPT combined Top plots show number of Monte Carlo scaled signal events, bottom plots - significance $\sigma = S/\sqrt{S+B}$ of the scaled Monte Carlo signal.

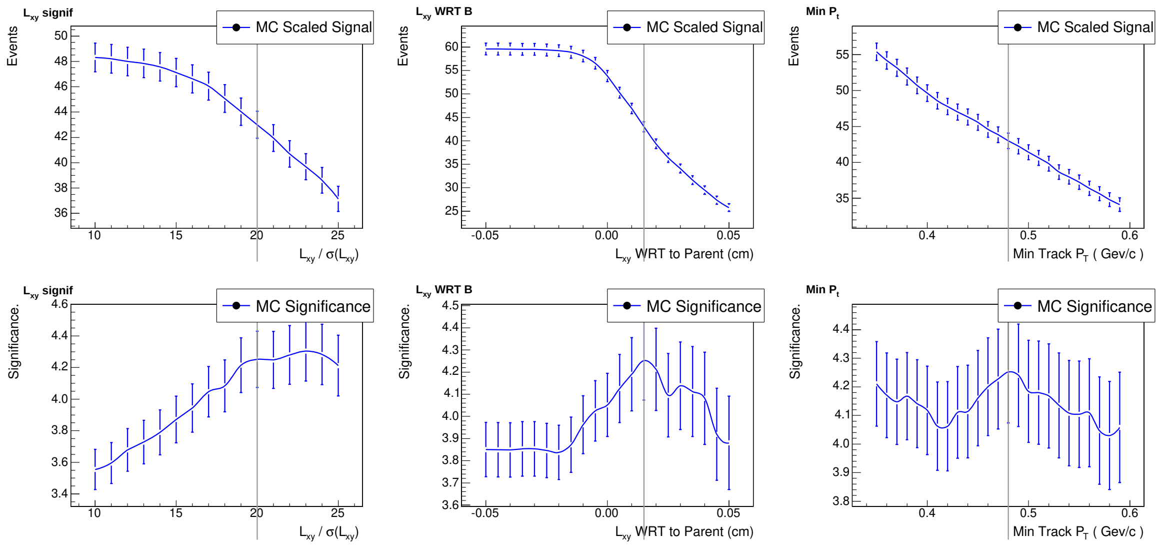

Figure 28: Cut optimization plots for $B_s^0 \rightarrow\ D_s^+ 3\pi, D_s \rightarrow \pi\pi\pi$: L_{xy} significance of the D^+, L_{xy} of the D^+ with respect to B and minimum P_T of the track for B_CHARM and LOWPT combined Top plots show number of Monte Carlo scaled signal events, bottom plots - significance $\sigma = S/\sqrt{S+B}$ of the scaled Monte Carlo signal.

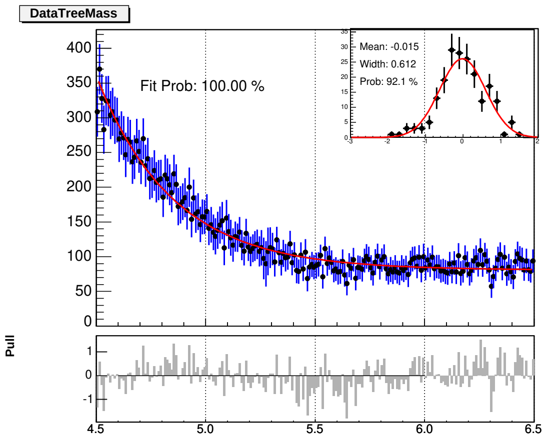

Figure 29: Templates for combinatorial background. Candidates with worng charge assignment are used.

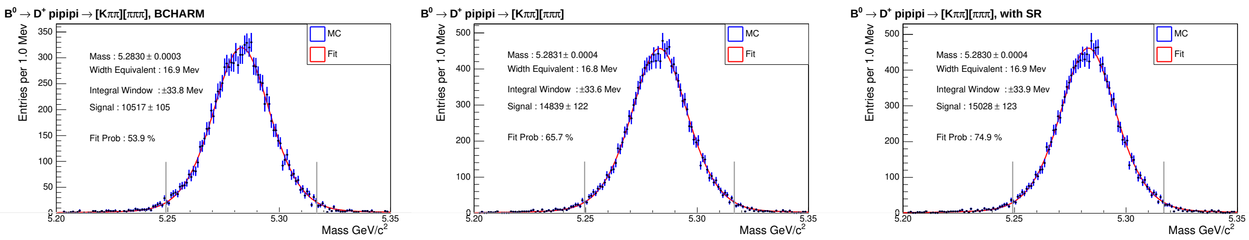

Figure 30: Signal Monte Carlo $B^0 \rightarrow D^- 3\pi$. `B_CHARM` on the left, `B_CHARM` and `LOWPT` combined in the middle and with self reflections not removed on the right. Used to extract template parameters and for efficiency studies.

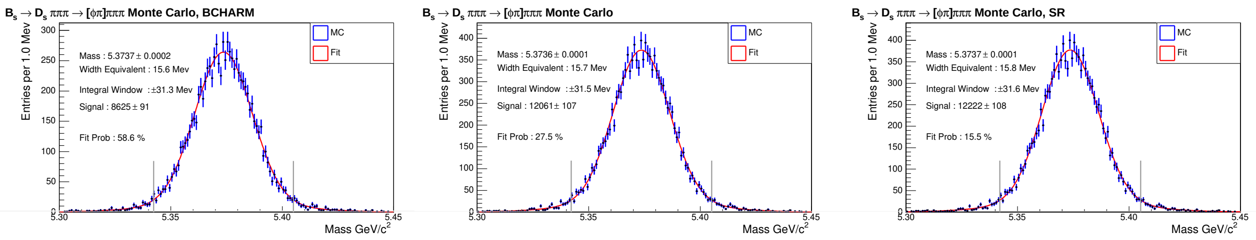

Figure 31: Signal Monte Carlo $B_s^0 \to D_s^+ 3\pi, D_s \to \phi\pi$. `B_CHARM` on the left, `B_CHARM` and `LOWPT` combined in the middle and with self reflections not removed on the right. Used to extract template parameters and for efficiency studies.

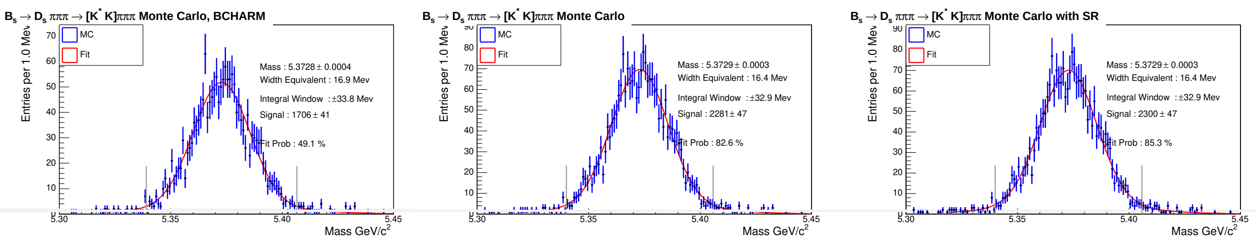

Figure 32: Signal Monte Carlo $B_s^0 \to D_s^+ 3\pi, D_s \to K^* K$. `B_CHARM` on the left, `B_CHARM` and `LOWPT` combined in the middle and with self reflections not removed on the right. Used to extract template parameters and for efficiency studies.

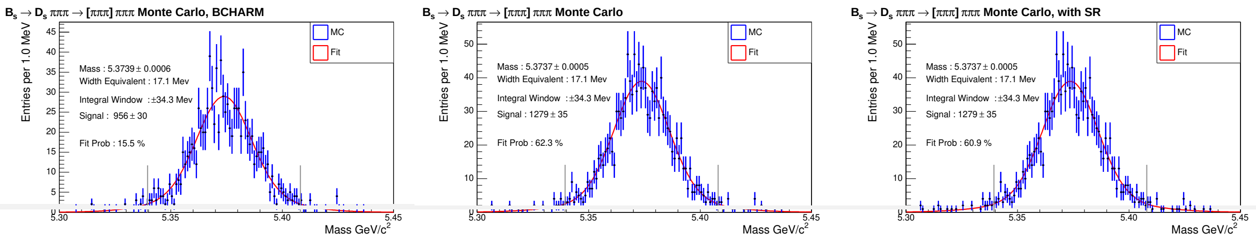

Figure 33: Signal Monte Carlo $B_s^0 \to D_s^+ 3\pi, D_s \to \pi\pi\pi$. `B_CHARM` on the left, `B_CHARM` and `LOWPT` combined in the middle and with self reflections not removed on the right. Used to extract template parameters and for efficiency studies.

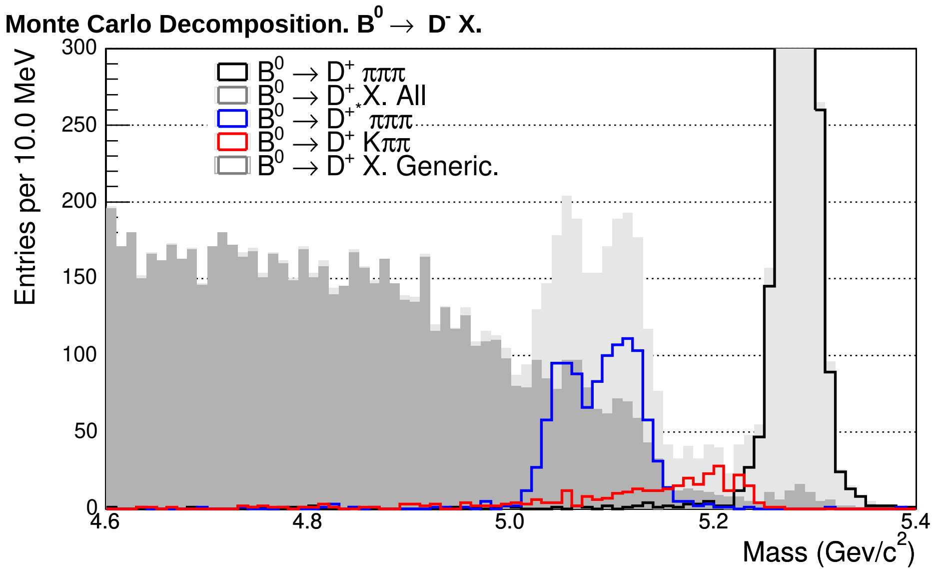

Figure 34: The decomposition of the semi-generic Monte Carlo into signal, Cabibo suppressed part, D^{+*} reflection and generic background.

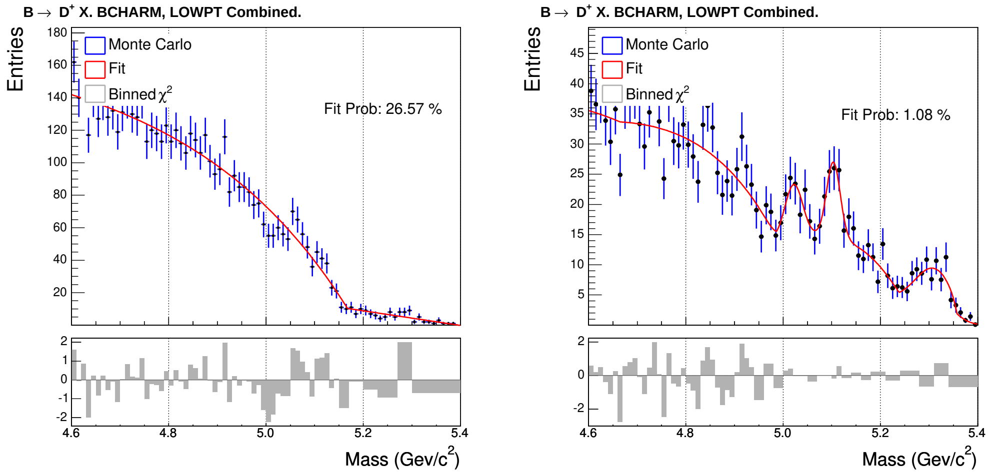

Figure 35: Templates for the generic background used in $B_d \to D^+ 3\pi$ fitting:

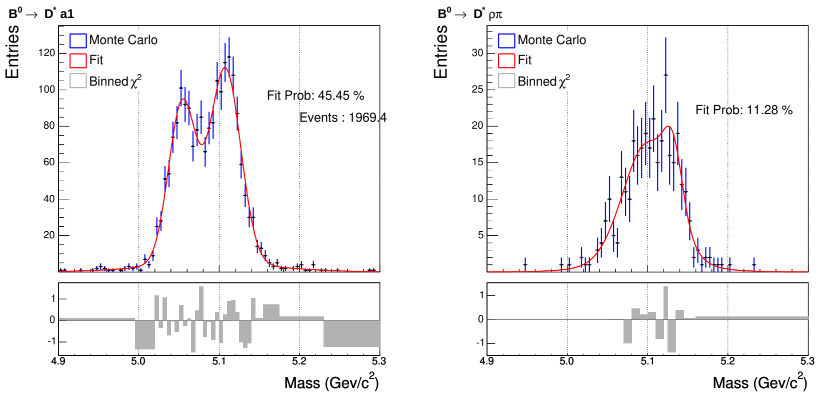

Figure 36: Templates for $B^0 \to D^* a_1$ and $B^0 \to D^* \rho\pi$ used to fit $B_d \to D^+ 3\pi$.

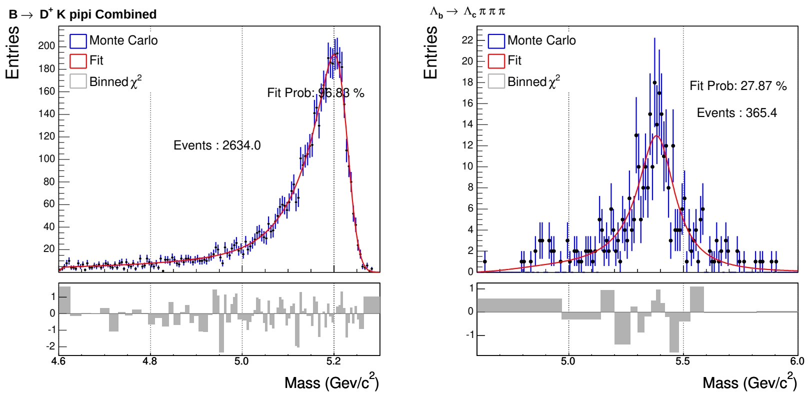

Figure 37: Templates for Cabibo and $\Lambda_b \to \Lambda_c \pi\pi\pi$ used to fit $B_d \to D^+ 3\pi$.

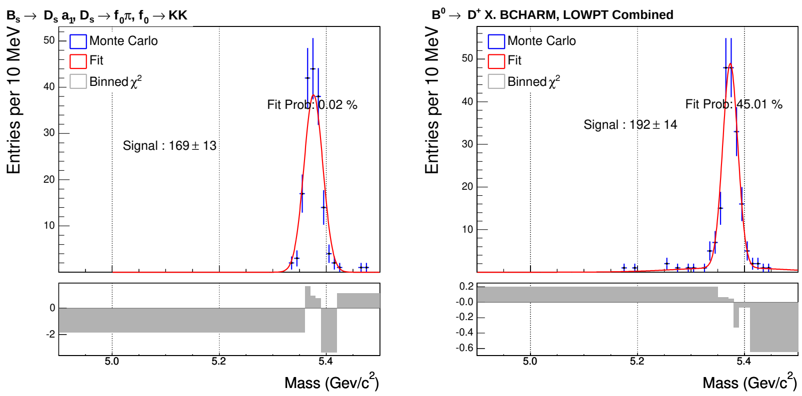

Figure 38: Templated for cross-talk. $B_s^0 \to D_s^+ 3\pi, D_s \to \phi\pi$ on the left and $B_s^0 \to D_s^+ 3\pi, D_s \to K^* K$ on the right.

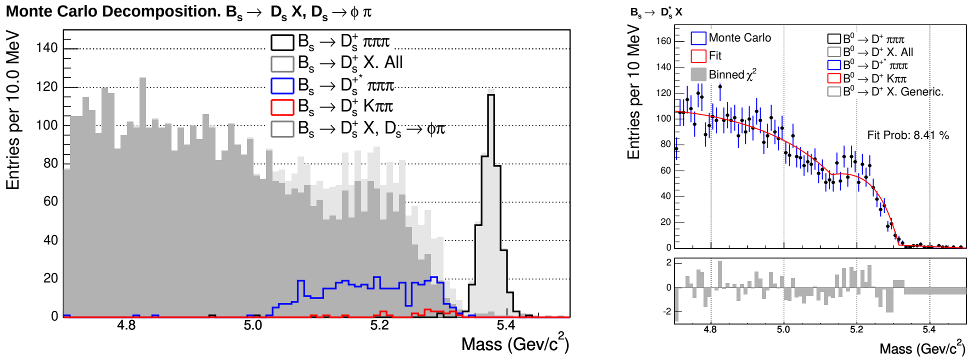

Figure 39: Background decomposition and templates for generic background used to fit $B_s^0 \to\ D_s^+ 3\pi, D_s \to \phi\pi$.

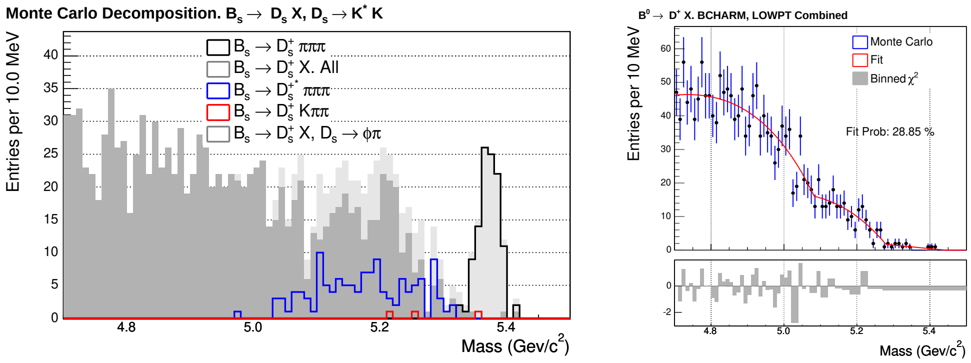

Figure 40: Background decomposition and templates for generic background used to fit $B_s^0 \to\ D_s^+ 3\pi, D_s \to K^* K$.

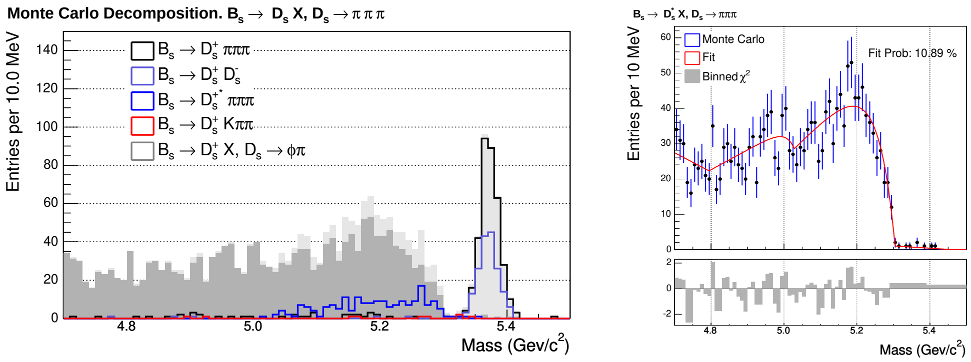

Figure 41: Background decomposition and generic background template for $B_s^0 \to\ D_s^+ 3\pi, D_s \to \pi\pi\pi$.

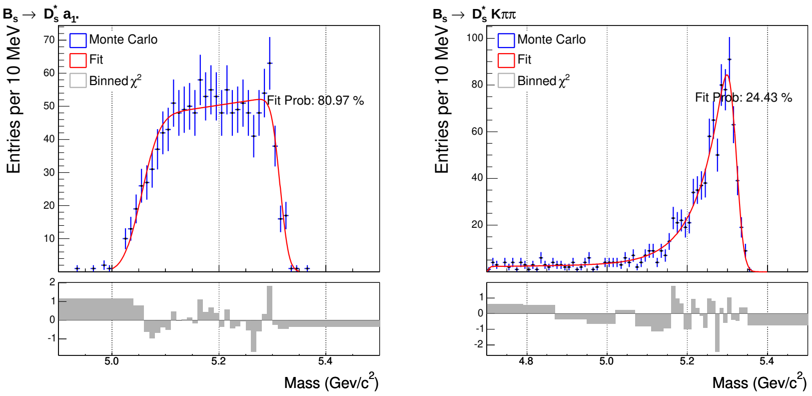

Figure 42: $B_S \to D_s^*$ and Cabibo templates for $B_s^0 \to \ D_s^+ 3\pi, D_s \to \phi\pi$.

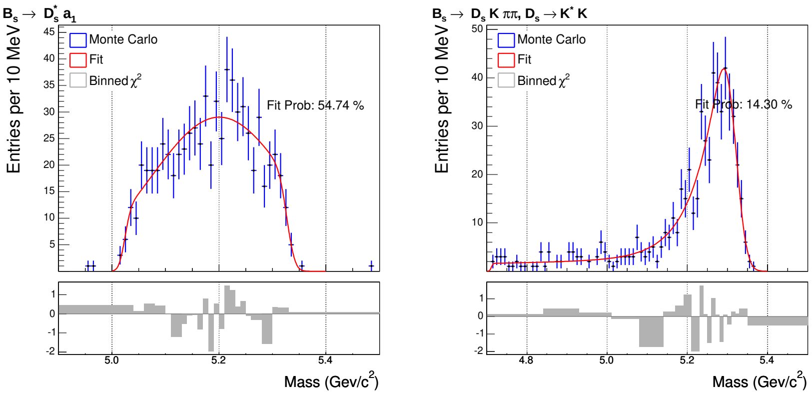

Figure 43: $B_S \to D_s^*$ and Cabibo templates for $\ B_s^0 \to \ D_s^+ 3\pi, D_s \to K^* K$.

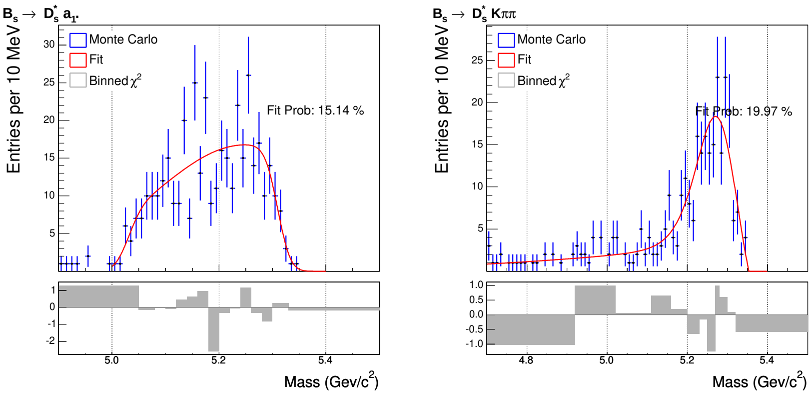

Figure 44: $B_S \to D_s^*$ and Cabibo templates for $B_s^0 \to \ D_s^+ 3\pi, D_s \to \pi\pi\pi$.

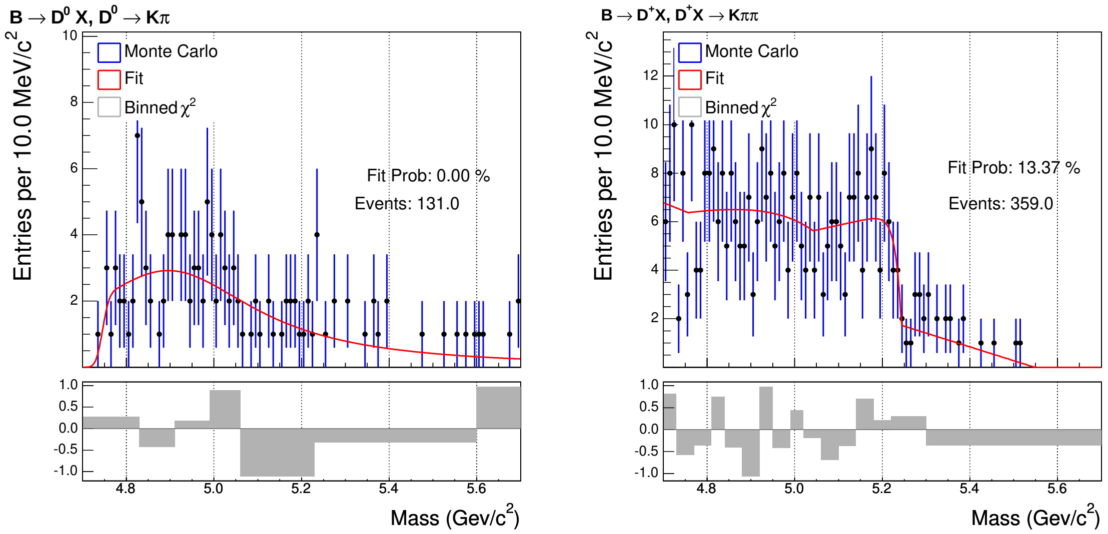

Figure 45: $B \to D^0 X, D^0 \to K\pi$ and $B \to D^+ X, D^+ \to K\pi\pi$ semi-generic templates used to fit $B_s^0 \to D_s^+ 3\pi, D_s \to K^* K$. $B^0 \to D^- 3\pi$ is removed.

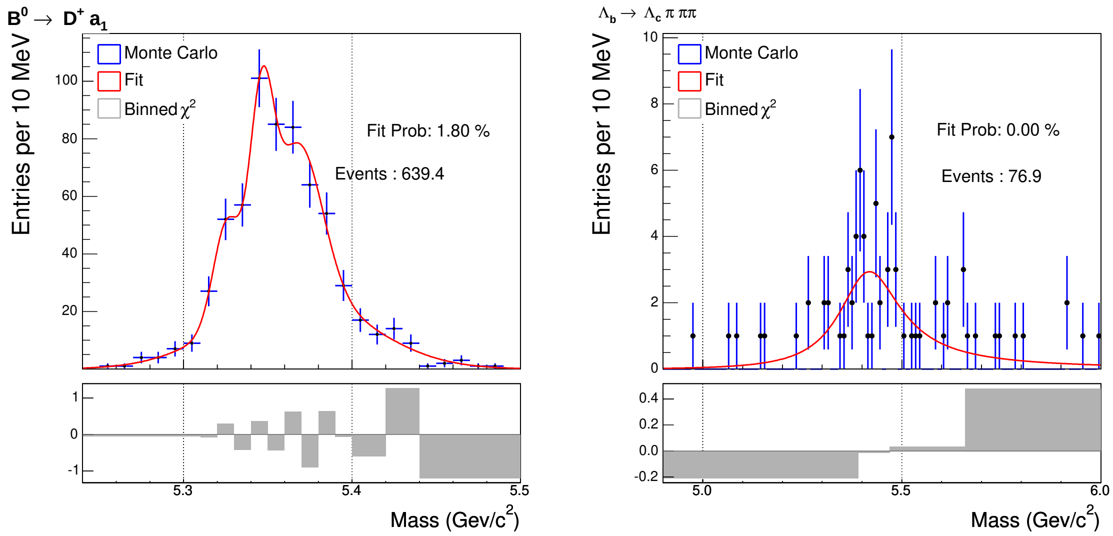

Figure 46: $B^0 \to D^- 3\pi$ and $\Lambda_b \to \Lambda_c \pi\pi\pi$ templates used to fit $B_s^0 \to D_s^+ 3\pi, D_s \to K^* K$.

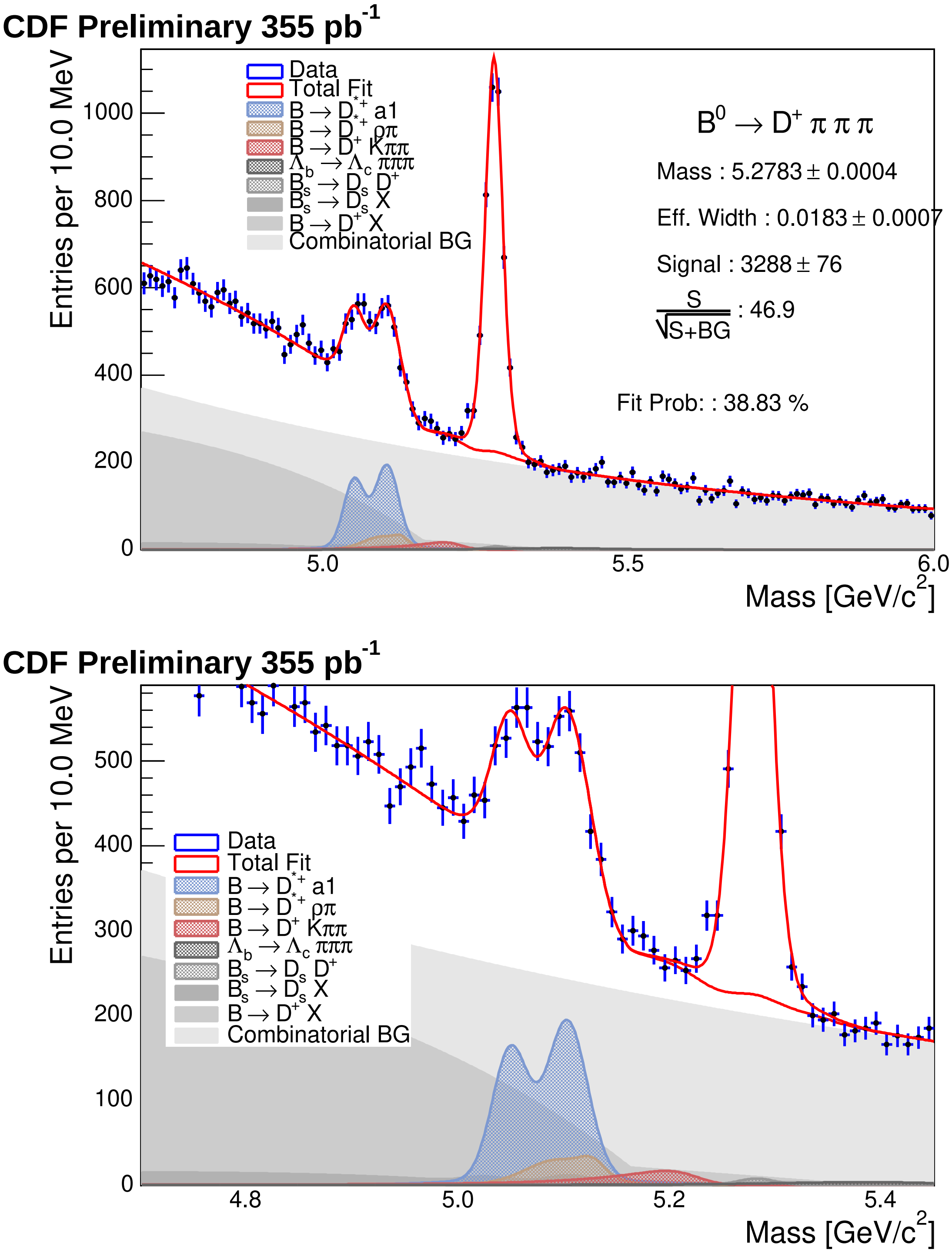

Figure 47: $B^0 \to\ D^- 3\pi$ Data Fit. Zoom into the signal region at the bottom.

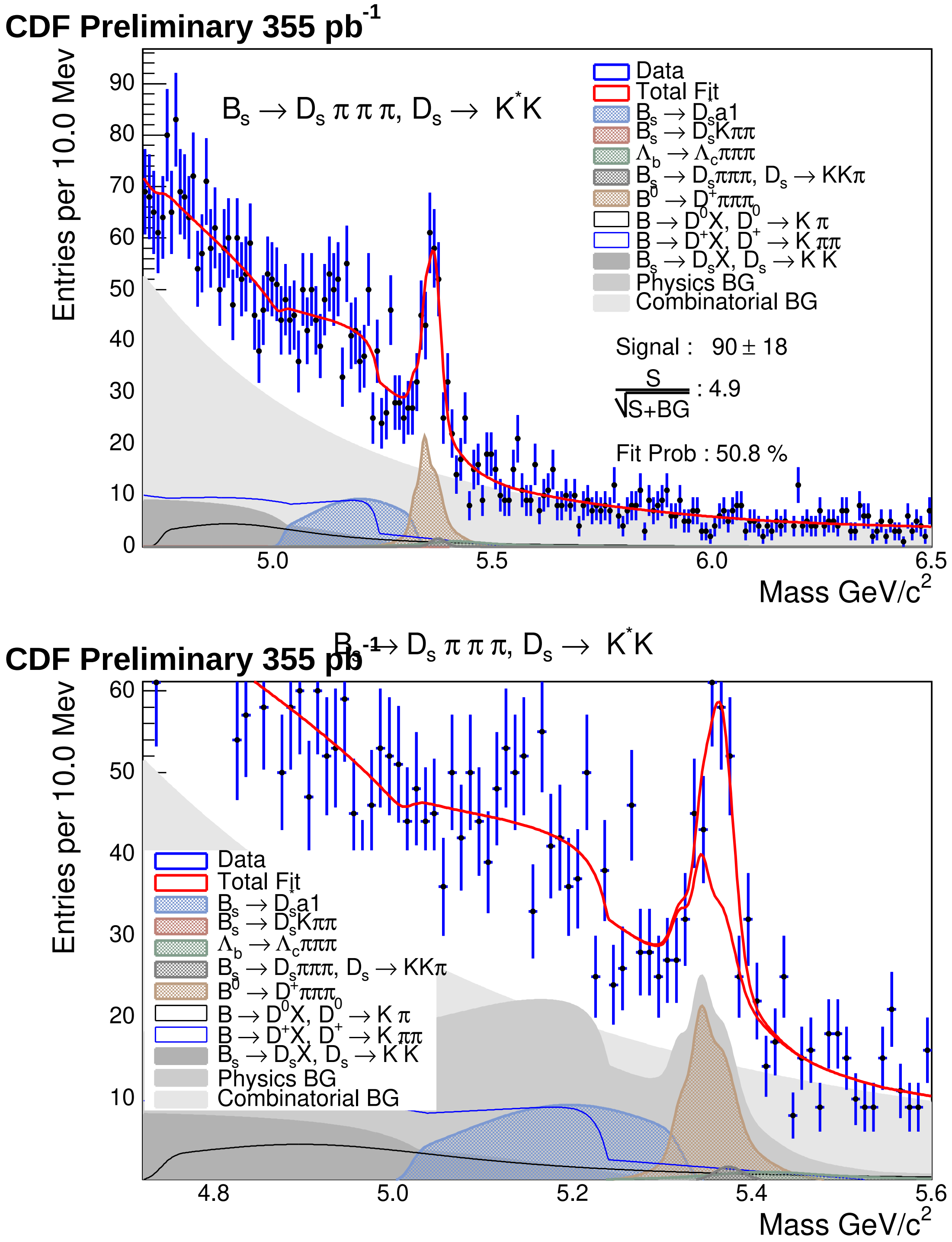

Figure 48: $B_s^0 \to\ D_s^+ 3\pi, D_s \to K^*K$ Data Fit. Zoom into the signal region at the bottom.

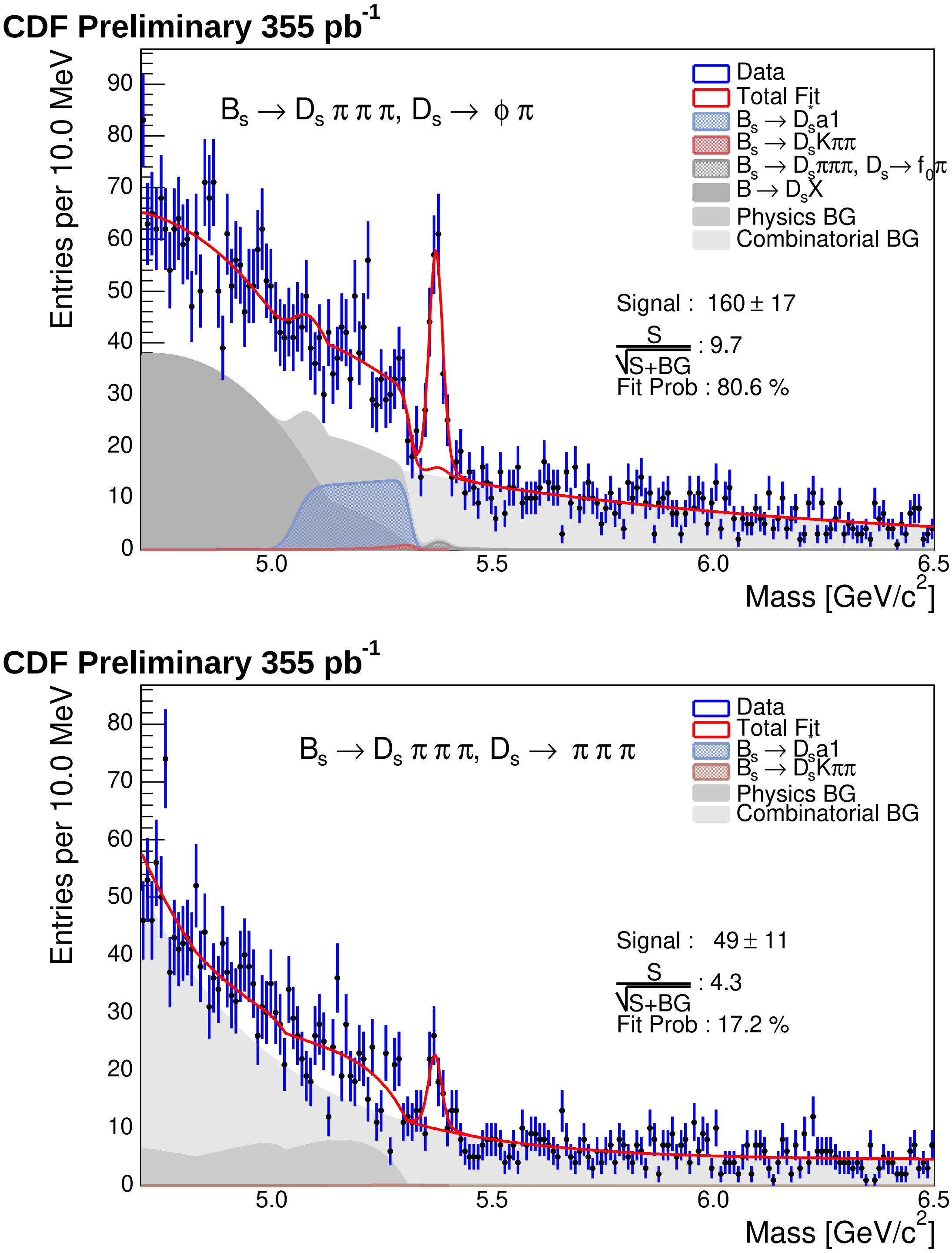

Figure 49: $B_s^0 \to\ D_s^+ 3\pi, D_s \to \phi\pi$ and $B_s^0 \to\ D_s^+ 3\pi, D_s \to \pi\pi\pi$ Data Fits.

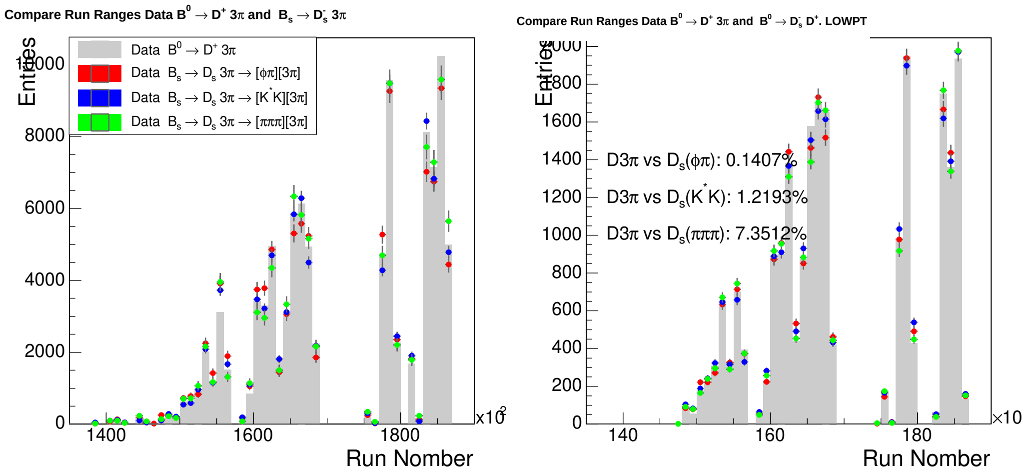

Figure 50: Comparing the run ranges for all four modes for Data and for Monte Carlo.

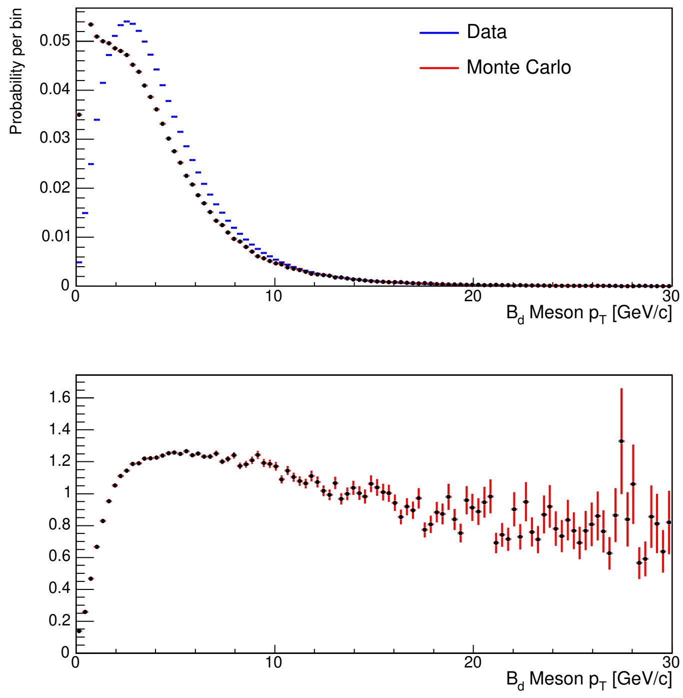

Figure 51: p_T spectra of B^0 mesons obtained from BGen Monte Carlo with Peterson fragmentation versus measured in $J/\psi X$ analysis.

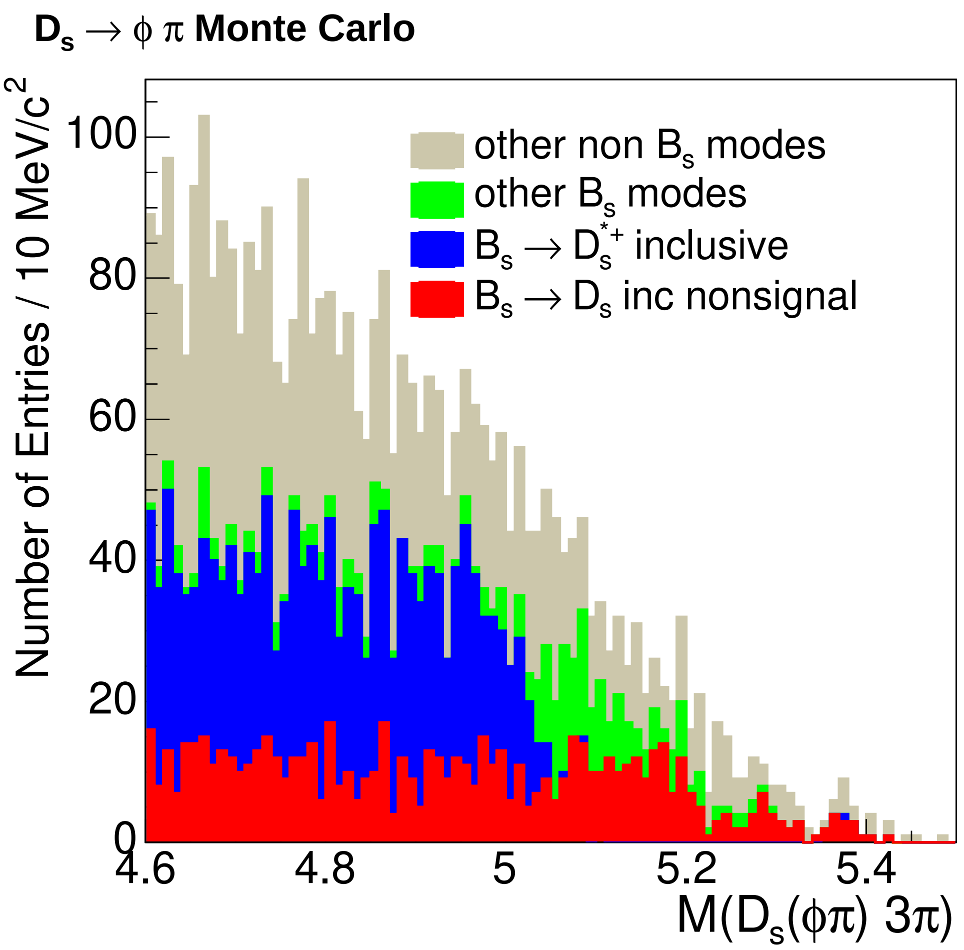

Figure 52: The plot shows the breakdown of continuum physics background for B_s meson into categories used to estimate the systematic error due to the limited knowledge of B_s branching fractions.

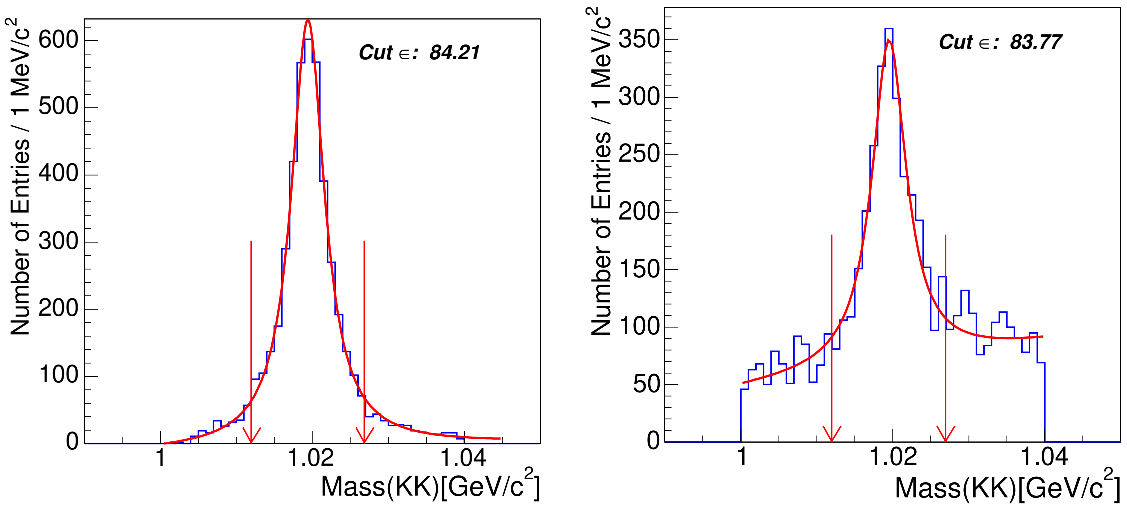

Figure 53: Comparison of ϕ^0 mass cut efficiency in Monte Carlo and data.

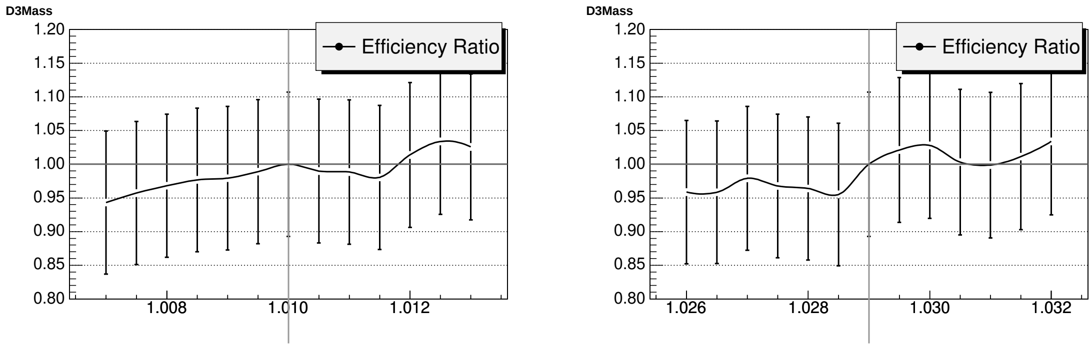

Figure 54: Ratio of ϕ^0 mass cut efficiency in Monte Carlo and data. The scans of the left and the right sides of the mass window.

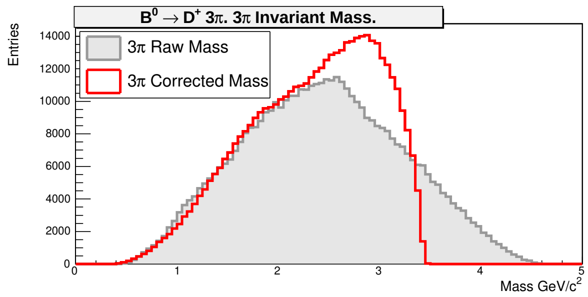

Figure 55: 3π invariant mass distribution for sideband corrected by sideband mass.

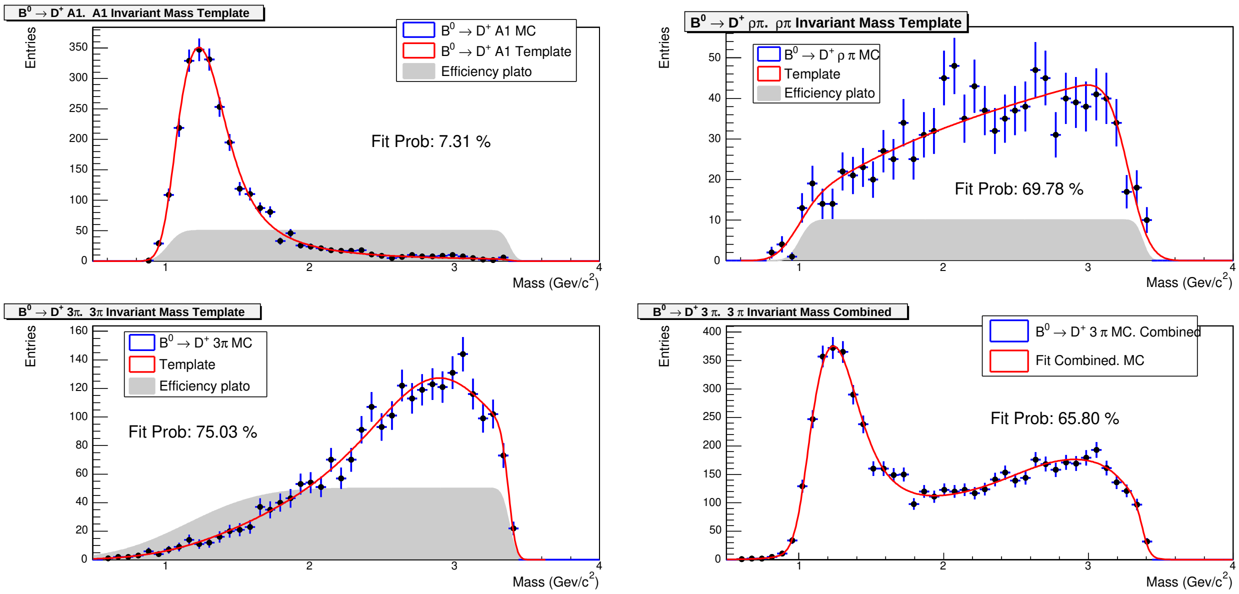

Figure 56: 3π invariant mass templates. $B^0 \to D^+a_1$ - top left, $B^0 \to D^+\rho\pi$ - top right, $B^0 \to D^+3\pi$- bottom left. Bottom right plot shows a combined templated fit of the default Monte Carlo.

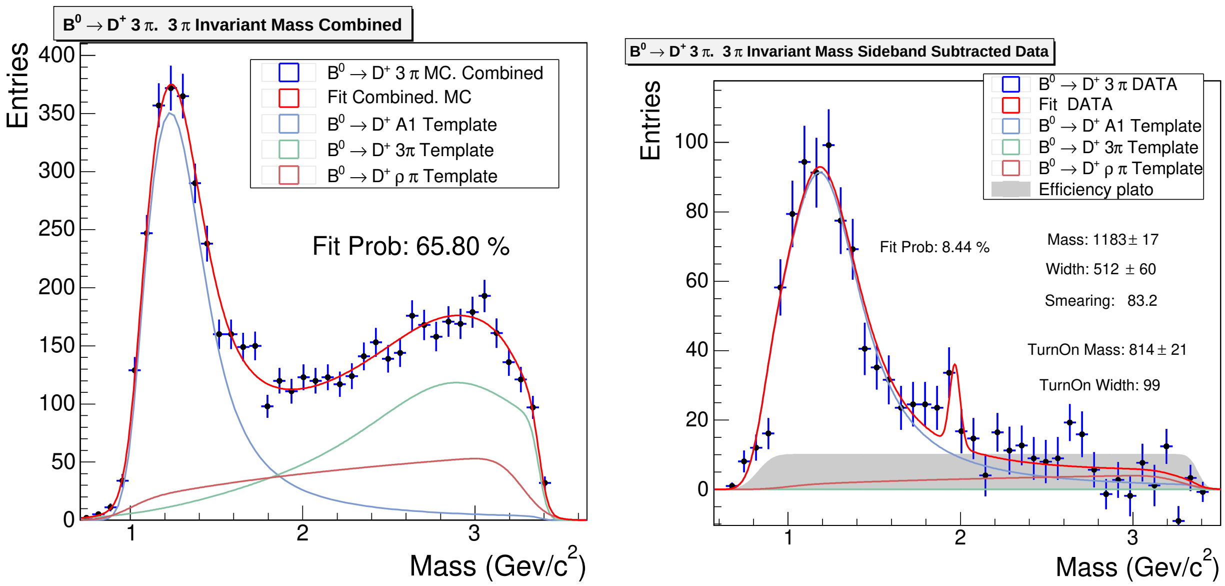

Figure 57: 3π invariant mass temlated fits. Default Monte Carlo on the left, $241pb^{-1}$ of B_CHARM data on the right.

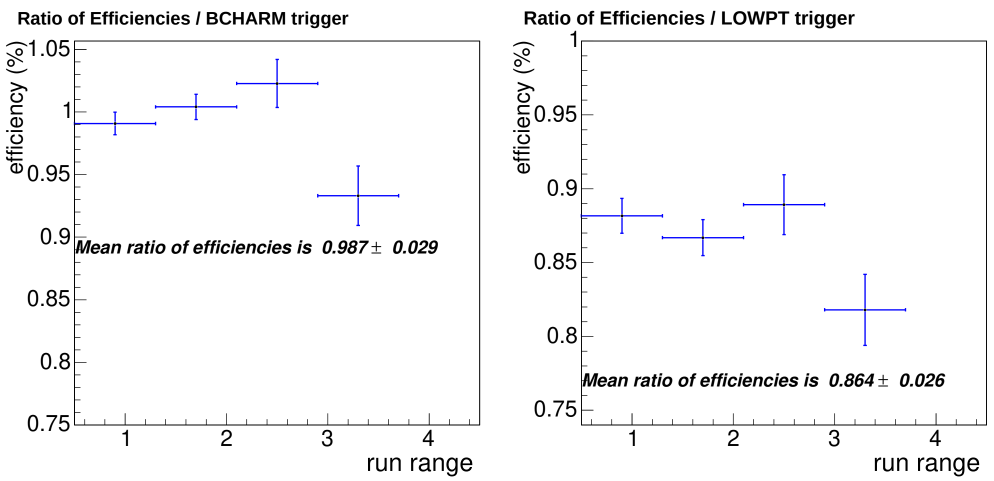

Figure 58: Ratio of efficiencies of $B^0 \rightarrow D^- 3\pi$ and $B^0_s \rightarrow D^+_s 3\pi$ calculated for four representative run ranges. `B_CHARM` data on the left, `LOWPT` data on the right.

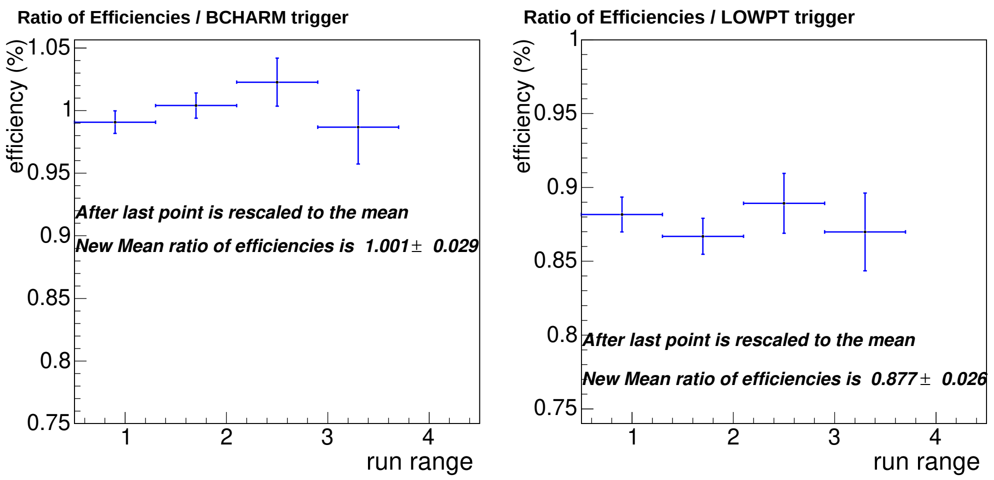

Figure 59: Ratio of efficiencies of $B^0 \rightarrow D^- 3\pi$ and $B^0_s \rightarrow D^+_s 3\pi$ calculated for four representative run ranges after the rescale of the last bin. `B_CHARM` data on the left, `LOWPT` data on the right.

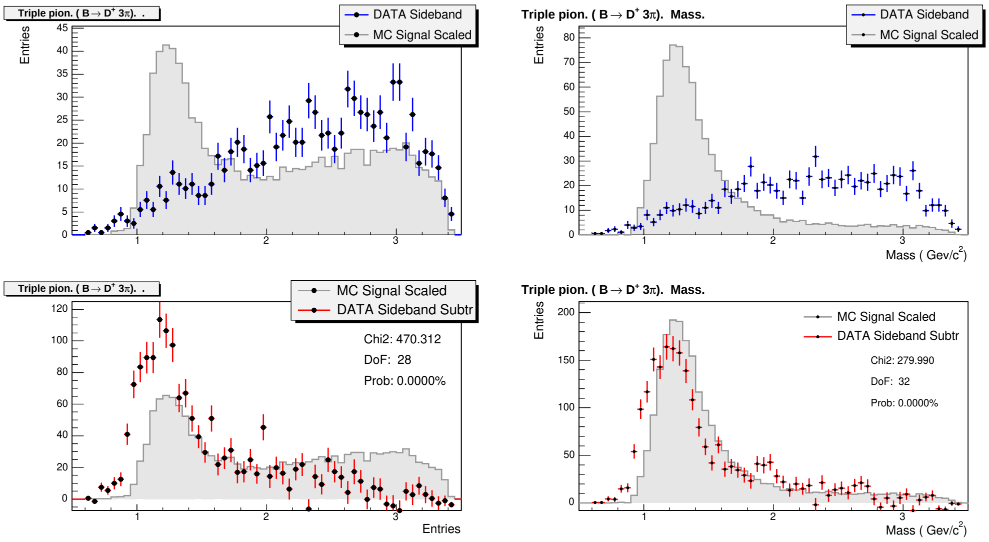

Figure 60: Separation and signal data comparison for the invariant Mass of 3π of B^0 meson. Default decay file compared with $241pb^{-1}$ of B_CHARM data on the left. Updated decay file compared with $355pb^{-1}$ of B_CHARM data on the right.

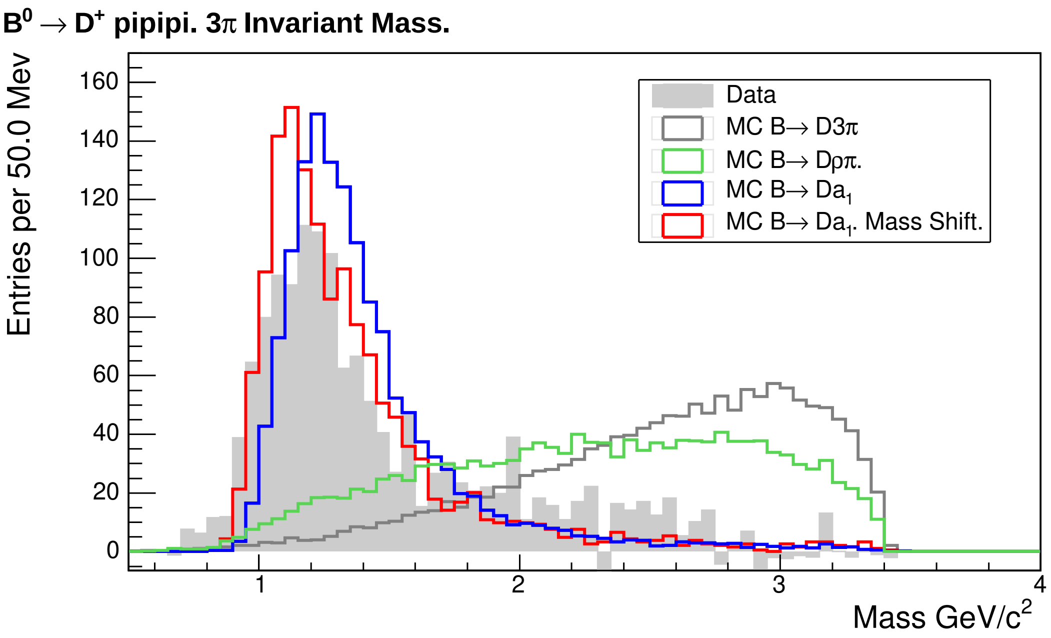

Figure 61: Comparing Monte Carlo 3π invariant mass spectrum for different signal components with data.

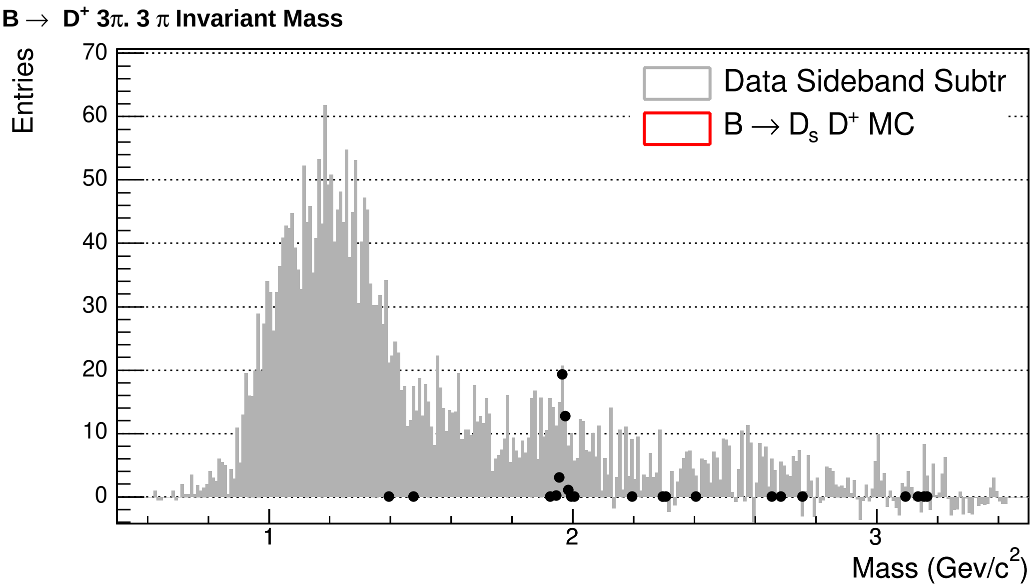

Figure 62: Comparing the 3π invariant mass data spectrum with scaled $B^0 \rightarrow\ D_s^+ D^-, D_s^+ \rightarrow$ $\pi\pi\pi$Monte Carlo contribution.

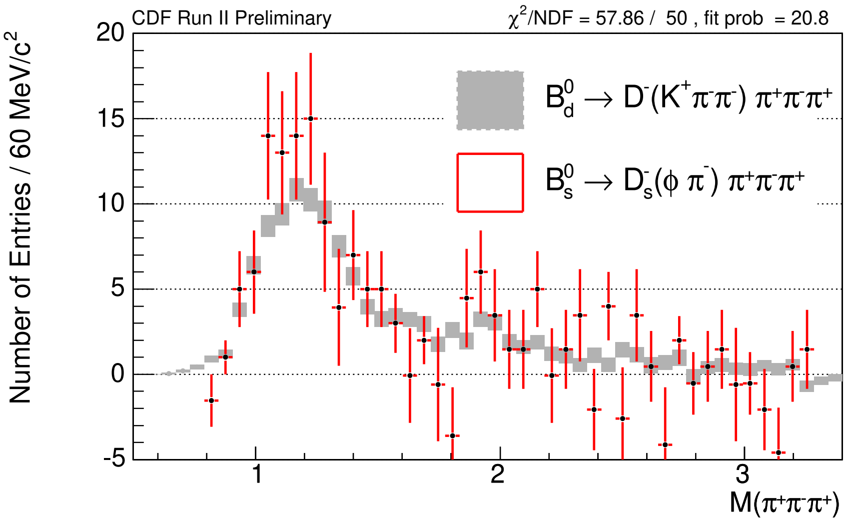

Figure 63: 3π invariant mass data comparison $B^0 \rightarrow\ D^- 3\pi$ and $B_s^0 \rightarrow\ D_s^+ 3\pi, D_s \rightarrow \phi\pi$.

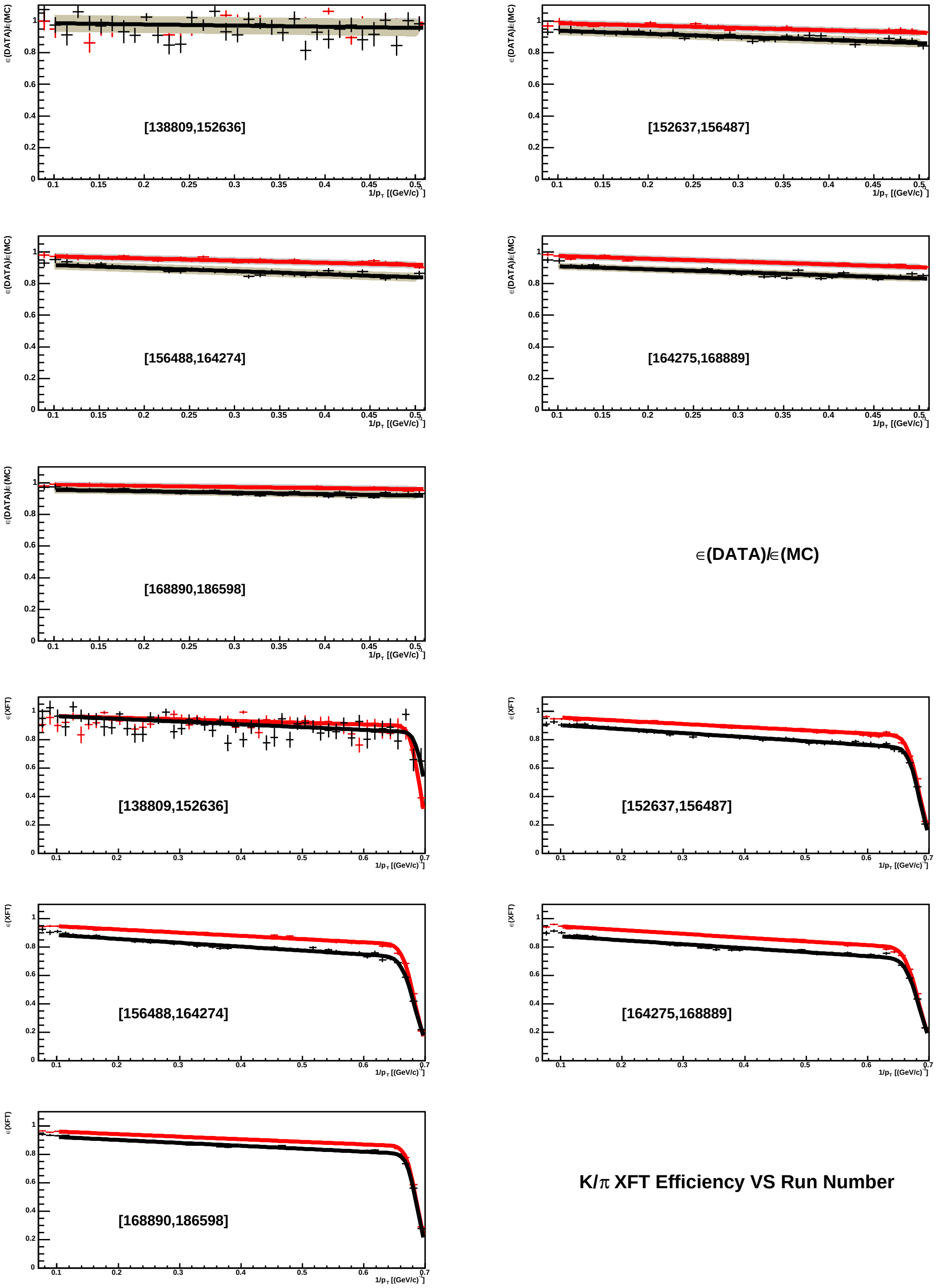

Figure 64: Plots showing the XFT efficiency of kaons relative to pions as a function of run number and inverse p_T of the track. Provided by [21].

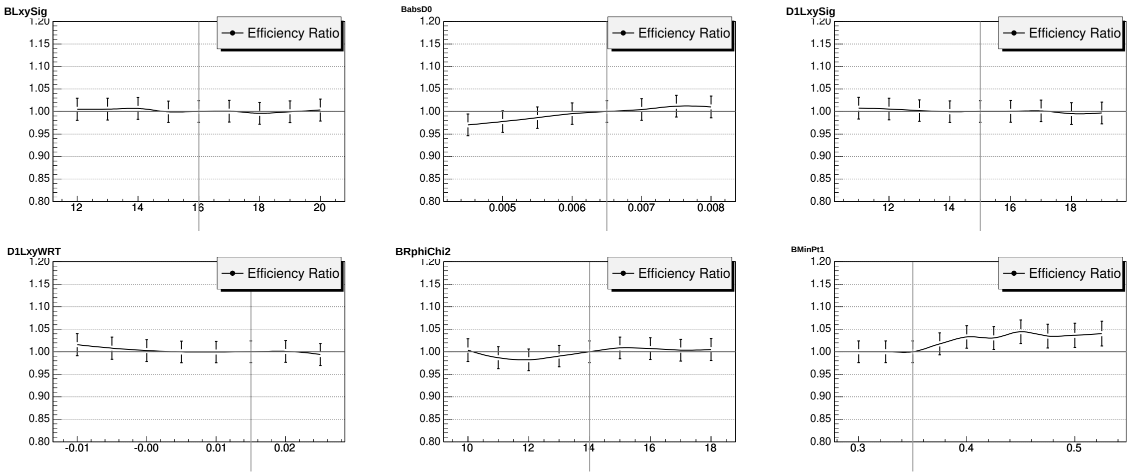

Figure 65: Cut systematics for $B^0 \to\ D^-3\pi$.

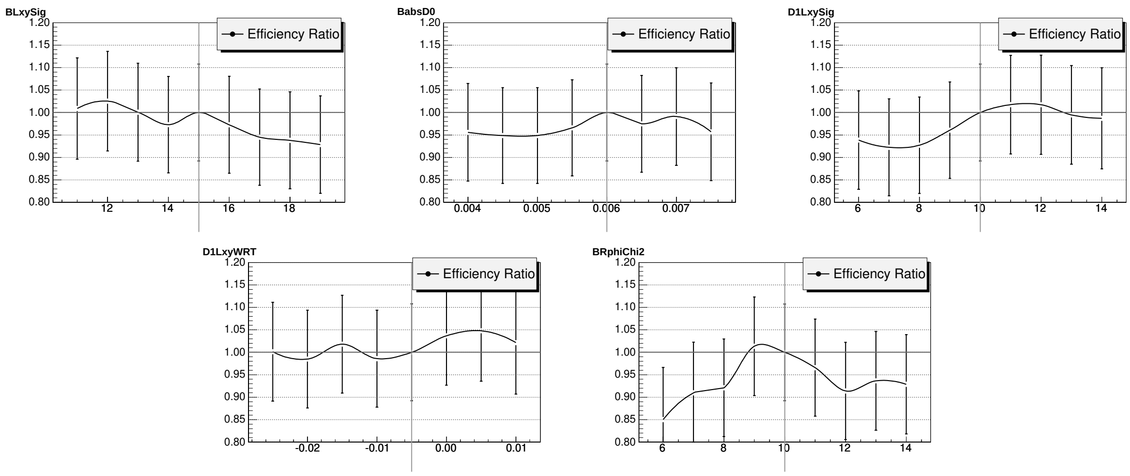

Figure 66: Cut systematics for $B_s^0 \to\ D_s^+3\pi$.

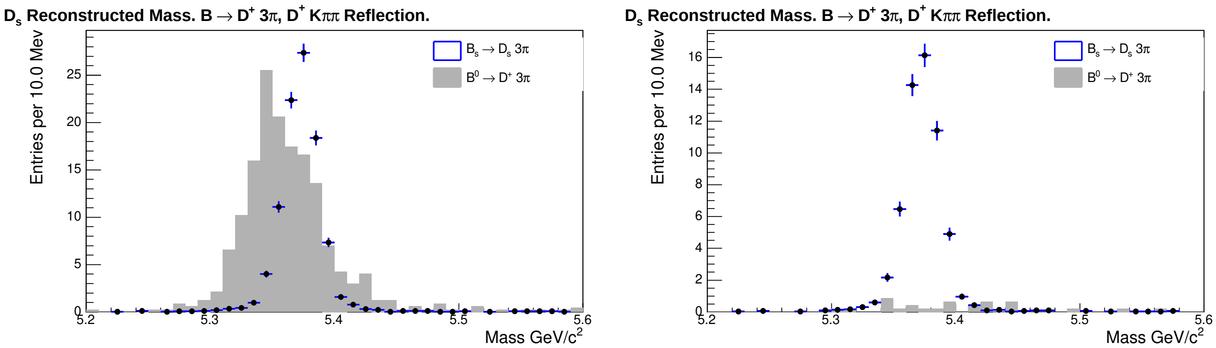

Figure 67: Reconstructed $B_s^0 \rightarrow D_s^+ 3\pi, D_s \rightarrow K^*K$ mass distribution. Signal Monte Carlo and $B^0 \rightarrow D^- 3\pi$ Monte Carlo scaled to the size of the data sample. No D^+ veto on the left. Veto applied on the right.

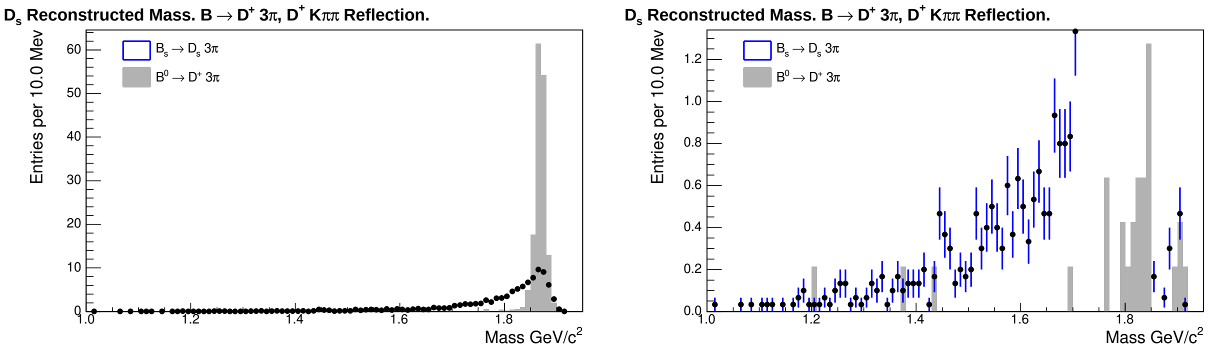

Figure 68: Reconstructed $D_s \rightarrow K^*K$ mass distribution. Signal Monte Carlo and $B^0 \rightarrow D^- 3\pi$ Monte Carlo scaled to the size of the data sample. No D^+ veto on the left. Veto applied on the right.

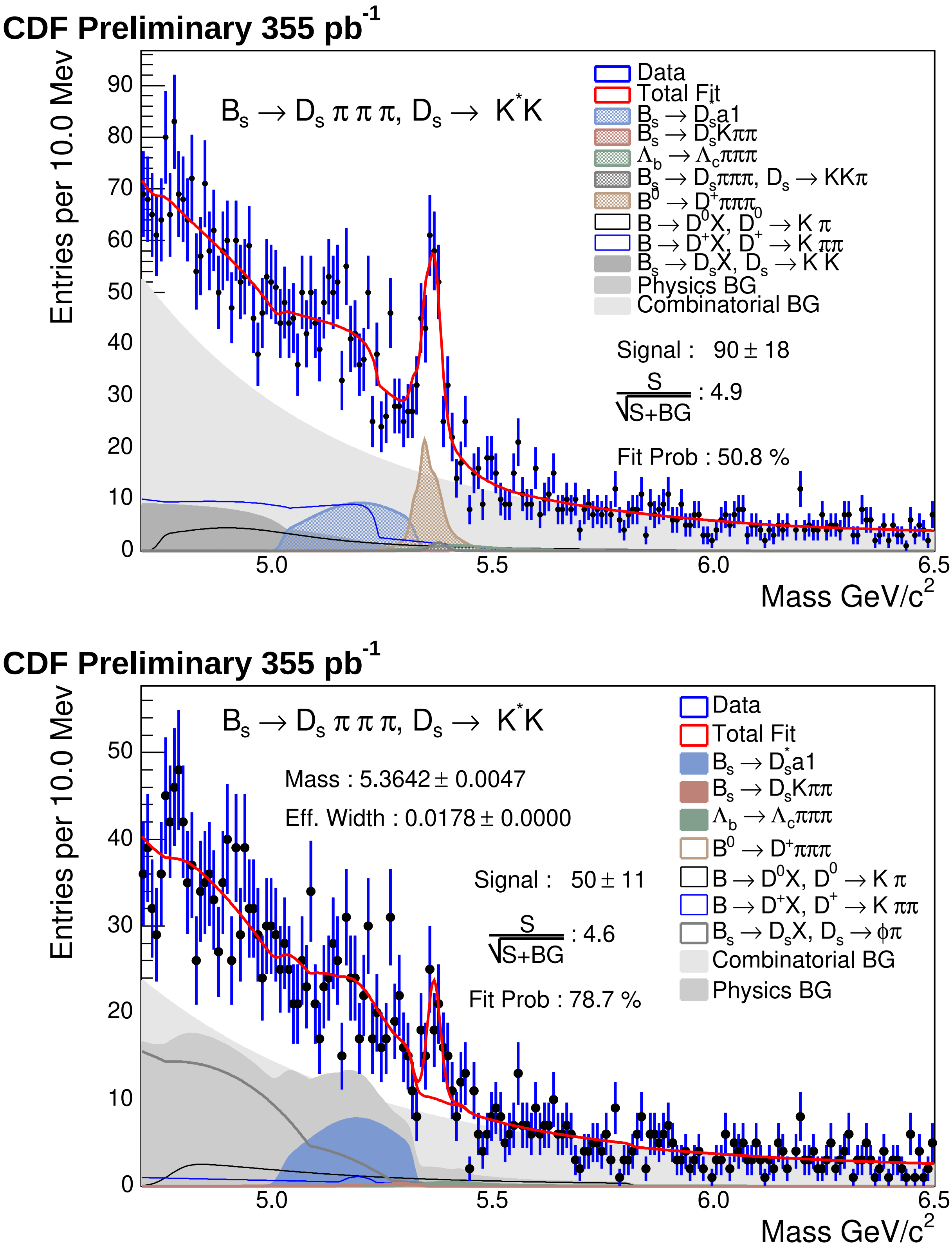

Figure 69: Reconstructed $B_s^0 \to \ D_s^+ 3\pi, D_s \to K^* K$ mass distribution. No D^+ veto on top. Veto applied at the bottom.